Title
Stochastic Models for the Control of Mosquito-borne Pathogens

Author
Wu, Sean Lawrence

Publication Date
2020

Peer reviewed|Thesis/dissertation

Stochastic Models for the Control of Mosquito-borne Pathogens

by

Sean L. Wu

A dissertation submitted in partial satisfaction of the

requirements for the degree of

Doctor of Philosophy

in

Epidemiology

and the Designated Emphasis

in

Computational Biology

in the

Graduate Division

of the

University of California, Berkeley

Committee in charge:

Assistant Professor in Residence John M. Marshall, Chair
Assistant Professor Joseph A. Lewnard
Professor Alan E. Hubbard
Professor Emeritus Robert C. Spear

Fall 2020

Stochastic Models for the Control of Mosquito-borne Pathogens

Abstract

Stochastic Models for the Control of Mosquito-borne Pathogens

by

Sean L. Wu

Doctor of Philosophy in Epidemiology

and the Designated Emphasis in

Computational Biology

University of California, Berkeley

Assistant Professor in Residence John M. Marshall, Chair

In this dissertation mechanistic stochastic models of mosquito population dynamics relevant for the control of mosquito borne pathogens are discussed. The first chapter reexamines the classical theory of vector control, which has been developed since its inception over a century ago and has produced a set of quantitative metrics that are the basis for measuring pathogen transmission. One metric is vectorial capacity, which describes the ability of a local mosquito population to transmit pathogens, expressed in a single equation. Despite its appealing simplicity, the formula is too coarse a description to describe mosquitoes in any particular place. Vectorial capacity is reevaluated as an emergent property arising from how mosquitoes use resources on a landscape according to biological imperatives, using a stochastic model based on behavioral state transitions. The second chapter builds a simulation modeling framework to evaluate the effects of gene drive and other genetic control strategies on epidemiological and entomological outcomes. The simulation modeling framework is constructed using stochastic Petri nets (SPN), a mathematical modeling language that succinctly expresses state and events in a bipartite network. The SPN can be interpreted as describing either a deterministic or stochastic system, and associated software is developed to numerically solve the resulting system of ordinary differential equations or continuous-time Markov chain. In the final chapter, an algorithm is developed to simulate stochastic jump processes as disaggregated agent-based models (ABM). To speed up simulation times, the algorithm approximates a subset of hazard rates used to specify the model, but also converges upon the true process as the time step goes to zero. The simulation technique is relevant to a wide variety of contagion processes of interest to epidemiology, and also related fields such as ecology and the quantitative social sciences.

Contents

Contents **i**

List of Figures **iii**

List of Tables **xi**

1 Introduction **1**

2 Vector bionomics and vectorial capacity as emergent properties of mosquito behaviors and ecology **4**
2.1 Introduction 4
2.2 Methods 7
2.3 Results 22
2.4 Discussion 33

3 MGDrivE 2: A simulation framework for gene drive systems incorporating seasonality and epidemiological dynamics **40**
3.1 Introduction 40
3.2 Design and Implementation 41
3.3 Results 48
3.4 Future directions 52

4 Principled simulation of agent-based models in epidemiology **55**
4.1 Introduction 55
4.2 Materials and methods 57
4.3 Results 63
4.4 Discussion 71

Bibliography **74**

A MBDETES: Duration of Feeding Cycle **86**

B MGDrivE 2: Description of the Modeling Framework **88**

B.1 Lifecycle Model 88
B.2 Epidemiological Dynamics 96
B.3 Stochastic Petri Net 106

C Brief Description of Step Operators **113**

D Derivation of Final Epidemic Size Distributions **116**

E Principled simulation of agent-based models in epidemiology: supplemental figures **118**

List of Figures

2.1 **Structure of an Activity Bout. Top)** MBITES and MBDETES model mosquito behavioral states and state transitions required for the gonotrophic cycle. The first two columnns list the behavioral states, and the last two columns describe the potential state transitions. A mosquito is either searching for a blood host (F) or attempting to blood feed (B), searching for aquatic habitat (L) or attempting to oviposit (O), or resting (R). Transitions depend on whether the last bout was a success or failure, and optionally on refeeding behavior[†] or laying a partial egg batch and skip oviposit[‡]. The next activity bout is also affected by whether a mosquito decides to make an attempt or initiate a search[*]. **Bottom)** In MBITES models, each behavioral state has an associated activity bout that has a common structure, as illustrated in the diagram. The activity bout involves a sequence of four phases: launch, do an activity (either a search or an attempt), land, and rest. The type of activity is determined both by its behavioral state and by presence and availability of resources. A mosquito will stay (S) unless there are no resources present or if the mosquito has become frustrated ([*]), in which case it will initiate a search. If the mosquito decides to stay, it makes a choice and an approach that may or may not succeed at what it was trying to do. When a mosquito lands, it selects a micro-site for a resting spot from the set of possibilities at that site. During the resting period, data from the last bout are logged, the behavioral state is updated, and the waiting time to the next launch is determined. A mosquito enters the bout either after emerging from aquatic habitat or after exiting its previous bout and surviving. 13

2.2 **The structure of a blood feeding attempt bout in MBITES.** The flowchart follows the progression of a mosquito through simulated events, from the launch (dark grey oval), choosing a host from the atRiskQ (aquamarine diamond), and the events that follow depending on what sort of host was chosen (yellow rectangles). If a human is chosen (or more generally, a blood host that is also a host for the pathogen), then each mosquito must approach and attempt to probe (salmon rectangle) and then blood feed (red rectangle). If a non-human host is, probing is ignored. Traps mimicking a blood host can also be chosen. After a blood meal (red rectangle), a mosquito must land and choose a resting spot (yellow diamonds). A post-prandial resting period follows a successful blood meal which has its own hazards (purple oval), including additional hazards associated with a flight laden with blood, which may be followed by decision to feed again (dark red diamond). Similarly, after failing the attempt (green pentagons to green rectangle), a mosquito must land and choose a resting spot (yellow diamonds). At each step, it is possible to die (light grey ovals). At any point when failure occurs or during landing, a mosquito could choose to leave the haunt and initiate a search on the next bout. This condition is checked after completing the bout (pink diamond). At the end of a bout, the mosquito's behavioral state and other state variables are updated. The endpoint of each bout is either death (grey ovals), a repeated blood feeding attempt (dark red oval) or a state transition to either a blood feeding search (pink oval) or to oviposit (blue ovals). 16

2.3 **The structure of an egg laying attempt bout in MBITES.** The flowchart follows the progression of a mosquito through simulated events, from the launch, choosing a habitat or trap from the eggQ (aquamarine diamond), and the events that follow depending on whether the mosquito chose a habitat or a trap (yellow rectangles). If a mosquito approaches the habitat, it could lay eggs. Alternatively, a mosquito could approach a trap and fail in the approach (thus surviving) or die (light grey ovals). If a mosquito is deterred in the approach to its habitat or the trap, it fails (green pentagons to green rectangle). After a successful approach to a habitat, a mosquito lays eggs (blue rectangle). After laying eggs or failing, a mosquito must land and survive (yellow diamonds). If not all eggs were laid, a mosquito can choose another habitat to lay (light blue diamond). At any point when failure occurs or during landing, a mosquito could choose to leave the haunt and initiate a search on the next bout. This condition is checked after completing the bout (pink diamonds). At the end of a bout, the mosquito's behavioral state and other state variables are updated. The outcome of each bout is either death (light grey ovals), a repeated egg laying attempt bout (dark blue ovals) or a state transition to either an egg laying search (light blue ovals) or a blood feeding attempt (red or pink ovals). 17

2.4 **Comparison of results from MBITES and MBDETES under restricted (Markovian) assumptions on waiting times and state transition probabilities.** B: Egg laying rate is the number of eggs laid, per female, per day. C: Blood feeding by age is the age distribution of mosquitoes taking bloodmeals. D: Feeding cycle duration is the time between post-prandial resting periods. In each panel, MBITES is summarized as a red histogram overlaid against the smooth density (in blue) predicted by MBDETES. All cases see excellent agreement, with MBITES fluctuating around MBDETES due to finite sample size of mosquitoes in the stochastic simulation. 27

2.5 **Measures of Mosquito Dispersion.** Smoothed distribution (red line) and density (blue area) functions are displayed for summary statistics calculated for one particular landscape (50% peri-domestic habitats). A: The spatially averaged movement kernel is simply the probability of movement by distance, averaged over all haunts on the landscape. B: Cumulative movement, gives the distribution of total distance traveled by mosquitoes over their entire lifetime, and has a long right tail. C: Lifetime displacement is the absolute *displacement* of a mosquito, that is, the distance between the natal aquatic habitat they emerged from and the site at which their died. D: Dispersion of VC shows the distribution of secondary bites by distance, and follows closely absolute displacement of mosquitoes. All plots are calibrated to the same x-axis for comparison. 28

2.6 **Simulated Landscapes.** 3 simulated landscapes at A: 0%, B: 50%, and C: 100% peri-domestic habitats. Haunts that contain only blood feeding haunts are plotted as red circles, haunts that contain only aquatic habitats are plotted as green triangles, and those haunts that contain both types of resources are shown as blue squares (*i.e.*, peri-domestic habitats). Dispersal kernels were calibrated as if this was an area of about 100 km^2. 30

2.7 **Vectorial Capacity.** In MBITES, vectorial capacity (VC) is computed directly as the average number of infectious bites (*i.e.*, probing) arising from all the mosquitoes blood feeding on a single human on a single day; it is effectively the number of pairs of events where a blood meal by a mosquito is followed at least EIP days later by that same mosquito probing in attempt to feed on a human, measured per human, per day. Summary VC A,B,C: and number of human blood meals per mosquito over its lifespan (D,E,F; referred to as the *stability index* by Macdonald) are shown by column for 0%, 50%, and 100% peri-domestic habitats. Each histogram gives the distribution of VC or the number of human blood hosts across mosquitoes for that percent peri-domestic habitats. 31

2.8 **Behavioral State Distribution.** Chord diagrams showing the empirical state transition matrices for three of the 26 experiments: A: 0%, B: 50%, and C: 100% peri-domestic habitats. These were calculated for each experiment by summing transitions for each mosquito between two states and then averaging to produce a Markov transition matrix. The width of the directed edges between each behavioral state is proportional to the probability of that transition, and the area on the perimeter of the circle labeled for each state is proportional to the mean time spent in that state. The three chord diagrams are accompanied below (D-F) by quasi-stationary probability distributions which give the asymptotic distribution of how a mosquito spends time across behavioral states conditional on survival. 33

2.9 **Binomic Parameters.** Simulations in MBITES illustrate that all of the bionomic parameters are sensitive to the proportion of peri-domestic habitats, which gives a measure of how frequently a mosquito must search. The x-axis of each plot ranges from 0% to 100%, and each summary bionomic parameter is plotted as mean (solid line), median (dashed line), and the shaded area covers the 20-80% quantile range of the data. The distribution of number of blood hosts B: exhibits significant right skew, such that the mean exceeds the 80% quantile at low proportion peri-domestic breeding habitats. Because the simulations are stochastic, the exact number of mosquitoes from which Monte Carlo estimates of the bionomic parameters were computed varied somewhat over the 26 landscapes, the mean was 456,579 mosquitoes with a standard deviation of 754 mosquitoes. 34

2.10 **Dispersion and Movement Parameters.** In MBITES, vectorial capacity (VC) and its dispersion are highly sensitive to the proportion of peri-domestic habitats. Interpretation of axes follows Fig 2.9, and each summary bionomic parameter is plotted as mean (solid line), median (dashed line), and the shaded area covers the 20-80% quantile range of the data. A: Number of secondary bites produced increases dramatically as a function of peri-domestic habitats. B: Spatial dispersion shows no strong trend however, due to the strong clustering of haunts in the landscape (it largely follows the trend of absolute lifetime displacement (C), as opposed to cumulative movement (D). At low percent peri-domestic breeding habitats, significant right skew in the distribution of VC pulls the mean above the 80% quantile. 35

3.1 **Modules in the MGDrivE 2 framework. (A)** Genetic inheritance is embodied by a three-dimensional tensor referred to as an "inheritance cube". Maternal and paternal genotypes are depicted on the x and y-axes and offspring genotypes on the z-axis. **(B)** Mosquito life history is modeled according to an egg-larva-pupa-adult (female and male) life cycle in which density dependence occurs at the larval stage, and life cycle parameters may vary as a function of environmental variables over time. Genotypes are tracked across all life stages, and females obtain a composite genotype upon mating - their own and that of the male they mate with. Egg genotypes are determined by the inheritance cube. **(C)** The landscape represents a metapopulation in which mosquitoes are distributed across population nodes and move between them according to a dispersal kernel. Population sizes and movement rates may vary as a function of environmental variables. **(D)** The epidemiology module describes reciprocal transmission of a vector-borne pathogen between mosquitoes and humans. This requires modeling human as well as mosquito populations, and the number of individuals having each infectious state. Epidemiological parameters may vary as a function of environmental variables. 43

3.2 **Epidemiology module.** MGDrivE 2 includes two basic models for reciprocal pathogen transmission between mosquitoes and humans - one for malaria **(A)**, and one for arboviruses **(B)**. In both cases, female mosquitoes emerge from pupae at a rate equal to $d_P/2$ as susceptible adults (S_V), become exposed/latently infected ($E_{V,1}$) at a rate equal to the force of infection in mosquitoes, λ_V, and progress to infectiousness (I_V) through the extrinsic incubation period (EIP = $1/\gamma_V$), which is divided into n bins to give an Erlang-distributed dwell time. The mortality rate, μ_F, is the same for female mosquitoes in each of these states. For malaria **(A)**, susceptible humans (S_H) become infected/infectious (I_H) at a rate equal to the force of infection in humans, λ_H, and recover at rate r, becoming susceptible again. For arboviruses **(B)**, susceptible humans (S_H) become exposed/latently infected (EH) at a rate equal to λ_H, progress to infectiousness (I_H) at rate equal to γ_H, and recover (R_H) at rate, r. Infection dynamics couple the mosquito and human systems via the force of infection terms; λ_V is a function of I_H, and λ_H is a function of I_V, shown via red edges. 45

3.3 **Stochastic Petri net (SPN) implementation of MGDrivE 2. (A)** Petri net representation of the life history module. The set of purple circles corresponds to places, P, and red rectangles to transitions, T. This Petri net shows a model in which development times for the egg stage are Erlang-distributed with shape parameter $n = 2$, and for the larval stage are Erlang-distributed with shape parameter $n = 3$. Population dynamics are derived directly from this graph; *e.g.*, the transition corresponding to oviposition has one edge beginning at F, meaning at least one female mosquito must be present for oviposition to occur. When oviposition occurs, a token is added to E_1 (new eggs are laid) and a token is returned to F. **(B)** Conceptual representation of the SPN software architecture showing the separation between the model representation (blue circles) and set of sampling algorithms (red rectangles). These two components of the codebase meet at the simulation API, enabling users to match models and simulation algorithms interchangeably. Output may be returned as an array in R for exploratory work, or written to CSV files for large simulations. 49

3.4 **Example MGDrivE 2 simulations.** Example MGDrivE 2 simulations for a population replacement gene drive system designed to drive a malaria-refractory gene into an *An. gambiae s.l.* mosquito population with seasonal population dynamics and transmission intensity calibrated to a setting resembling the island of Grand Comore, Union of the Comoros. The gene drive system resembles one recently engineered in *An. stephensi* [3] for which four alleles are considered: an intact homing allele and malaria-refractory gene (denoted by "H"), a wild-type allele (denoted by "W"), a functional, cost-free resistant allele (denoted by "R"), and a non-functional or otherwise costly resistant allele (denoted by "B"). Model parameters describing the construct, mosquito bionomics and malaria transmission are summarized in Table 3.1. **(A)** Climatological time-series data - temperature in red and rainfall in purple - that were used to calculate time-varying adult mosquito mortality rate and larval carrying capacity, respectively. The resulting adult female population size is shown in green. **(B)** Allele frequencies for adult female mosquitoes over the simulation period. Grey vertical bars beginning at year three denote eight consecutive weekly releases of 10,000 male mosquitoes homozygous for the drive allele (HH). **(C)** Spread of the malaria-refractory trait through the female mosquito population, and consequences for mosquito and human infection status. Following the release of the drive system at year three, the proportion of refractory female mosquitoes (dotted light purple line) increases and the proportion of infectious mosquitoes (dotted dark purple line) declines. As humans recover from infection and less develop new infections, the P. falciparum parasite rate (solid red line) declines until it reaches near undetectable levels by year five. **(D)** Human malaria incidence is halted by the beginning of year four. 53

4.1 **Approximate infection hazard over a time.** The left filled circle and unfilled right circle indicate that time steps are closed on the left and open on the right. 59
4.2 **Comparison of Rejection Sampler and Direct Inversion for sampling first event times.** Panel A: using integrated hazard to sample, Panel B: using accept-reject algorithm to sample. Red curves in both panels are the exact density, from numerical integration. 61
4.3 **Graphical representation of simulation algorithm with three agents.** Rows $s_1(t), s_2(t), s_3(t)$ are piecewise constant functions that give each agent's state in the state space (S, I, R) at time t; each agents' trajectory will be a piecewise constant function through state space. S (susceptible) is green, I (infectious) is blue, and R (recovered) is violet. The blue stripe $\lambda_3(t)$ gives the FOI on agent 3 (the only one to begin as susceptible). 63
4.4 **Comparison of exact transition probabilities to MNRM and ABM transition probabilities.** Panel A: Comparison of MNRM (dashed contours) against exact probability distribution (solid contours), Panel B: Comparison of ABM (dashed contours) against exact probability distribution (solid contours). In both panels the x-axis and y-axis give the probability of having that number of susceptible and infectious individuals at $t = 5$, respectively. 66
4.5 **Absolute error between ABM and exact transition probabilities for different sized time steps.** Panels show absolute error between transition probabilities calculated from the ABM versus exact distribution, from smallest time step (0.001) in the upper left to largest (1.0) in lower right. Darker areas correspond to small error while lighter regions correspond to higher error. 67
4.6 **Final epidemic size distributions for Markovian SIR model.** Panel A: Analytic final epidemic size distribution (red) versus empirical distribution (purple) from MNRM [7], Panel B: same, but empirical distribution (purple) from ABM. For each possible final size value we plotted the mean of simulation results as a purple dot with error bars indicating the pointwise 95% confidence interval from Wilson's score method. 68
4.7 **Comparison of exact transition probabilities to MNRM and ABM transition probabilities.** Comparison of transition probability distribution sampled from MNRM (solid contours) to distribution sampled from the ABM (dashed contours). The x-axis and y-axis give the probability of having that number of susceptible and infectious individuals at $t = 5$, respectively. 71
4.8 **Final epidemic size distributions for non-Markovian SIR model.** Panel A: Analytic final epidemic size distribution (red) versus empirical distribution (purple) from MNRM [7], Panel B: same, but empirical distribution (purple) from ABM. For each possible final size value we plotted the mean of simulation results as a purple dot with error bars indicating the pointwise 95% confidence interval from Wilson's score method. 72

A.1 Graphical representation of Equation A.1, edges are colored by their origin compartment, and correspond to elements in the matrix ODE. 87

B.1 SEI-SIS pathogen transmission system; orange arrows denote the contribution of each species to the force of infection term on the other. 97
B.2 Susceptible-infected-susceptible (SIS) human infection dynamics 98
B.3 Susceptible-exposed-infected (SEI) mosquito infection dynamics 101

E.1 **Truncated Exponential distribution of infection time on time step where the $\widehat{\tau}_{S\to I}$ is accepted.** An Exponential distribution truncated at Δt with rate parameter λ has the density $f(\tau;\lambda,\Delta t)=\frac{\lambda e^{-\lambda\tau}}{1-e^{-\lambda\Delta t}}$. 118
E.2 **Nonhomogeneous diurnal intensity function.** Continuous intensity function $\tilde{\lambda}(t)$ (red solid line) and piecewise approximation $\lambda(t)$ (purple step function; approximation used for simulation is on much finer time-step, coarse approximation is purely for visual effect). 119
E.3 **Comparison of simulation trajectories from exact stochastic simulation and ABM.** Panel A: Markovian SIR trajectories. Panel B: non-Markovian SIR trajectories. For each panel we drew 10^4 trajectories from the MNRM and ABM simulation algorithms and summarized the results by plotting the mean and 95% simulation interval. The MNRM trajectory is denoted by dashed lines and the ABM by solid lines. 120

List of Tables

2.1 **Vectorial Capacity** The five parameters comprising the classical formula for vectorial capacity (VC or denoted V), describing the total number of infectious bites arising from all the mosquitoes feeding on a single human on a single day under the assumptions of the Ross-Macdonald model [105, 141, 138]. The expected number of blood meals on the pathogen's hosts, summed over a mosquito lifespan, is given by the term $S = fQ/g$. The probability of surviving the EIP is $P = e^{-gn}$. Mosquito population density is $m = \lambda/g$. Under the assumptions, the formula for VC is $V = \lambda S^2 P$. In the Ross-Macdonald model, the entomological inoculation rate, $\mathcal{E}$, is related to VC by a formula: $\mathcal{E} = V\kappa/(1 + S\kappa) \approx V\kappa$, where κ is the proportion of bites on humans that infects a mosquito; the approximation holds when κ is small, such that mosquito super-infection is rare. In MBITES, the same quantity can be computed directly by Monte Carlo simulation. 5

2.2 **State Transitions & Waiting Times** In MBITES, it is possible to compute the expected state transitions and waiting times from any state to the next state. In MBDETES and limiting cases of MBITES, these single-state transition expectations can be used to estimate the state transition probabilities and waiting times from one state to every other state, including the length of a gonotrophic cycle, from resting to resting (*i.e.*, from $R \to R$). The table gives formulas for the probability of surviving to reach the behavioral state Y starting from another state X, $\Psi_{X,Y}$, where $X, Y \in \{L, O, F, B, R\}$. Note that $P_{X,Y}$ denotes the single activity bout probability of a state transition. It also gives the expected waiting time to Y from X is $T_{X,Y}$. These formulae are expressed in terms of the single bout state transitions and waiting times, $P_{X,Y}$ and $T_X = \gamma_X^{-1}$ (or they can be by making a simple substitution from one of the formulas appearing in the table above it.) 14

3.1 **Parameters for example simulation output.** Model parameters describing the gene drive construct, mosquito bionomics and malaria epidemiology for simulations resembling releases on Grand Comore, Union of the Comoros.) 54

Acknowledgments

This dissertation, while bearing my name and being the product of my own work and learning, would not have been possible without the assistance, mentorship, and friendship of a great many people. I ask forgiveness from those whose names I omit, due to my own forgetful nature.

First I wish to give my sincere thanks to my advisor, John M. Marshall. It is quite incredible to me, years later, to consider the gamble you took on a motivated but not particularly focused MPH student. Your encouragement and willingness to talk frankly when things were not so smooth were instrumental in getting me across the finish line, and I thank you for everything. I hope we will continue to be friends and collaborators for years to come. Second I would like to give my deepest thanks to my unofficial advisor, David L. Smith. Beyond being a brilliant mathematician and ecologist, your uncompromising stance to do the right thing will never leave me. Your words have been a source of encouragement in dark times and I think others feel the same. I hope to work together with you for many years to come. Next I would like to thank my dear friend and colleague Andrew J. Dolgert. Your infectious enthusiasm for all things stochastic is an affliction I expect I shall never recover from. I have fond memories of our many talks, both those with equations in them and without. I know we will be friends for many years to come. I would also like to extend my gratitude to Robert C. Spear; from the outset you have always treated me as a colleague despite our very large gap in knowledge, years, and experience. I am forever grateful to have gone to Sichuan with you and gotten my feet wet for my first experience as an epidemiologist. My only (selfish) regret is that we had not met earlier and had the chance to be collaborators throughout our careers.

Next I wish to thank my friends that I have made on this journey. Amanda Mok, Justin Batchellor, Héctor M. Sánchez C., Cameron J. Adams, Alexandra M. Jurgens, Falko Goettsch, Yoshika Crider, Maria Ma, Daniel T. Citron, Biyonka Liang, Fausto A. Bustos C., and Qu Cheng. I would also like to thank older friends who have accompanied me on this journey. Harry J. Kao, Don Paul Whigan, Tess E. Smidt. I also owe my parents, Cynthia J. Anfinson and Frederick Wood the greatest thanks for their neverending encouragement and interest in my journey. I would like to thank Jupiter in downtown Berkeley for their stout brews which have fueled many a long conversation. Finally I would like to give my deepest, sincerest thanks to Xunfei Li for her steadfast support and love.

Chapter 1

Introduction

The use of mathematical models to understand and control mosquito borne pathogens has a long and distinguished history, beginning with Ronald Ross's initial investigations into the relationship between prevalence of malaria parasites in human hosts and mosquito vectors after he demonstrated mosquitoes were responsible for transmission of the disease causing pathogen. Ross's model was analyzed by the famed mathematician Alfred Lotka, and later extended to incorporate insights and synthesis by malariologist George Macdonald, and has since been known as the Ross-Macdonald (RM) model. These early mathematical models resemble demonstrations of simple physical laws in ideal media, neglecting (or relegating to fixed constants) details such as abiotic interactions, uneven distribution of bites, immune response, and finite populations [139, 140].

Nontheless, their parsimonious construction succinctly represents the most important events in the process of malaria transmission: bloodfeeding and infection of susceptible humans or mosquitoes, death of infectious mosquitoes, and recovery of infected humans. The RM model is expressed as a pair of coupled nonlinear ordinary differential equations requiring 7 parameters, each of which has an unambiguous definition (though not necessarily always easy to measure in the field). At equilibrium, the equations can be manipulated to provide simple, intuitive expressions for vectorial capacity and the basic reproduction number, giving insight into the effect sizes of interventions that target different features of malaria ecology [138]. Perhaps due to the clarity of thought and persuasive conclusions drawn from the RM model, most models developed since Ross's original mathematical insights still incorporate most of their simplifying assumptions [125].

While the original RM model was used to demonstrate large-scale, strategic aspects of malaria control, such as Ross's insight that malaria elimination required only that the adult mosquito population be brought below some critical value necessary to sustain endemic transmission, or George Macdonald's later use of the model to argue forcefully for adult vector control which guided the Global Malaria Eradication Program (1955-1969), the model is too abstract to provide real insights about any specific place [141]. Making models more relevant for specific locations means making more complicated models. In some cases, sufficiently increased complexity means that one must turn to new methods

of *building models* to effectively grapple with the required complexity, a topic investigated in the final chapter of this dissertation.

The first two chapters in this dissertation develop theory and methods to mechanistically model mosquito borne pathogen transmission systems. The first chapter, "Vector bionomics and vectorial capacity as emergent properties of mosquito behaviors and ecology" takes a critical view at mechanistic models of adult mosquito population dynamics, many of which still fulfill some or most of the canonical set of assumptions used in RM-style models [125]. By constructing micro-scale models of adult behavior based on the smallest atomic unit of mosquito behavior, the flight bout, where a mosquito launches into the air to fulfill a biological imperative, succeeds or fails, and lands to rest, dependence of bionomic parameters describing mosquito populations relevant for disease transmission and control were shown to be highly sensitive to details of the spatial arrangement of resources that mosquitoes use throughout their life. Relative density or sparsity of resources in an area changes the way that a mosquito spends its time, given the same biological imperatives, giving a mechanistic explanation of the way that transmission dynamics depend on local setting. The stochastic simulation algorithm used is described fully in the final chapter, where it is verified against closed form analytical results.

In the second chapter, a simulation framework (MGDrivE 2) is developed to model meso-scale population dynamics of mosquitoes with special application to modeling genetic inheritance and genetic control strategies for mosquito borne pathogen transmission. The modeling framework is designed using stochastic Petri nets (SPN), a mathematical modeling language that represents state and events as two sets of nodes on a bipartite graph. Used to great effect in operations research and chemical physics especially, SPNs are seldom used in epidemiological simulation despite their ability to succinctly structure complex state spaces and design the events that affect state. The mathematical and computational framework builds upon previous work by [130] and is available as an open source R package on CRAN [156]. Mathematical models developed with MGDrivE 2 can be used to gain insight into how genetic control strategies may affect disease transmission at an intermediate scale in which humans and mosquitoes move among nodes in a metapopulation network. Such a scale is amenable to mathematical analysis if necessary, but incorporates enough details to suggest how genetic control may work in realistic settings.

The final chapter in this dissertation develops a new method to reformulate stochastic models of epidemiological interest as agent-based models (ABM). The simulation algorithm considers the ABM to be a disaggregated representation of a stochastic jump process, of which the continuous-time Markov chain models commonly use to simulate stochastic epidemics are a special case [4]) For complicated state spaces, ABMs can often be the most convenient and intuitive way to specify a model, but model updating can be a point of friction for researchers attempting to use the agent-based representation to simulate a system of interest. What is missing for mathematical epidemiologists is a clear recipe to turn systems in which in which agents interact through a discrete set of

events which are allowed to change their internal state into a simulation algorithm with desirable properties. A problem of *ad hoc* simulation algorithms is that they may be either unacceptably slow or induce unwanted or even unnoticed approximations. The method developed in this chapter allows for each agent's internal dynamics to update exactly in continuous time, but events that depend on the state of other agents (such as infection) are approximated over a time step.

The work presented in this dissertation investigates interactions between mosquitoes, environment, humans, and genetics, through stochastic mechanistic models, and also devises a new way to build complex models. While in the age of Big Data and machine learning an investigation of mechanistic models may seem quaint, the process of model building and refinement, and falsification if a model is incapable of reproducing observed patterns, is a core activity of science. Subjecting mathematical models of physical laws to statistical testing has been used for no less an august purpose than putting to the test Newtonian mechanics versus Einstein's General Theory of Relativity [110, pp. 119-125]. On a more earthly scale, Ross's original models of malaria were shown to be inadequate and subsequently modified by Macdonald in the 1950s to account for the omitted phenomenon of *superinfection*, in which a given host may be simultaneously infected by multiple genetically distinct parasite broods [111, 141], leading to qualitatively different predictions. While recent advances in mechanistic models may in some cases exceed the ability of field biologists to measure all relevant metrics which would be required to evaluate their adequacy, the concurrent development in statistical theory and computation for complex stochastic models, such as data augmentation, history matching, filtering techniques, and various Bayesian approaches mean that iterated model building, testing, and refinement is possible for even complicated mechanistic descriptions of a process [25, 154]. Understanding how phenomenon in the world came about requires a critical mind to imagine not only how a process operates but how one might be fooled by other, hidden mechanisms. Mechanistic models are excellent tools for developing these faculties, and advanced statistical techniques can sift away those which do not meet some level of rigorous testing. The following chapters are my attempt to grapple with understanding the processes behind mosquito borne pathogen transmission, genetic control, and how to go about the actual business of model building. I hope they prove useful.

Chapter 2

Vector bionomics and vectorial capacity as emergent properties of mosquito behaviors and ecology

2.1 Introduction[1]

Mosquitoes transmit the pathogens that cause malaria, filariasis, dengue, and other diseases that account for approximately 17% of the global burden of infectious diseases [70]. Mosquito-borne pathogens are transmitted to a vertebrate host while mosquitoes probe or blood feed, so the intensity of transmission and the risk of infection are related to mosquito blood feeding behaviors and local population density. Development of concepts and metrics to measure transmission intensity by mosquitoes, such as the entomological inoculation rate (EIR) and vectorial capacity (VC), were motivated by or derived from mathematical models of pathogen transmission by mosquitoes [38, 119, 105, 48, 141]. Entomologists meanwhile identified and developed field methods to measure some of the parameters that are key determinants of the EIR and VC: mosquito survival, mosquito population density, the overall blood feeding frequency, and human blood index, the ratio of mosquitoes to humans in the area, and the pathogen's extrinsic incubation period (EIP) [49, 136]. These parameters are also important determinants of vector population responses to vector control interventions, such as insecticide-treated nets, indoor residual spraying, and spatial repellents, to name but a few. These parameters and metrics arise from basic mosquito behavioral algorithms for finding and using resources, avoiding hazards, and adjusting to weather and other factors that characterize mosquito ecology [91, 18]. An important question is how parameters relevant for pathogen transmission and vector control are co-determined by basic behavioral algorithms and genetically determined preferences of each vector species and by the availability and distribution of resources and other ecological factors.

[1]This chapter has been previously published [157]

The canonical model of the entomological aspects of malaria transmission, called the Ross-Macdonald model, describes changes in the sporozoite rate [105]. The associated formulae for VC and EIR, which arise from a common conceptual and mathematical basis, summarize transmission intensity in terms of a few parameters (Table 2.1) [138, 141]. Both formulae count the expected number of events occurring on one human on one day: VC measures the number of infectious bites that would arise from all mosquitoes blood feeding on a typical human, as if that human were perfectly infectious; and the daily EIR measures the number of infectious bites received by a typical human. The number of bites arising must approximately balance the number of bites received, after accounting for time lags (e.g. the EIP), mosquito migration, and imperfect transmission from infected humans. Mathematical formulas for VC and the EIR derived *a priori* are consequently related by a simple formula [22]. The quantitative logic supporting these metrics is both parsimonious and compelling, and these metrics and associated bionomic parameters form the basis of medical entomology and most models of mosquito-borne pathogen transmission [125].

m	The number of female mosquitoes per human
f	The blood feeding rate, per mosquito, per day
Q	Proportion of blood meals on the pathogens' hosts
g	The mosquito death rate, per mosquito, per day
n	Extrinsic Incubation Period (EIP), in days
$\lambda = gm$	The number of female mosquitoes emerging, per human, per day
$S = fQ/g$	The expected number of human blood meals per mosquito
$P = e^{-gn}$	The probability of surviving the EIP

Table 2.1: **Vectorial Capacity** The five parameters comprising the classical formula for vectorial capacity (VC or denoted V), describing the total number of infectious bites arising from all the mosquitoes feeding on a single human on a single day under the assumptions of the Ross-Macdonald model [105, 141, 138]. The expected number of blood meals on the pathogen's hosts, summed over a mosquito lifespan, is given by the term $S = fQ/g$. The probability of surviving the EIP is $P = e^{-gn}$. Mosquito population density is $m = \lambda/g$. Under the assumptions, the formula for VC is $V = \lambda S^2 P$. In the Ross-Macdonald model, the entomological inoculation rate, $\mathcal{E}$, is related to VC by a formula: $\mathcal{E} = V\kappa/(1 + S\kappa) \approx V\kappa$, where κ is the proportion of bites on humans that infects a mosquito; the approximation holds when κ is small, such that mosquito super-infection is rare. In MBITES, the same quantity can be computed directly by Monte Carlo simulation.

While the Ross-Macdonald model and associated bionomic parameters are a useful way of summarizing overall transmission intensity, a weakness of the model is that it does not include many other parameters and metrics that are important for pathogen transmission dynamics, the measurement of transmission, and responses to vector control. These

include metrics for heterogeneous biting by mosquitoes [34], the spatial dimensions of transmission or control [120, 30, 29], vector contact rates with and quantitative responses to various kinds of vector control deployed in myriad combinations and coverage levels [92], environmental factors that affect variance in the number of mosquitoes caught [84], and nuances of behavior affecting the accuracy of various field methods [136]. Models describing effect sizes of vector control rely on assumptions about the way interventions alter the basic bionomic parameters [94], but there has been very little theory developed to understand either what contextual factors determine baseline bionomic parameters or how contextual factors influence the effect sizes of control [50]. What is needed is a synthetic framework for weighing entomological heterogeneity: spatial and temporal heterogeneity in the availability of hosts and the rates of blood feeding on hosts; heterogeneity in the availability of habitats, egg laying, and mosquito population dynamics; age-specific mosquito mortality; mating and the availability of mates; energetics, sugar feeding and the availability of sugar sources; and the risks and costs associated with searching for all these resources. Understanding and quantifying the inter-dependency of mosquito behavior on hazards and resources through observation presents enormous challenges.

One way to forge a new synthesis is to model mosquito behavior at its most irreducible level and in extreme detail in order to prioritize new research. To that end, we here present a new framework for building individual-based models based on the concept of an "activity bout". A bout is initiated when a mosquito launches itself in the air to do something and ends after a mosquito has landed, rested, and is about to launch itself into the air again. It includes a sequence of events which may be of varying duration depending on factors both internal and external to the mosquito. In the models we present here, a bout is the irreducible unit of mosquito activity. Specific actions during the bout depend on the mosquito's current behavioral state. This behavioral state depends on cues from local ecology and the mosquito's current physiological state and determines what activity the mosquito is intent on accomplishing at any given time, such as seeking to blood feed or oviposit. Success and survival through each bout depend on context and chance. Probabilities are affected by the resources and hazards in its vicinity, the cues it uses to find those resources, its efficiency in using those resources, and other factors such as vector interventions that suppress transmission by killing mosquitoes or altering their behavior. This description of behavioral states makes clear the joint dependence of behavioral state transitions on the mosquito's biology as well as local ecology.

To understand how ecology and behavior jointly affect transmission, we developed bout-based behavioral state models for mosquitoes to show how the values of bionomic parameters in the Ross-Macdonald model arise from basic mosquito behavioral algorithms in response to ecology. These models consider a behavioral state space and model the dynamic transitions between states as they follow the biological imperatives of their state and succeed or fail depending on the availability of local resources and other factors. MBITES (Mosquito Bout-based and Individual-based Transmission Ecology Simulator) is a framework for building individual-based simulation models of mosquito behavioral activity bouts in exquisite detail. Simulated mosquito activities are implemented as algo-

rithms executing activity bouts and behavioral transitions in response to resources that are organized on spatially explicit landscapes. MBDETES (Mosquito Bout-based Differential Equation-based Transmission Ecology Simulator) is a differential equation based model of behavioral state transitions that is more analytically tractable than MBITES. Under a restricted set of assumptions, some MBITES models can be represented as a continuous-time Markov process, for which MBDETES is the set of master equations. Because MBDETES describes the expected behavior of some MBITES models, we use the two frameworks for mutual verification through both simulation and analysis.

These two bout-based behavioral state models make it possible to investigate how behavioral algorithms and resource distributions affect local decisions and give rise to the parameters that are widely acknowledged to be important for pathogen transmission. Through Monte Carlo simulation of models developed in MBITES, it is possible to compute any quantity describing adult mosquito reproductive success or capability to act as effective pathogen vectors and, through careful *in silico* analysis, to learn what factors determine their values. To this end, MBITES provides algorithms to compute from simulation output: lifespans, metrics of mosquito dispersal from the natal aquatic habitat, stability index (number of human blood meals per mosquito lifetime), the length of a feeding cycle, survival through one feeding cycle, blood feeding rate, entomological inoculation rate (EIR), egg production and dispersal, vectorial capacity (VC), and the spatial scales over with VC is dispersed. By summarizing models according to these values, we can map these behavioral models to regularly discussed and estimated metrics that are the target of inference and control in many intervention studies. We show how the classical mosquito bionomic parameters used by the Ross-Macdonald model arise from mosquito behavioral algorithms in their ecological context, but we also describe their distribution and spatial dimensions. These behavioral state models thus provide a way of synthesizing more than a century of studies that have observed and measured aspects of individual mosquito behavior in a variety of contexts, from laboratory through the field.

2.2 Methods

MBITES

MBITES is a framework for building individual-based continuous-time discrete-event simulation models for adult mosquito behavior and ecology. The framework is highly mimetic: simulated mosquito activity is designed to resemble what we believe actual mosquitoes are doing. The descriptions of mosquito behavior in the sections below map onto the structures and algorithms that are built into MBITES. For each simulated mosquito, MBITES samples events and outputs a lifetime trajectory through behavioral state space as well as spatial location. The framework accommodates differences in behavioral algorithms and life-history traits across species, different ecological contexts, and different purposes. To make it useful as a research tool, some pre-defined behavioral states are

optional. An important feature of MBITES is a resource landscape can be configured to suit any situation. MBITES has a modular design: several functions can be called to model each biological or ecological process, and it is comparatively easy to add, remove or modify new functions or features. Mathematical and computational details, including functional forms and some options are documented in the code.

MBITES is under active development and it is being maintained with version control. This document describes MBITES version 1.0. The code was written in R and C [123]. Source code for MBITES are released at a permanent GitHub archive (`https://github.com/dd-harp/MBITES/tree/v1.0/MBITES`); configuration files for simulations are also available here (`https://github.com/dd-harp/MBITES/tree/v1.0/scripts`).

The Landscape

MBITES simulates mosquito behavior on a set of points in space called *haunts*, small areas where mosquitoes can rest between long range search flights. *Resources* may be present at some of these haunts. Landing spots within a *haunt* are represented as a set of micro-sites. The set of points and associated resources is called the *landscape*.

Each adult mosquito emerges from one of these haunts and moves among the haunts throughout its life as it searches for and utilizes the resources it needs. In this manuscript we consider only two types of resources. First, blood feeding haunts are places where vertebrate animals are typically found such that mosquitoes could take a blood meal, which could include the area around a family dwelling or other structure, a field where farming occurs, or an outdoor spot where humans or other vertebrate animals are found. Second, some haunts include aquatic *habitats* where mosquitoes attempt to lay eggs. In this manuscript we do not consider density-dependent dynamics in aquatic habitats, as our focus is on the behavioral algorithms that structure how cohorts of mosquitoes behave after emergence. We acknowledge the possibility and importance of nonlinear dependence in adult mosquito behaviors, such as the choice of where to oviposit, and competition for resources by larval mosquitoes in aquatic habitats. However, we feel confident in presenting the current set of *adult* behavioral algorithms as an initial step, to be followed up with development of detailed *aquatic* algorithms which will incorporate such dynamics; the modular design patterns we have used in MBITES allows for such development to be feasible and transparent.

Two other types of resources included in MBITES, which will be described in detail in future manuscripts, are sugar sources and mating sites. Each haunt may have one or more resource type and more than one of each type of resource; more than one potential blood host could be present, and there could be more than one suitable aquatic habitat, such as a pond and a rain-storage barrel in the backyard of a home, for instance. The question of how to model a landscape – how many haunts make up the landscape, how large an area is represented by each haunt, whether to include haunts without other resources, and how many micro-sites in each haunt – is flexible. In some instances, a haunt could represent

a small area around a habitat or the area immediately surrounding a single household. The question is intrinsically related to mosquito search and dispersal, a question that may require some tuning, depending on the purpose of a simulation.

In addition to the resources present, each haunt is assigned a set of *local hazards*, or parameters that affect survival at the site, which reflects highly local conditions (such as predators) that may make a haunt more or less dangerous than others of the same type.

Each haunt is also characterized by a set of micro-sites, which define specific aspects of the places within a haunt where the mosquito lands to rest. Different *types* of haunts may have different sets of micro-sites with different resting surfaces. A *homestead* is a pre-defined haunt type with three micro-sites" a mosquito may rest either in the house, or outside on the house, or outside on surrounding vegetation. If there is no human dwelling at a haunt, it could have only vegetation. Other types can be easily constructed (*e.g.*, a homestead with livestock sheds) with their own set of relevant micro-sites for resting.

These micro-sites were devised to simulate survival through the post-prandial resting period or contact with various kinds of vector control in a highly realistic way, including exposure to residual pesticides and house entering. Housing quality and housing improvements can affect the probability of entering a house; when a mosquito attempts to enter a house, it may encounter an eave tube; insecticide spraying can be applied to the interior walls of houses (or not), their exterior walls (or not), or vegetation (or not) so that contact is simulated only if a mosquito lands on the type of micro-site that has been sprayed; and area repellents or other local features can make it more likely a mosquito will leave the haunt, thereby initiating a new search bout. Encounter with environmental vector based intervention, such as indoor residual spraying (excluding personal-level interventions, such as topical repellents, which we considered separately) at any point may incur death or physiological damage.

Modular Design

MBITES is designed to be nested within a broader framework for simulating the transmission dynamics and control of mosquito-borne pathogens. Because individual mosquitoes are simulated as a continuous-time discrete-event process, a mosquito's actions can be simulated exactly and do not need to be discretized to the nearest time step. While each mosquito agent is simulated exactly, between-agent synchronization occurs at fixed time steps. Synchronization allows agents to update each other on where they are, how many resources have been consumed, etc. in order to simulate interaction. In all simulations for this paper we chose the synchronization time step as one day. In principle, any synchronization time step can be used so long as it is short enough that the consequences of one mosquito (or agent) are synchronized before they would affect another.

Because agents in MBITES interact on the landscape, it is necessary for haunts to have associated data structures that record information to pass between different parts of the model. For example, when a human visits a certain blood feeding haunt, they must leave

a piece of information denoting their id, when they arrived, and the duration of their stay so that during the mosquito portion of the MBITES simulation, mosquitoes visiting that haunt have a list of potential blood hosts they can select from to take a blood meal. We call these data structures *queues*, and they allow different modules to interact in a generic way, facilitating a design that is both flexible and extensible. To continue the blood feeding example, it is not important for mosquitoes to know the specific algorithms by which human movement between blood feeding haunts is simulated, as long as when a mosquito arrives at a haunt to take a blood meal, it can query the queue there to find out which blood hosts are available. It is information contained in these queues that are synchronized in each time step.

As described, at each blood feeding haunt, MBITES tracks all available blood meal hosts in a queue called the *atRiskQ*. Because not all hosts present at a haunt are equally available or attractive to the mosquito, the atRiskQ stores not only the identities of blood hosts but also a biting weight for each human and other potential blood host. These biting weights reflect a combination of time spent and comparative attractiveness of all the hosts. When a mosquito chooses a blood host, she samples from the discrete distribution on blood hosts parameterized by those biting weights.

Each haunt also has a queue object called the *eggQ* that lists aquatic habitats at the haunt and ovitraps. The eggQ stores any eggs laid by mosquitoes for potential use by linked models of immature mosquito population dynamics in aquatic habitats. Like potential blood hosts, these habitats are not equally available or attractive to the mosquito, so each eggQ has a search weight. These weights can be changed dynamically to mimic specific behaviors; for example, it is possible to change the search weight if larvae are present [115].

A landscape is thus comprised of the locations of multiple points in space called haunts where mosquitoes rest, their resources, a set of micro-sites describing landing spots (*e.g.* homestead, shed, field, forest edge), local hazards, and queues. Importantly, the ability to characterize landing spots in varying granular levels of detail allows for specific simulations that can adapt to levels of detail present in field data. In this way, complex composite types of haunts can be built up by adding the basic elements, as in our previous example of a single blood feeding haunt with several independent aquatic habitats representing a large house with multiple mosquito breeding ponds in the backyard; the flexibility can accommodate complex ecological dynamics of structured habitat and behavior such as skip oviposition. All these elements determine where a mosquito attempts to do something on the landscape and affects its probability of success and survival.

Mosquito Dispersal

Mosquito movement in MBITES may occur during a behavioral bout if a *search* is triggered. It is a relocation from one haunt to a different haunt. A mosquito may decide to leave a haunt for several reasons; if the mosquito survives the search flight, it picks

a destination according to a probability mass function, which we call the haunt-specific movement kernel. While movement is random in the sense that it is sampled from this distribution, the form of this distribution is not constrained. Diffusive movement could be approximated by a landscape sufficiently rich in haunts where the haunt-specific movement kernel followed simple nearest neighbor rules, but other models are also possible.

The decision of how to configure haunts and how to model movement is not determined within MBITES. A user chooses the number of haunts and their locations knowing these are the only locations where a mosquito can be. Computation of the probability distribution functions describing dispersal to each haunts from any starting point is done prior to the MBITES simulation; the simulation accepts as input the computed probability vectors giving inter-point movement. Haunts could thus include a set of points describing all areas where mosquitoes rest or only those that are significant because of the presence of other resources. Since dispersal is modeled during pre-processing, the user has complete control over the proportion that survive dispersal and the probability of reaching each one of the other haunts.

As utilities for setting up simulations, MBITES has developed some simple parametric functions to compute these probabilities as a function of distance and an activity-specific *search weight*, ω_x, where x denotes a particular blood feeding haunt or aquatic habitat [34]. These functions thus provide multiple ways of computing the probability of moving from one haunt to any other haunt, optionally conditional on behavioral state.

Behavioral States and Other Variables

Simulations in MBITES include variables describing mosquito behavioral states and other states that maybe relevant for survival [136]. At any point during a mosquito's lifespan, it will seek to mate, sugar feed, blood feed, or lay eggs; these are biological imperatives that must be accomplished to survive and reproduce. In terms of simulation, this means that at all points in time a mosquito is alive, it belongs to one of a discrete set of behavioral states that govern its actions while in that state, as well as what state it is likely to transition to next.

Transitions between behavioral states were developed around a basic description of adult mosquito behavior. A newly emerged female mosquito must harden and mate before it is mature, whereupon it begins a cycle of blood feeding and egg laying throughout the rest of its life. After a search to find suitable blood meal hosts, the mosquito selects a host and approaches it in an attempt to blood feed. Assuming it is successful, after the blood meal, the mosquito typically rests to lose some of the water weight in a post-prandial resting period. During this time, blood is provisioned into eggs that require some time to mature. Once the egg batch is mature, the mosquito initiates a search to find a suitable aquatic habitat and then lays eggs. Sugar feeding occurs frequently throughout a mosquito's life, depending on availability of resources and energy levels, and both sexes participate in the activity [45].

In order to allow detailed simulation of activities mosquitoes undertake during each behavioral state, as well as allowing for flexibility to account for differences among species, behavioral algorithms simulate specific actions mosquitoes take as they attempt to accomplish goals associated with each state, as well as transitions to future states. While there is a general pattern to be followed (*e.g.*, blood feed, rest, lay eggs, and repeat), each mosquito follows a probabilistic sequence through a set of distinct phases surrounding the activity bout as they seek to accomplish their goals. Transitions between behavioral states depend on various internal characteristics of the individual mosquito and logical prerequisites. Egg batches must mature before a mosquito is considered gravid and enters the egg laying state. If a mosquito is gravid, it will tend to lay eggs, though re-feeding can occur regardless (see below). Otherwise, disregarding sugar feeding and mating for the moment, a mosquito's state is oriented towards blood feeding. A mosquito must leave a haunt to initiate a search if the resources it needs are not present, but a decision to leave the haunt and initiate a search can also occur even if resources are present, depending on other events that occur during a bout and properties of a haunt. For example, area repellents could increase the probability of a failure, and force a mosquito to initiate a new search.

In addition to a mosquito's behavioral states, MBITES includes a set of other variables making it possible to model heterogeneity among individual mosquitoes in extreme detail. Each mosquito in MBITES is described by internal variables that include but are not limited to: physical and physiological condition, energy reserves, size of the most recent blood meal, the number of mature eggs ready to be laid, infection status, physical condition, and a set of variables related to sugar feeding and mating. For example, inter-site movement is physiologically stressful on the mosquito, and during travel between haunts, a mosquito's energy level (an optional variable) can be decremented. The energy level can be replenished by blood meals (for females), or sugar feeding, and could be modeled as an important source of mortality while searching in resource-sparse environments. A random variate is drawn to determine the amount of physical damage (*e.g.*, wing tattering) that was incurred and modifies its physical condition or physiological damage (*e.g.*, after exposure to insecticides). Physical and physiological damage takes a cumulative toll on the mosquito.

MBITES is capable of modeling both female and male mosquito populations and behavior. For female mosquitoes, the primary behavioral states are blood feeding and egg laying (the two necessary components of the gonotrophic cycle). In this manuscript, male mosquitoes are not considered and the optional behavioral states of sugar feeding and mating and all associated variables have been turned off in order to introduce and focus on algorithms describing blood feeding and egg laying by females.

Each behavioral state – blood feeding or egg laying – requires one or more activity bouts. Additionally, each behavioral state may require one or more *types* of activity, namely *searching* or *attempting*. Thus the set of possible activity bout types each associated with a behavioral state has been denoted by a letter (Fig 2.1, Table 2.2): the blood feeding search bout (F); the blood feeding attempt bout (B); the search bout for egg laying

(L); the egg laying attempt bout (O). A letter is also assigned to the post-prandial resting period (R) that always follows a blood meal, which is a part of the blood feeding attempt bout. If a mosquito dies, it's behavioral state is set to (D).

State / Activity	**Name**	**Success**	**Fail** or **Repeat**†
Blood Feeding Search Bout	**F**	**B**	**F**
Blood Feeding Attempt Bout	**B**	**R**	**B** | **F***
Post Prandial Resting Period	**R**	**L** | **O***	**B**†
Egg Laying Search Bout	**L**	**O**	**L**
Egg Laying Attempt Bout	**O**	**B** | **F***	**L** | **O**‡

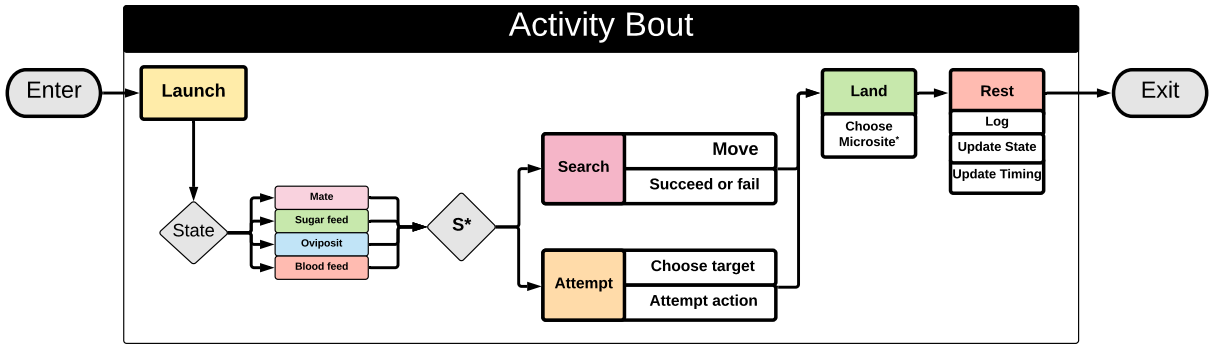

]

Figure 2.1: **Structure of an Activity Bout. Top)** MBITES and MBDETES model mosquito behavioral states and state transitions required for the gonotrophic cycle. The first two columnns list the behavioral states, and the last two columns describe the potential state transitions. A mosquito is either searching for a blood host (F) or attempting to blood feed (B), searching for aquatic habitat (L) or attempting to oviposit (O), or resting (R). Transitions depend on whether the last bout was a success or failure, and optionally on refeeding behavior† or laying a partial egg batch and skip oviposit‡. The next activity bout is also affected by whether a mosquito decides to make an attempt or initiate a search*. **Bottom)** In MBITES models, each behavioral state has an associated activity bout that has a common structure, as illustrated in the diagram. The activity bout involves a sequence of four phases: launch, do an activity (either a search or an attempt), land, and rest. The type of activity is determined both by its behavioral state and by presence and availability of resources. A mosquito will stay (S) unless there are no resources present or if the mosquito has become frustrated (*), in which case it will initiate a search. If the mosquito decides to stay, it makes a choice and an approach that may or may not succeed at what it was trying to do. When a mosquito lands, it selects a micro-site for a resting spot from the set of possibilities at that site. During the resting period, data from the last bout are logged, the behavioral state is updated, and the waiting time to the next launch is determined. A mosquito enters the bout either after emerging from aquatic habitat or after exiting its previous bout and surviving.

	$\Psi_{X,Y}$	$T_{X,Y}$
$L \to O$	$\frac{P_{L,O}}{1-P_{L,L}}$	$\frac{T_L}{1-P_{L,L}}$
$O \to F$	$\frac{P_{O,F}}{1-P_{O,O}-P_{O,L}\Psi_{L,O}}$	$\frac{T_O+P_{O,L}\Psi_{L,O}T_{L,O}}{1-P_{O,O}-P_{O,L}\Psi_{L,O}}$
$O \to B$	$\frac{P_{O,B}}{1-P_{O,O}-P_{O,L}\Psi_{L,O}}$	$\frac{T_O+P_{O,L}\Psi_{L,O}T_{L,O}}{1-P_{O,O}-P_{O,L}\Psi_{L,O}}$
$F \to B$	$\frac{P_{F,B}}{1-P_{F,F}}$	$\frac{T_F}{1-P_{F,F}}$
$B \to R$	$\frac{P_{B,R}}{1-P_{B,B}-P_{B,F}\Psi_{B,F}}$	$\frac{T_B+P_{B,F}\Psi_{F,B}T_{F,B}}{1-P_{B,B}-P_{B,F}\Psi_{F,B}}$
$F \to R$	$\Psi_{F,B}\Psi_{B,R}$	$T_{F,B}+T_{B,R}$
$O \to R$	$\Psi_{O,F}\Psi_{F,R}+$ $\Psi_{O,B}\Psi_{B,R}$	$\frac{P_{O,F}}{P_{O,F}+P_{O,B}}(T_{O,F}+T_{F,R})+$ $\frac{P_{O,B}}{P_{O,F}+P_{O,B}}(T_{O,B}+T_{B,R})$
$L \to R$	$\Psi_{L,O}\Psi_{O,R}$	$T_{L,O}+T_{O,R}$
$R \to R$	$\sum_{X\neq R} P_{R,X}\Psi_{X,R}$	$T_R+\sum_{X\neq R} P_{R,X}T_{X,R}$

Table 2.2: **State Transitions & Waiting Times** In MBITES, it is possible to compute the expected state transitions and waiting times from any state to the next state. In MBDETES and limiting cases of MBITES, these single-state transition expectations can be used to estimate the state transition probabilities and waiting times from one state to every other state, including the length of a gonotrophic cycle, from resting to resting (*i.e.*, from $R \to R$). The table gives formulas for the probability of surviving to reach the behavioral state Y starting from another state X, $\Psi_{X,Y}$, where $X, Y \in \{L, O, F, B, R\}$. Note that $P_{X,Y}$ denotes the single activity bout probability of a state transition. It also gives the expected waiting time to Y from X is $T_{X,Y}$. These formulae are expressed in terms of the single bout state transitions and waiting times, $P_{X,Y}$ and $T_X = \gamma_X^{-1}$ (or they can be by making a simple substitution from one of the formulas appearing in the table above it.)

The Activity Bout

Regardless of behavioral state, all activity bouts have four phases: launch, do an activity, land, and rest (Fig 2.1). Launching itself into the air, finding a suitable landing spot, and resting prior to the next launch must occur regardless of the biological state of the mosquito (blood feeding or oviposition, in this manuscript) and are a common part of each behavioral state and activity bout. However because the purpose of activity bouts is to accomplish different biological goals, the activity phase of each bout depends on the behavioral state. The specific activities undertaken differ depending on behavioral state, and it is possible to modify these activities to describe what happens during each bout in virtually unlimited detail. The endpoint of each bout is either death or another bout and possibly a behavioral state transition (Table 2.2, Fig 2.1).

The paths through a bout are sampled from appropriate distributions that determine whether the bout resulted in death, success (state transition), or failure (remain in the same behavioral state). These activity bouts, prefaced by a launch and ending with a rest, may be of varying duration, but encompasses all of the activity by a mosquito from

launch to launch.

The modular nature of MBITES makes it possible to configure all these options to consider a biological process of interest. While all bouts share similar structure and call on similar functions (*e.g.* optionally, flights could expend energy or contribute to cumulative wing damage), the activities and outcomes will differ based on each individual mosquito's internal physiological state. Thus, a mosquito's life consists of a series of transitions between behavioral states, each of which may take several bouts to accomplish, completely determining a mosquito's activity throughout its life.

Launch and Timing

A new bout begins the moment a mosquito launches itself into the air. The timing of the start of the launch phase is determined during the previous bout during the resting phase following landing. By sampling the time to next launch at this point in the simulation, launch times can be (optionally) conditional on events that have taken place during the previous bout.

Do an Activity — Search of Attempt

After launching, the specific behavioral algorithms called by the mosquito depend on its behavioral state (decision point "state" in Fig 2.1), as well as the local distribution of resources necessary to fulfill the mosquito's current biological needs. A mosquito will either "attempt" to accomplish the task required by their behavioral state or "search" for the resource it needs to accomplish that task. In any particular activity bout, a mosquito will either search or attempt, but not both. Searching or attempting algorithms are behavioral state-specific, and will be called during that phase of the bout (attempting to blood feed, as illustrated in Fig 2.2, for example, means something very different behaviorally than attempting to oviposit, as illustrated in Fig 2.3). Details of the attempt algorithms are described below.

The searching algorithm moves a mosquito to a new haunt on the landscape to find resources, as described earlier in section Mosquito Dispersal, while the attempting algorithm describes how a mosquito fulfills its behavioral imperatives once necessary resources are present, which will be described below for egg laying and blood feeding.

There are many factors that determine whether a mosquito will make an attempt or begin a search. A mosquito will stay and make an attempt if the necessary resource is present at the haunt, but it could leave and initiate a search if it has previously been frustrated in its attempts or if the resource is not present. Many events occurring during the bout can trigger a decision to leave and initiate a search during the next bout. For example, if the mosquito is primed to blood feed and blood hosts are present, the mosquito will tend to approach a potential blood host and try to blood feed. If there are no blood hosts present, the mosquito will search and move to a new haunt. Even if blood hosts are

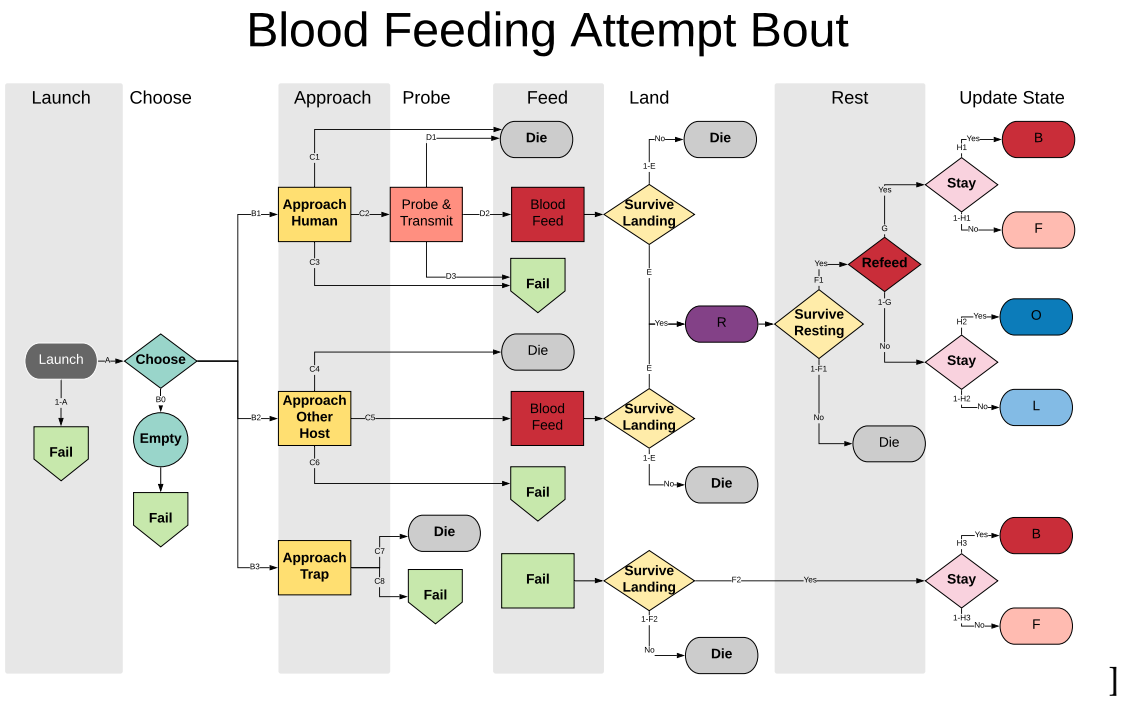

Figure 2.2: **The structure of a blood feeding attempt bout in MBITES.** The flowchart follows the progression of a mosquito through simulated events, from the launch (dark grey oval), choosing a host from the atRiskQ (aquamarine diamond), and the events that follow depending on what sort of host was chosen (yellow rectangles). If a human is chosen (or more generally, a blood host that is also a host for the pathogen), then each mosquito must approach and attempt to probe (salmon rectangle) and then blood feed (red rectangle). If a non-human host is, probing is ignored. Traps mimicking a blood host can also be chosen. After a blood meal (red rectangle), a mosquito must land and choose a resting spot (yellow diamonds). A post-prandial resting period follows a successful blood meal which has its own hazards (purple oval), including additional hazards associated with a flight laden with blood, which may be followed by decision to feed again (dark red diamond). Similarly, after failing the attempt (green pentagons to green rectangle), a mosquito must land and choose a resting spot (yellow diamonds). At each step, it is possible to die (light grey ovals). At any point when failure occurs or during landing, a mosquito could choose to leave the haunt and initiate a search on the next bout. This condition is checked after completing the bout (pink diamond). At the end of a bout, the mosquito's behavioral state and other state variables are updated. The endpoint of each bout is either death (grey ovals), a repeated blood feeding attempt (dark red oval) or a state transition to either a blood feeding search (pink oval) or to oviposit (blue ovals).

present, after multiple failed attempts, or if the blood hosts are not sufficiently attractive, a mosquito may become frustrated and leave.

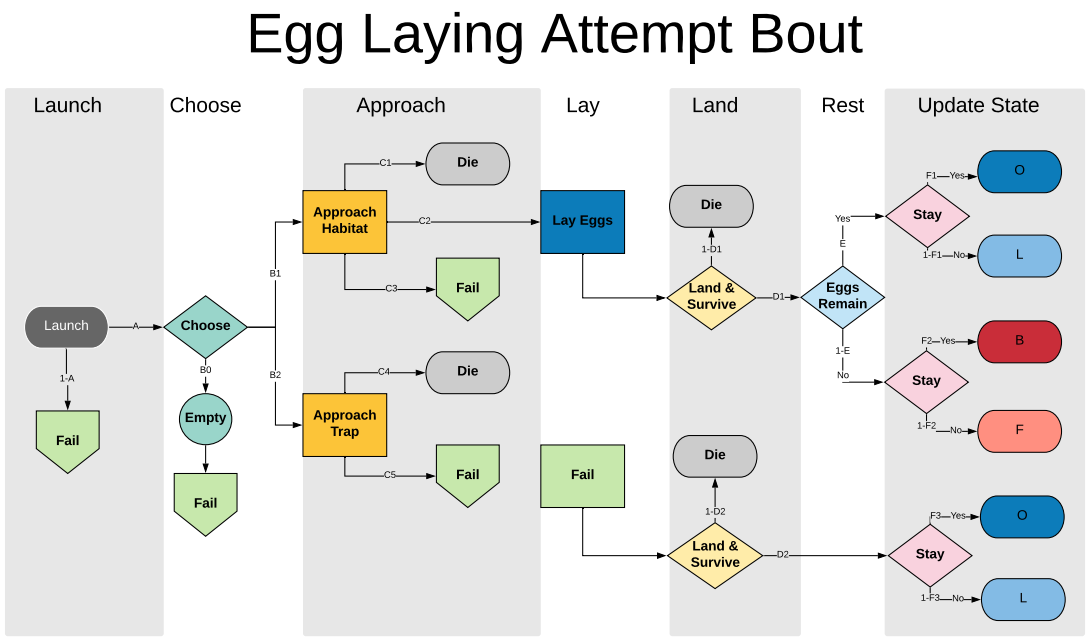

]

Figure 2.3: **The structure of an egg laying attempt bout in MBITES.** The flowchart follows the progression of a mosquito through simulated events, from the launch, choosing a habitat or trap from the eggQ (aquamarine diamond), and the events that follow depending on whether the mosquito chose a habitat or a trap (yellow rectangles). If a mosquito approaches the habitat, it could lay eggs. Alternatively, a mosquito could approach a trap and fail in the approach (thus surviving) or die (light grey ovals). If a mosquito is deterred in the approach to its habitat or the trap, it fails (green pentagons to green rectangle). After a successful approach to a habitat, a mosquito lays eggs (blue rectangle). After laying eggs or failing, a mosquito must land and survive (yellow diamonds). If not all eggs were laid, a mosquito can choose another habitat to lay (light blue diamond). At any point when failure occurs or during landing, a mosquito could choose to leave the haunt and initiate a search on the next bout. This condition is checked after completing the bout (pink diamonds). At the end of a bout, the mosquito's behavioral state and other state variables are updated. The outcome of each bout is either death (light grey ovals), a repeated egg laying attempt bout (dark blue ovals) or a state transition to either an egg laying search (light blue ovals) or a blood feeding attempt (red or pink ovals).

Land

After its flight, a mosquito must land and rest. This must occur at one of the micro-sites at a haunt, as described earlier. During the landing phase, an algorithm called *restingSpot* simulates the mosquitoes choice of micro-site, and to simulate the consequences of landing there (*e.g.* encountering a sprayed surface or entering or leaving a house). Movement

to a micro-site within a haunt to land and rest is designed to emulate short hops (*e.g.*, < 10m) a mosquito may take that differs from longer range searching behavior. The algorithm also tracks if the attempt was successful. Repeated failures at the same site may lead to the mosquito becoming frustrated, in which case the next activity bout will include a search regardless of resources availability.

Rest

The duration of the resting phase, the time elapsed between landing and the next launch, will in general differ based on behavioral state, other state variables, and events that may have transpired during the bout. Several probability distribution functions functions are available to simulate heterogeneity in the time required by mosquitoes to accomplish certain tasks based on individual characteristics and spatial location. The default option is for these times to follow an exponential distribution.

During the resting phase, internal characteristics of the mosquito are updated, including cumulative wing damage, and internal energy reserves which have been used for flight. Egg batches (if present) are also checked for maturity, depending on if the mosquito has successfully blood fed, and if so how much. The next behavioral state is determined by the success or failure of the current bout. Other variables are also updated during this time, such as age and (if a pathogen model is present), infection status.

Survival

A mosquito can die at many points during a bout as a result of specific events, such as being swatted while attempting to blood feed, or as a result of contact with some vector control device. Survival through a bout is also computed during every resting phase. Mortality is associated with the stress of flight, which sets a baseline mortality probability (per flight). A mosquito must also survive any *local hazards*, which determine the site-specific probability of dying while landing or flying at each site, such as from predation by jumping spiders or dragon flies.

Attempt Algorithms

The following sections describe in detail the algorithms that determine how a mosquito makes an attempt to blood feed or oviposit. In addition, a separate section discusses the post-prandial resting period and algorithms for simulating oogenesis and re-feeding.

Blood Feeding Attempt and Pathogen Transmission [B]

During an activity bout in which a mosquito attempts to blood feed (Fig 2.2), a detailed sequence of events describing the blood feeding attempt is simulated, any of which can result in a failure (the green nodes in Fig 2.2) with its associated state transitions (the green box in lower right of Fig 2.2). In the event of failure, the mosquito could either fail

to survive the landing, be frustrated and leave the site to search for other blood hosts (a blood feeding search, F), or remain and try again (B).

When the mosquito attempts to feed on a blood host after launching, a sequence of critical processes must be simulated. Upon arriving at a site with viable blood hosts, the mosquito chooses a particular host at that site to approach from the atRiskQ object at that site, which maintains a list of available hosts (described in the section Modular Design).

If the mosquito chooses a human host, a detailed sequence of events is simulated. First, the mosquito must approach and land on the host successfully. The approach can result in failure or death if it is deterred by swatting or a sudden movement or something else. If the mosquito survives the approach and lands on the human host, it will try to probe the host, which can also result in failure or death. Finally, if probing is successful, the mosquito proceeds to feed. When a mosquito blood feeds, a random variable is drawn to determine the blood meal size, which affects egg maturation and batch size. Notably, the blood meal could infect a mosquito if the human host is infectious. Following successful feeding, the mosquito will make a short hop within the current site and find a resting spot to digest the blood meal (post-prandial rest, purple oval), simulated by the *restingSpot* algorithm, where the specific micro-site for resting is chosen from the set of micro-sites available.

Note that it is during probing that mosquitoes could transmit pathogens from their salivary glands into humans infecting them. During blood feeding, mosquitoes could take up pathogens in blood and become infected. This functionality is part of MBITES, but the details are beyond the scope of this paper.

If the mosquito chooses a non-human host (or more generally, a blood host that is not suitable for the pathogen), probing is not modeled. A mosquito can either survive and blood feed, survive without blood feeding, or die. If the mosquito survives, restingSpot is called (as above).

The Post-Prandial Resting Period and Oogenesis [R]

The postprandial resting period is part of the blood feeding attempt bout following landing (purple oval, Fig 2.2), but it requires special consideration. After calling restingSpot, a long delay is simulated which represents the time needed for diuresis and the early stages of digestion to occur. Several options are available for modeling survival and the events that follow as blood is concentrated and provisioned into eggs. First, mortality rates can be higher because the mosquito is heavy with blood, increasing the chance that they fall victim to successful predation [127]. Second, a function has been provided to model overfeeding: the physiological stress of processing a blood meal can kill a mosquito, so it is possible to model mortality as an increasing function of blood meal size. A function determines how much, if at all, the energy reserves are topped up by the blood in the blood meal.

During the resting period, an egg batch is produced; however, the mosquito will not be considered *gravid* until the batch is mature. The number of eggs in a batch is de-

termined by a probability distribution function family, such as a discretized Gaussian distribution. Oogenesis (production of an egg batch) and the time delay to egg maturation is modeled explicitly in MBITES. Oogenesis is modeled in three ways: first, a simple phenomenological model, which simply draws a random variate from a Gaussian distribution with mean and variance parameterized to match entomological understanding; second, a semi-mechanistic model in which the size of the egg batch is linearly proportional to the size of the blood meal, in which a new blood meal adds to the egg batch size; and third, a model in which the egg batch is linearly proportional to the size of the blood meal, but eggs from a new blood meal completely replace a previous egg batch. The third model is unrealistic but mathematically convenient (*i.e.*, it was included so that there would be a memoryless model that could exactly match the assumptions of MBDETES).

In the first oogenesis model, each egg in the egg batch is considered to require a certain provision of blood for its maturation. Because each egg requires its own resources, the total blood provision needed for a batch is a linear function of the egg batch size. After the blood provision has been fulfilled, which could require multiple blood meals, the egg batch is mature and the mosquito will become *gravid*.

In the other two models, time to maturation is modeled as a delay between the initial biological commitment of the mosquito to produce a batch of eggs, and the time when the mosquito is considered gravid, upon which it will be primed to transition to the egg laying behavioral state. The time to maturation implements a simple phenomenological model, where a random variate is drawn for the maturation time which is coincident with the resting period; after this time delay, the mosquito will become gravid and either search for suitable aquatic habitats (L) or attempt to oviposit (O), depending on the local availability of resources. Re-feeding can occur in both these models.

Re-feeding

Re-feeding (the red diamond in Fig 2.2) is possible. A mosquito may take multiple blood meals prior to oviposition, which lengthens the time interval between successive oviposition attempts. Re-feeding depends in part on the model for oogenesis, as an oogenesis model could explicitly force re-feeding when a batch of eggs is not yet mature.

When re-feeding is not forced by the oogenesis model, MBITES allows for probabilistic re-feeding behavior that can optionally be disabled. Re-feeding behavior is a Bernoulli event that occurs when a mosquito is exiting the post-prandial rest (R) at the end of a blood feeding attempt bout. The probability of re-feeding is a function of either the size of the previous blood meal or the previous egg batch, accounting for mosquito propensity to top up the size of the egg batch before ovipositing.

Egg Laying Attempt and Oviposition [O]

After arriving at a haunt containing an aquatic habitat (i.e. after a search), or if the mosquito is already at a suitable haunt with one or more aquatic habitats, the mosquito

chooses a particular habitat, or possibly an ovitrap (Fig 2.3). If a mosquito chooses an aquatic habitat, it will approach the habitat and attempt to lay eggs. The outcome of an egg laying attempt bout is either death, a failed attempt, or oviposition. Like the blood feeding attempt bout, mosquitoes can fail at any time during the attempt (green pentagons), which, if the mosquito survives the failed attempt, will lead it to either reattempt at the current site (L), or become frustrated and search for a new site (O). If a mosquito is successful it lays some fraction of her eggs in an aquatic habitat. If an ovitrap exists at a site, it competes for attractiveness with other aquatic habitats that may be present, and ovipositing mosquitoes could become trapped and die in it.

MBDETES

MBDETES (Mosquito Bout-based Differential Equation Transmission Ecology Simulator) is a system of coupled ordinary differential equations for modeling mosquito bout-based behavioral states and state transitions that offers analytical tractability but reduced flexibility compared with MBITES. MBDETES was developed as a way of approximating some models developed in MBITES: any MBITES model in which the behavioral state transitions are memoryless and the waiting time to the next state transition is always exponentially distributed is the the stochastic analogue of a model in MBDETES.

The analytic tractability of MBDETES and speed of numerical solutions serves several purposes. First, we can check that the complex behavioral algorithms in MBITES are indeed functioning correctly, by comparing the output of Monte Carlo simulations against analytic solutions in situations where their expected behavior is known. Second, MBDETES provides a simple null case against which the importance of process stochasticity and individual level heterogeneity can be judged, allowing examination of situations where estimation of mean quantities through Monte Carlo simulation (*e.g.*, running MBITES repeatedly) deviates from the deterministic approximation. It is not the goal of MBDETES to produce a full deterministic approximation of the complete spatial dynamics of MBITES, but for model checking and investigating the importance of stochasticity on the individual level.

The variables in MBDETES equations represent the density of mosquitoes that are in each behavioral state, and the parameters describe state transition probabilities and associated waiting times. Let a variable name denote the population density of mosquitoes in each state, where the variable names in MBDETES matches the code letter for the behavioral states and the postprandial resting period in MBITES: blood feeding (B), egg laying (O), searching for blood (F), searching for habitats (L), and post-prandial resting (R), for each site. Let P_{XY} denote the proportion of mosquitoes transitioning from state X to Y after one bout, $1/\gamma_X$ denote the duration of time to complete one bout in state X, and let $\Lambda_F(t)$ and $\Lambda_B(t)$ denote the rates of mosquitoes emerging end entering into F and B states, respectively:

$$\begin{aligned}
\frac{dF}{dt} &= \Lambda_F(t) + \gamma_B P_{BF} B + \gamma_O P_{OF} O + \gamma_R P_{RF} R - \gamma_F(1 - P_{FF})F \\
\frac{dB}{dt} &= \Lambda_B(t) + \gamma_F P_{FB} F + \gamma_R P_{RB} R + \gamma_O P_{OB} O - \gamma_B(1 - P_{BB})B \\
\frac{dR}{dt} &= \gamma_B P_{BR} B - \gamma_R R \\
\frac{dL}{dt} &= \gamma_R P_{RL} R + \gamma_O P_{OL} O - \gamma_L(1 - P_{LL})L \\
\frac{dO}{dt} &= \gamma_R P_{RO} R + \gamma_L P_{LO} L - \gamma_O(1 - P_{OO})O
\end{aligned} \tag{2.1}$$

Note that there are some more general cases of MBITES (*i.e.*, with mating and sugar feeding) in which behavioral state transitions can be formulated as a continuous-time Markov process and could thus be described by similar systems of equations. MBITES models that build up state memory over time in a mosquito, breaking the memoryless assumption of Markovian systems (by depending on age, oogenesis, egg-batch size, or other variables which depend on previous states), could possibly be modeled, but they would require more complex systems of equations. In particular, the model of oogenesis in which re-feeding depends on previous blood meals would require modifying the state space to track egg batch size, or use integro-differential equations. We note also that it is possible to develop MBDETES models that are "spatial." While such models can be built, they are beyond the scope of this paper.

2.3 Results

Behavioral state models, such as MBDETES and models developed in MBITES, are based on a detailed description of mosquito behaviors, behavioral states, and behavioral state transitions. These models do not supply the standard bionomic parameters. Instead, they show how mosquito bionomic parameters most relevant for pathogen transmission arise from the simple algorithms that drive the mosquito behavior. In addition, MBITES has additional built-in flexibility to show how these parameters are affected by geography (distribution of resources), ecology (interactions of mosquitoes with other biotic and abiotic elements of their environment), climate, and other factors external to the individual mosquito. The small set of summary statistics that has been traditionally used to describe aspects of mosquitoes relevant for transmission (Table 1) are thus emergent features of a complex interaction of mosquito behavior in an environment. In MBITES, these parameters arise naturally from mosquito behavior for a given place, shedding light into what aspects of ecology affect these population level summary metrics the most.

Here, using some models that were developed within the MBITES framework, we show how to compute these parameters and illustrate some basic features of mosquito ecology relevant for transmission. We also use MBDETES to verify MBITES (and *vice versa*).

Vectorial Capacity and Bionomic Parameters

VC in MBITES models can be computed in two ways. First, VC could be estimated by taking the product of the average bionomic parameters, using standard formulas (Table 2.1). Second, the bionomic parameters are not specified as parameters in MBITES, but they can be computed as a summary description of mosquito behavior through Monte Carlo simulation.

It has been shown that the traditional formula for VC can be reduced to just three terms – the number of emerging adult female mosquitoes, per human, per day (λ); the probability of mosquito survival through the extrinsic incubation period (EIP) of the pathogen (P); and the stability index (S) [138]. The Ross-Macdonald formula for the VC is equivalent to: $V = \lambda S^2 P$. The stability index appears twice because pathogen transmission requires a mosquito to take two distinct human blood meals – one to infect the mosquito and another to infect the pathogen's human host (after surviving the EIP and becoming infectious). Unlike the entomological inoculation rate, the VC does not rely on any information about the parasite reservoir in humans; that is, VC measures only the entomological capacity of a particular setting to sustain pathogen transmission, and is independent of prevalence of human infection [138].

Expectations in MBITES and MBDETES

One method to compute the bionomic parameters is by computing the expected transition probabilities from each state to all other states accessible from it. This discrete distribution can be calculated by following the sequence of Bernoulli events in Figures 2.2 and 2.3, for example, taking expectation values at each step. By averaging in this way, the $P_{X,Y}$ quantities for MBDETES can be computed from MBITES. The exact multinomial probability distribution over outcomes ($P_{X,Y}$) for each bout can also be calculated numerically without simulation, by summing the relative probability of each path through the bout; certain branch points are based on random sampling, such as blood meal size, in these cases, we calculate the expectation with respect to the random variable by numerical integration (these functions can be found in the file `https://github.com/dd-harp/MBITES/blob/v1.0/MBITES/R/MBDETES-Calibration.R` in the MBITES package).

Using these methods, we can then compute quantities in MBITES or MBDETES linking estimates back to the bionomics commonly used as input (or derived as equilibrium) in Ross-Macdonald style models. From the single-bout transition probabilities and waiting times for each bout type, P_{XY} and T_X, we derived formulas for the proportion surviving and the waiting time for surviving mosquitoes to make the transition from: F to B, including loops back into F; from B to R including loops back into F and B; from L to O; including loops back into L; and from O to L, including loops back into L and O. The waiting time in each state T_X is determined by parameter, and the inverse is the rate parameter γ_X used for simulation in MBDETES (Table 2.2). These closed-form solutions for the means of these bionomics allow us to compare MBDETES to classical Ross-Macdonald

parameters.

The inverse of this resting period to resting period waiting time maps onto the feeding rate parameter f in the Ross-Macdonald model (see Table 2.1); $T_{R,R} \mapsto 1/f$. The rest to rest survival probability is also needed to link MBDETES to Ross-Macdonald parameters; this maps onto the probability of surviving through one feeding cycle, $P_{R,R} \mapsto e^{-g/f}$, or $\frac{-\ln P_{R,R}}{T_{R,R}} \mapsto g$.

Monte Carlo Simulation in MBITES

In these simulations, there is a more direct way of computing the VC. For each mosquito from emergence to death, MBITES logs each activity bout, including the time, location, behavioral state, the values of other variables, the identity of every human host probed, and the identity of every host who gave a blood meal. Mosquito survival can be computed simply from the distribution of the mosquito age at death. Similarly, the overall feeding frequency can be computed from the distribution of time intervals between successive blood meals.

The formulas for VC arise from an anthropocentric concept that counts events happening to a human on a day. Here, we compute VC directly by following every bite occurring on a single person on a single day, and then summing all secondary bites by the initial biting mosquito separated from the initial bite by at least EIP days. To put it another way, the average VC is the number of pairs of human bites given by one mosquito that are separated by at least EIP days, summed over all mosquitoes and divided by the number of humans, reported per day. The distribution of VC uses the infecting human as the reference (thus VC is in units of $\mathrm{human}^{-1}\ \mathrm{day}^{-1}$).

To compute the VC in this way, MBITES simulation output was summarized as follows: 1) the first bite in the pair must have been a blood meal; only blood feeding can infect a mosquito; and 2) the second bite in the pair included all events in which a human was probed (as parasites or pathogens usually enter the wound in a matrix of salivary proteins during probing); 3) the time interval between the two events was greater than or equal to the EIP; 4) the number of secondary bites is tallied over all mosquitoes by adding them to the human who was bitten on the first encounter; 5) the total was divided by the number of days. Because all events in the simulation occur at a set of sites in space, the spatial dispersion of VC can be calculated by simply attaching the distance between these secondary bites from the primary bite to each pair of bites. This level of realism is possible because probing and blood feeding are accounted for separately and accurately in MBITES.

Notably, because MBITES simulates the blood meal as a process of probing followed by blood feeding, some mosquitoes may be killed or interrupted after probing but prior to blood feeding, so there could be small differences in the computed quantities of VC from the classic Ross-Macdonald formula and computation via MBITES.

Verifying MBITES and MBDETES

To address a challenge facing most complicated individual-based models, we have identified models in MBITES that are the stochastic analogues of models in MBDETES. The following sections illustrate how this was done.

Bionomic Parameters with MBDETES

To compute some of the bionomic quantities in MBDETES, we set $F(0) = 1$ and $\Lambda_F(t) + \Lambda_B(t) = 0$ such that the equations track a cohort as it ages. Using these equations, we track the proportion surviving by age: $F+B+R+L+O$, the laying rate $\gamma_O(P_{OF}+P_{OB})O$, and the blood feeding rate, $\gamma_B P_{BR} B$. In practice, given these initial conditions, this set of equations can be numerically solved to derive bionomic parameters of interest.

Because the length of a feeding cycle is a crucial determinant of transmission potential, we developed another set of equations to compute the probability distribution of the time needed to complete a single feeding cycle. Our equations describe all histories taken by a mosquito just beginning a post-prandial rest (R_1) which could lead to one of two absorbing states: death or the next rest, which implies successful feeding (R_2). By numerically solving these equations, the distribution of feeding cycle lengths, conditional on survival can be computed. Details on the equations and computation are presented in Appendix A.

Mapping MBITES onto MBDETES

A challenge for most complex individual-based models is having a method for verification. Here, for a comparatively simple model developed in MBITES, there is a theoretical match to a system of ordinary differential equations formulated in MBDETES. The two models can be used for mutual verification.

We developed a model in MBITES that maps onto a set of equations in MBDETES under a specific set of conditions. First, we use a "trivial" landscape in which there were three haunts with symmetric movement probabilities: one haunt with only a blood feeding resource, one haunt with only an aquatic habitat, and one haunt with both types of resources (*i.e.*, a peri-domestic haunt). Second, exponential distributions were used to sample all waiting times for behavioral state transitions. Third, re-feeding probability is only a function of blood meal size. We summarized the Monte Carlo simulation in MBITES by computing histograms, which were overlaid on top of density functions computed in MBDETES by numerically solving the system of Kolmogorov forward equations Eq (2.1).

The equations in MBDETES were parameterized following the method presented earlier (section Expectations in MBITES and MBDETES). Additionally, we set $\Lambda_F(t) = \Lambda_B(t) = 0$, and let $dD/dt = -dF/dt - dB/dt - dR/dt - dL/dt - dO/dt$, and initial conditions such that $F + B + R + L + O + D = 1$. Under these conditions the system of equations corresponds to the Kolmogorov forward equations for individual behavioral space trajectories,

averaging over the three haunts. In this interpretation, the state variables F, B, R, L, O, D represent the distribution of probability mass over the set of states a mosquito may belong to at any point in time t. If provided with an initial mass over states at $t = 0$, the numerical solution gives the time evolution of the probability to find a mosquito in any state at any time t.

In Fig 2.4 we show a comparison of MBDETES and MBITES for several bionomic parameters, where MBITES was simulated under a set of simplified conditions such that MBDETES correctly describes the predicted probability density functions of the parameters. Bionomic parameters for MBITES were computed from simulation output and compared to deterministic approximations from MBDETES by overlaying histograms over predicted density functions and comparing means (Fig 2.4). MBDETES was simulated by numerically solving the system of Kolmogorov forward equations Eq (2.1). Under this set of assumptions, the numerical results from MBDETES are matched by the results of the MBITES Monte Carlo simulation.

Dispersion in MBITES

Because the specific trajectory a mosquito takes is a random process that depends on the particular haunt containing the aquatic habitat from which it emerged, the complex interactions between a mosquito's internal behavioral state, the spatial arrangement of haunts and resources, and the movement of human (and non-human) blood hosts, it follows that the movement of mosquitoes on a landscape emerges from interactions among these components and algorithms. Averaging across all location-specific movement kernels gives a sense of how far mosquitoes are likely to travel (Fig 2.5), though the realized distribution for any particular simulation will differ depending on how often each route is used.

Dispersion in MBITES is a probability mass function describing the distances traveled as mosquitoes redistribute themselves among point sets: all distances traveled are drawn from the set of pairwise distances among sites. The dispersal kernels can be visualized directly for each site (*i.e.*, the probability mass on each distance), or from a simulation or overall: we compute the empirical cumulative distribution function (eCDF) of distances traveled; 2) fit a smooth curve to the eCDF; and 3) take the derivative of the smoothed eCDF. These smoothed kernels were estimated through the "lokern" package for R [71], and provide a rough estimate of how far mosquitoes will travel.

Distributions of mosquito movement by distance can also be directly calculated by Monte Carlo simulation through MBITES, allowing examination of characteristic scales of movement in the presence of specific models of human activity. Functionally relevant summaries of mosquito movement come from simulating MBITES and plotting these same kernels for spatial dispersion of VC as computed above (Fig 2.5). A key difference between these dispersal kernels and simulated empirical kernels is that the interactions between mosquitoes and humans will produce empirical kernels that are not necessarily the same as what one would obtain if we had simply used the dispersion kernels to smooth average bionomic parameters over space.

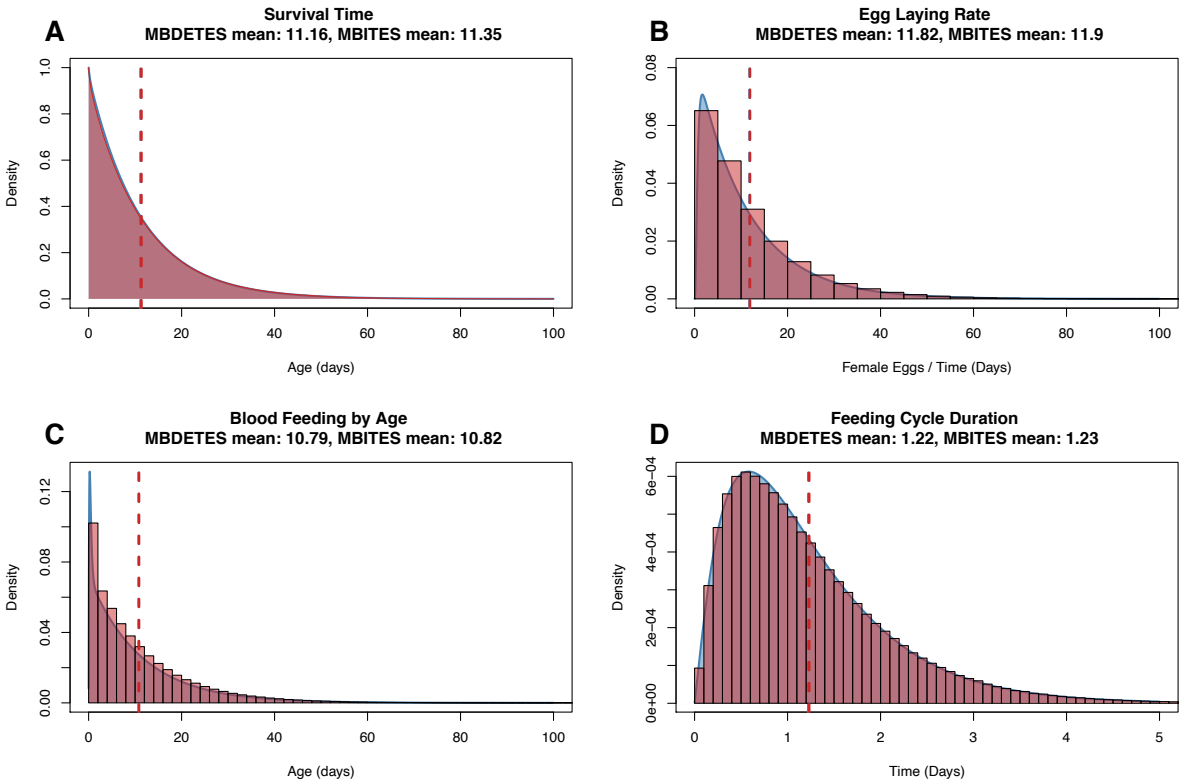

Figure 2.4: **Comparison of results from MBITES and MBDETES under restricted (Markovian) assumptions on waiting times and state transition probabilities.** B: Egg laying rate is the number of eggs laid, per female, per day. C: Blood feeding by age is the age distribution of mosquitoes taking bloodmeals. D: Feeding cycle duration is the time between post-prandial resting periods. In each panel, MBITES is summarized as a red histogram overlaid against the smooth density (in blue) predicted by MBDETES. All cases see excellent agreement, with MBITES fluctuating around MBDETES due to finite sample size of mosquitoes in the stochastic simulation.

Detailed measures of how far mosquitoes disperse through space, transport parasites, or distribute eggs relative to their natal aquatic habitat can be calculated and described by probability density functions. In Fig 2.5, densities for one particular landscape were calculated by taking the empirical cumulative distribution function (CDF) from simulation output, applying a smoothing algorithm to estimate a smooth CDF, and differentiating to estimate a probability density function (PDF) [71]. Four measures of dispersal were computed. First, the upper left density is the average site to site movement kernel, and shows the average "one hop" distance a mosquito will make during a activity bout if it leaves to search. Cumulative dispersion (upper right) is the average distance traveled by a mosquito summing over all hops in its lifetime. Absolute dispersion (lower left) summarizes the mean *displacement* of mosquitoes; that is, the distance between their na-

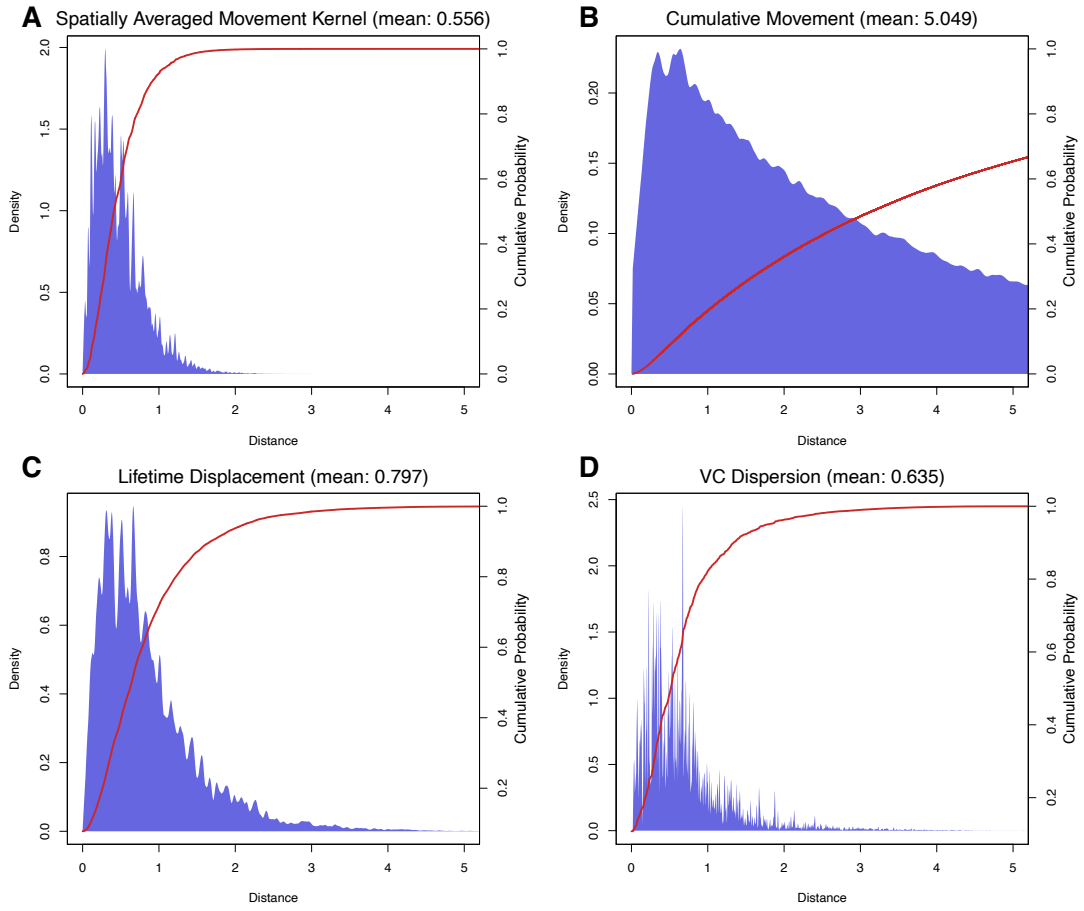

Figure 2.5: **Measures of Mosquito Dispersion.** Smoothed distribution (red line) and density (blue area) functions are displayed for summary statistics calculated for one particular landscape (50% peri-domestic habitats). A: The spatially averaged movement kernel is simply the probability of movement by distance, averaged over all haunts on the landscape. B: Cumulative movement, gives the distribution of total distance traveled by mosquitoes over their entire lifetime, and has a long right tail. C: Lifetime displacement is the absolute *displacement* of a mosquito, that is, the distance between the natal aquatic habitat they emerged from and the site at which their died. D: Dispersion of VC shows the distribution of secondary bites by distance, and follows closely absolute displacement of mosquitoes. All plots are calibrated to the same x-axis for comparison.

tal aquatic habitat they emerge as adults from and the site of death. Most relevant for pathogen transmission is VC, for which the average distance between each pair of secondary bites is a measure of the capability of the local ecology and vector population to sustain pathogen transmission spatially. Dispersion of secondary bites tracks much more closely measures of absolute dispersion rather than cumulative distance traveled, which will be explored in greater detail below.

Co-Distribution of Resources

Searching behavior, in which mosquitoes take long range flights or many short hopping flights to look for resources, plays a crucial role in mosquito behavior but also contributes an important source of mortality that could be avoided if local resources are plentiful. The distribution of local resources structures mosquito movement, therefore, holding all else constant, the amount of time a mosquito spends searching for resources should affect the various summary bionomics that describe the mosquito population and its ability to be effective vectors of pathogens. To illustrate the effect of distribution of resources on the bionomic parameters, we conducted a set of experiments showing the influence of resource co-distribution on summary bionomics.

The set of *in-silico* experiments was designed to explore how bionomics changed as a function of the availability of peri-domestic habitats, which describes the proportion of blood feeding at haunts that have a viable aquatic habitat in the local vicinity; in terms of simulation, a peri-domestic haunt has both types of resources present. The proportion of haunts with viable aquatic habitats nearby may differ depending on local distribution of resources. The extent to which the haunts get visited depends the extent to which there is significant correlation between the set of points at which mosquitoes can locate suitable blood meal hosts and the set of points at which mosquitoes can oviposit egg batches.

Peri-domestic Simulation

To examine the effect of peri-domestic habitats on generated mosquito bionomics, 26 resource landscapes were generated, each containing 250 blood feeding haunts, and 250 aquatic habitats. peri-domestic habitats (the percent of haunts that contained both resources), ranged from 0% in landscape 1, to 100% in landscape 26 (Fig 2.6). Put another way, in landscape 1, each site contained *either* a blood feeding haunt *or* an aquatic habitat, whereas in landscape 26, each site contained *both* types of resources. In all landscapes the total number of resources was held constant as described above. Spatial variance in location of haunts was simulated by choosing 25 parent points for blood feeding haunts, and then scattering 9 offspring blood feeding haunts around each parent, for a total of 250 haunts in 25 clusters. In the simulation where peri-domestic habitats was held at 0%, aquatic habitats were simulated independently using the same algorithm. For all other landscapes, overlap was simulated by selecting some fraction of the total number of aquatic habitats and attaching them randomly to blood feeding haunts.

In each simulation, all biological parameters were held constant such that the only varying parameter was the spatial arrangement of resources. In addition, mosquito emergence rates from each aquatic habitat was also held constant, such that on average, each habitat produced one adult female per day. We acknowledge that in the absence of population dynamic feedback effects the model may not correspond to any true ecological system. For the specific analysis considered here, we are specifically interested in how spatial arrangement of resources affects how mosquitoes distribute their time across be-

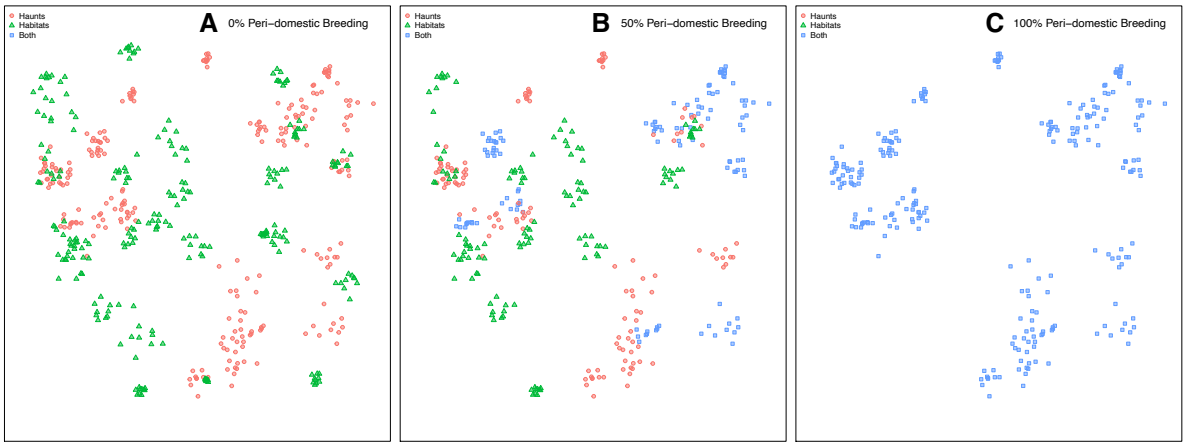

Figure 2.6: **Simulated Landscapes.** 3 simulated landscapes at A: 0%, B: 50%, and C: 100% peri-domestic habitats. Haunts that contain only blood feeding haunts are plotted as red circles, haunts that contain only aquatic habitats are plotted as green triangles, and those haunts that contain both types of resources are shown as blue squares (*i.e.*, peri-domestic habitats). Dispersal kernels were calibrated as if this was an area of about 100 km^2.

havioral states, and the effect it has on commonly used bionomic parameters. We intend to revisit the question of population dynamic feedback effects in future research.

Sensitivity of parameters to peri-domestic habitats

To study sensitivity of bionomics to peri-domestic habitats, we calculated all bionomic parameters for each of the 26 simulated landscapes. Of particular interest was the change in VC as a function of peri-domestic habitats. As the percentage of blood feeding haunts with associated peri-domestic mosquito aquatic habitats increased, mean VC (measured in units $\text{person}^{-1}\text{day}^{-1}$) increased by 2 orders of magnitude (Fig 2.7). While the stability index also increased as a function of peri-domestic habitats, the absolute difference between S evaluated at 0% and 100% peri-domestic was smaller, only increasing by one order of magnitude (Fig 2.7). Importantly, we currently assume no competition among mosquitoes during oviposition, but we note that nonlinear competition has been observed and can easily be included in the model, at the cost of complicating analytic analysis [115].

Significant differences were also observed in how mosquitoes transitioned between and partitioned their time over the set of behavioral states. To quantify, we computed empirical state transition matrices for each landscape, consisting of the behavioral states F, B, R, L, O, plus an absorbing state D for death. For each mosquito, all jumps between states were tabulated in the transitions matrix $\mathbf{T}$, which was then normalized such that $\mathbf{T}e' = 1$. These empirically estimated Markov transition matrices are displayed as chord diagrams in Fig 2.8 for 0%, 50%, and 100% peri-domestic habitats. Transitions between

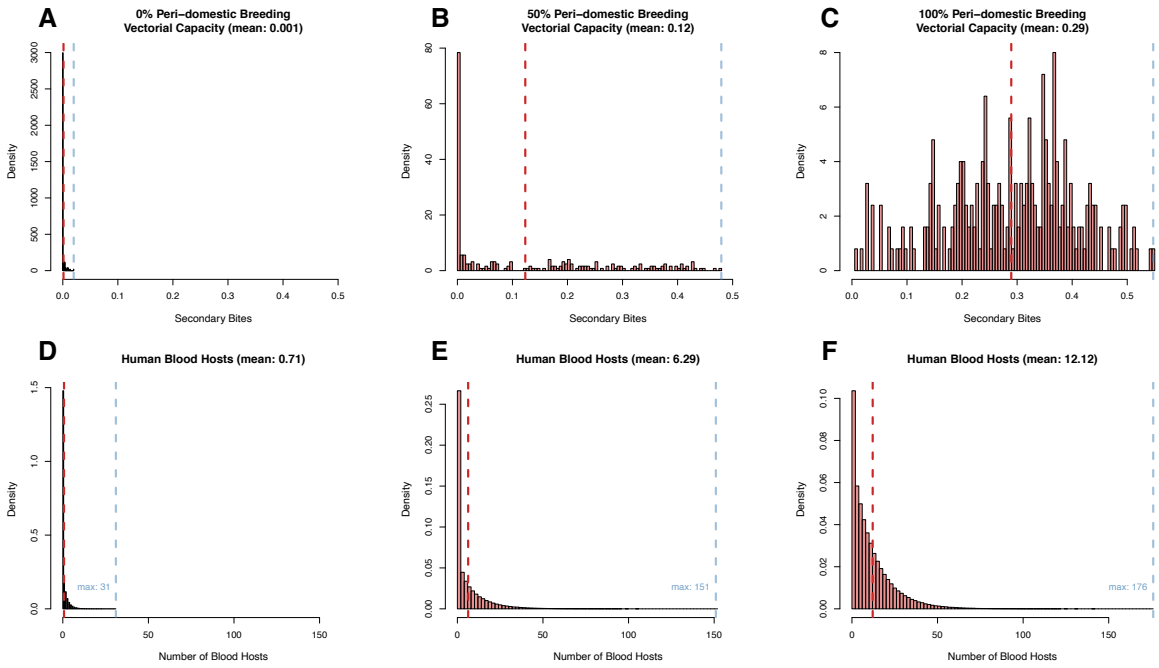

Figure 2.7: **Vectorial Capacity.** In MBITES, vectorial capacity (VC) is computed directly as the average number of infectious bites (*i.e.*, probing) arising from all the mosquitoes blood feeding on a single human on a single day; it is effectively the number of pairs of events where a blood meal by a mosquito is followed at least EIP days later by that same mosquito probing in attempt to feed on a human, measured per human, per day. Summary VC A,B,C: and number of human blood meals per mosquito over its lifespan (D,E,F; referred to as the *stability index* by Macdonald) are shown by column for 0%, 50%, and 100% peri-domestic habitats. Each histogram gives the distribution of VC or the number of human blood hosts across mosquitoes for that percent peri-domestic habitats.

states are represented by colored edges, where width of the edges is proportional to the probability of that transition. Colored areas on the circumference of the diagram represent the states, where size is proportional to that element of the quasi-stationary distribution for that landscape (the mean proportion of time spent in that state, conditional on survival). From 0% to 100% peri-domestic habitats the probability of a blood feeding search leading to another search dropped from 0.90 to 0.17 in the most resource-rich set-

ting, which we consider as easy access to local resources. To determine how mosquitoes partitioned their time across these states, for each normalized matrix $\mathbf{T}$, we calculated the quasi-stationary distribution across the transient states F, B, R, L, O [36]. This distribution describes how a mosquito spends its time, conditional on survival. At 0% peri-domestic, mosquitoes spend near 77% of their time prior to absorption searching for blood meals, and close to 12% of their time searching for suitable aquatic habitats to oviposit (Fig 2.8D). At 100% peri-domestic, these proportions drop to a mere 11% and 6%, respectively (Fig 2.8F).

For each of the 26 resources landscapes, we also calculated mosquito lifespan, stability index, duration of feeding cycle, blood feeding rate, absolute and cumulative mosquito dispersion, VC, and spatial dispersion of VC (Figures 2.9, 2.10). As the resources were rearranged to increase peri-domestic habitats, lifespan, number of blood hosts, and blood feeding rate increased, while duration of the feeding cycle decreased. Certain bionomics, such as blood feeding rate, and length of feeding cycle tended to reach a plateau after peri-domestic habitats increased beyond about 20%, as the mosquito life cycle does not allow these values to change indefinitely. Cumulative mosquito movement (the cumulative distance traveled in all activity bouts) decreases as peri-domestic habitats increases; as the environment becomes more resource rich, mosquitoes do not need to travel as far to fulfill their biological intent (their current behavioral state). In contrast, absolute dispersion (the *displacement* of a mosquito between the natal habitat they emerged from and where they died) stays relatively constant as a function of peri-domestic habitats. This apparent discrepancy between the simulation results and intuition can be understood by noting that while the percent of haunts that were considered peri-domestic changed between the 26 landscapes, the spatial arrangement of haunts did not (distances and clusters were preserved). Holding these spatial characteristics constant implies that observed differences are due solely to changes in search patterns of mosquitoes as resources become more or less locally dense.

As noted in Fig 2.7, VC increased dramatically as peri-domestic habitats increased. It is notable that at very low levels of peri-domestic habitats, the mean is strongly affected by a few outliers generating large numbers of secondary bites; the effect of these outliers is dampened as peri-domestic habitats increases and more humans contribute to secondary biting (Fig 2.10). Spatial dispersion of secondary bites remains relatively constant across landscapes; and follows closely the absolute dispersion of mosquitoes. This is primarily due to two effects. First, because VC was calculated assuming a pathogen with an EIP of 10 days, only mosquitoes that survived at least that long would be able to contribute secondary bites, so the site that secondary bites would be successfully delivered to would be close to the site of the eventual death of the mosquito. Additionally, because the spatial characteristics of the landscape were not affected to a large extent by the rearrangement of resource overlap, although the absolute value of VC changed dramatically, its spatial dispersion did not.

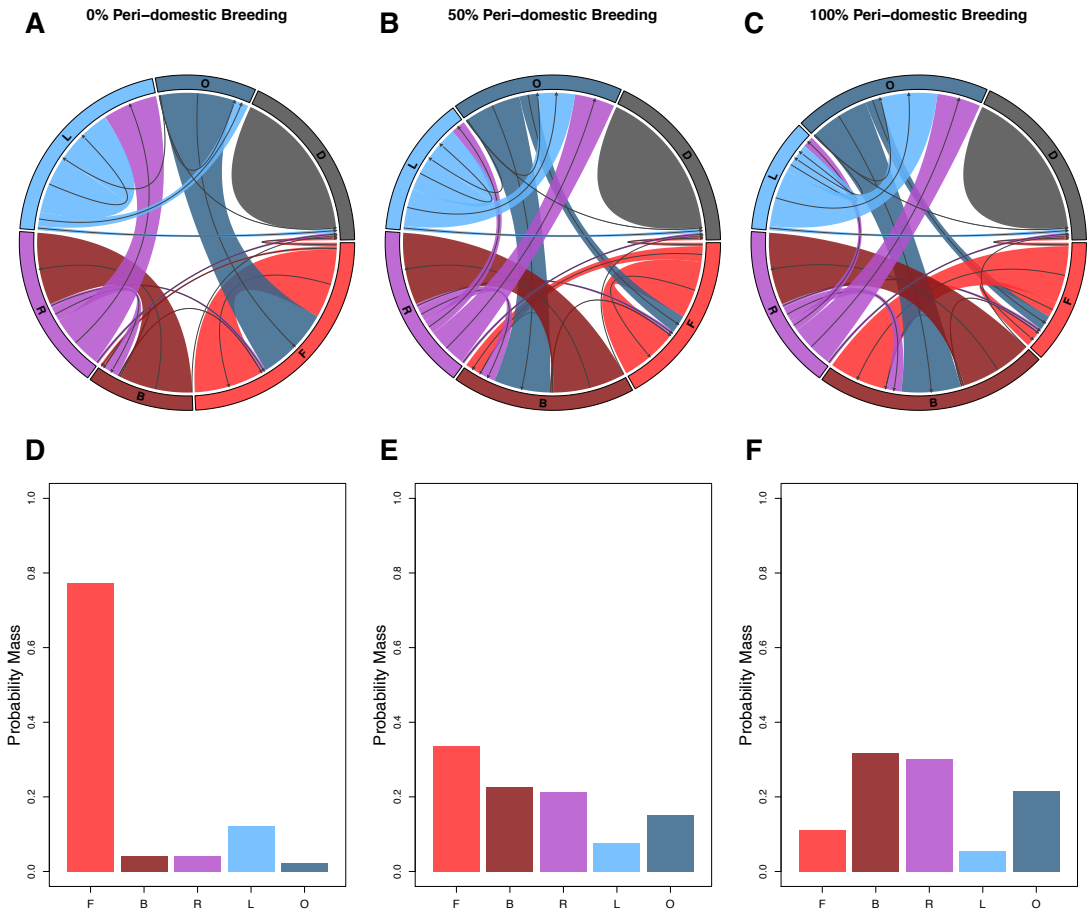

Figure 2.8: **Behavioral State Distribution.** Chord diagrams showing the empirical state transition matrices for three of the 26 experiments: A: 0%, B: 50%, and C: 100% peri-domestic habitats. These were calculated for each experiment by summing transitions for each mosquito between two states and then averaging to produce a Markov transition matrix. The width of the directed edges between each behavioral state is proportional to the probability of that transition, and the area on the perimeter of the circle labeled for each state is proportional to the mean time spent in that state. The three chord diagrams are accompanied below (D-F) by quasi-stationary probability distributions which give the asymptotic distribution of how a mosquito spends time across behavioral states conditional on survival.

2.4 Discussion

The sensitivity of standard bionomic parameters, including lifespan, stability index, and vectorial capacity, to the proportion of habitats that are peri-domestic has implications for disease transmission potential as well as response to control. By rearranging the spatial arrangement of the same resources, we showed that increasing proportion of peri-

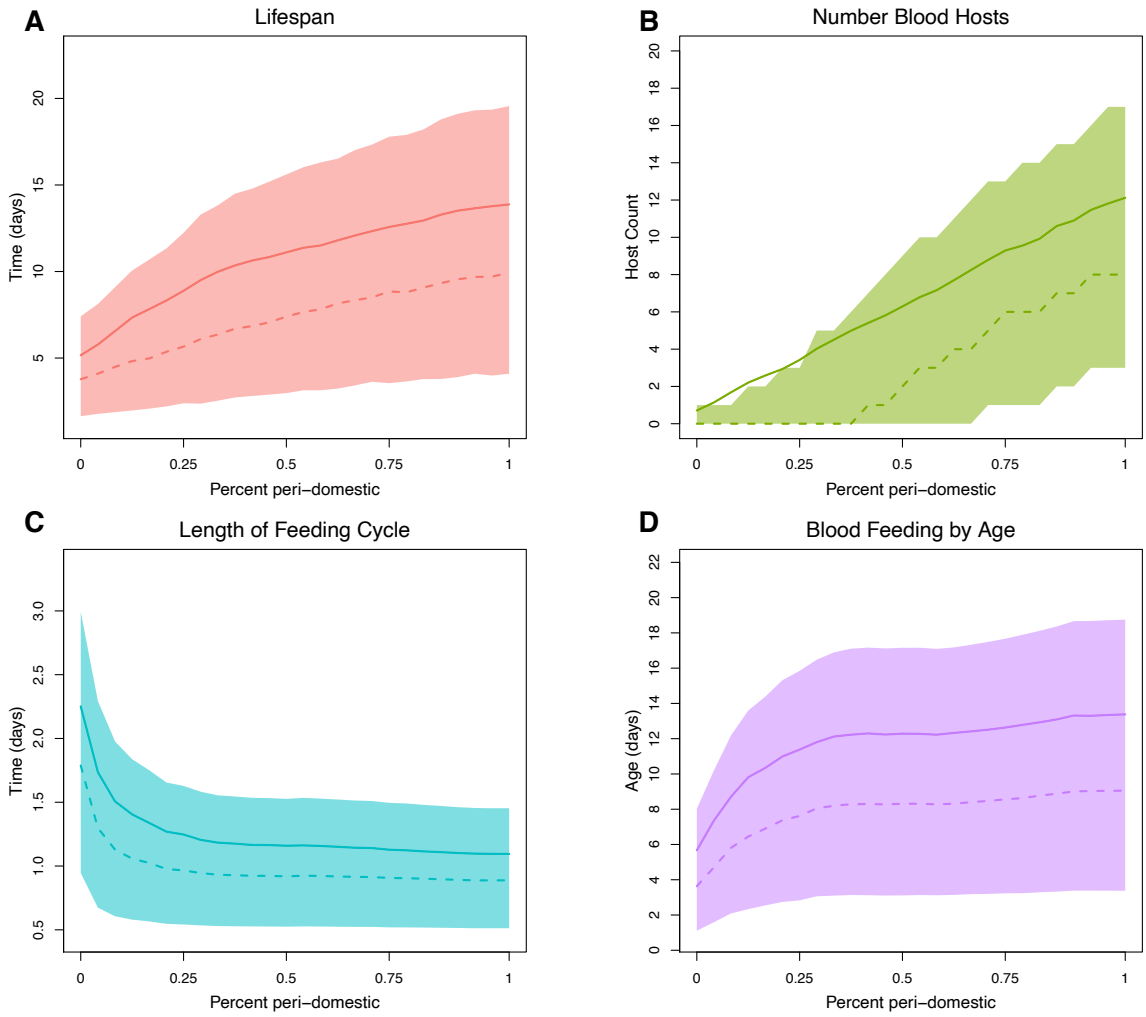

Figure 2.9: **Binomic Parameters.** Simulations in MBITES illustrate that all of the bionomic parameters are sensitive to the proportion of peri-domestic habitats, which gives a measure of how frequently a mosquito must search. The x-axis of each plot ranges from 0% to 100%, and each summary bionomic parameter is plotted as mean (solid line), median (dashed line), and the shaded area covers the 20-80% quantile range of the data. The distribution of number of blood hosts B: exhibits significant right skew, such that the mean exceeds the 80% quantile at low proportion peri-domestic breeding habitats. Because the simulations are stochastic, the exact number of mosquitoes from which Monte Carlo estimates of the bionomic parameters were computed varied somewhat over the 26 landscapes, the mean was 456,579 mosquitoes with a standard deviation of 754 mosquitoes.

domestic habitats causes proportionate increase in VC and affects the dispersion of these potential secondary bites. Each parameter that strongly affects VC is sensitive to the pro-

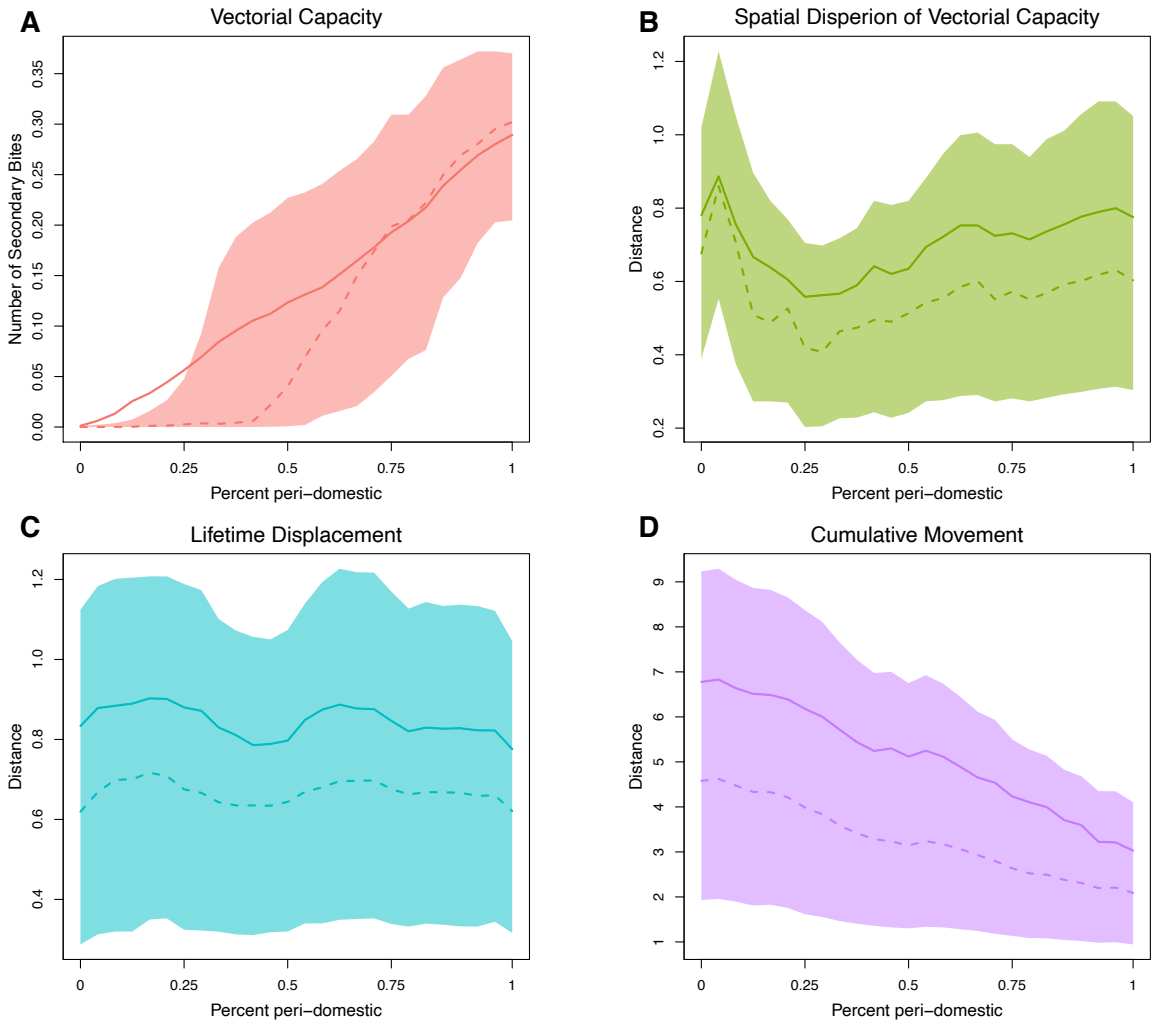

Figure 2.10: **Dispersion and Movement Parameters.** In MBITES, vectorial capacity (VC) and its dispersion are highly sensitive to the proportion of peri-domestic habitats. Interpretation of axes follows Fig 2.9, and each summary bionomic parameter is plotted as mean (solid line), median (dashed line), and the shaded area covers the 20-80% quantile range of the data. A: Number of secondary bites produced increases dramatically as a function of peri-domestic habitats. B: Spatial dispersion shows no strong trend however, due to the strong clustering of haunts in the landscape (it largely follows the trend of absolute lifetime displacement (C), as opposed to cumulative movement (D). At low percent peri-domestic breeding habitats, significant right skew in the distribution of VC pulls the mean above the 80% quantile.

portion of peri-domestic breeding sites (Figure 9, lifespan, mean age of blood-feeding mosquitoes, and length of gonotrophic cycle). This was alluded to in an earlier mathematical model [112] but this is the first demonstration of sensitivity to peri-domestic breeding

in a stochastic agent-based model. The strong dependence of bionomics upon the proximity of breeding sites to blood feeding haunts has encouraging implications for larval source management based vector control. In the case where enough such habitats are findable, sustained larval source management could potentially reduce the proportion of peri-domestic habitats and consequently reduce VC. Adult vector control methods could also be preferentially deployed based on the proportion of peri-domestic breeding sites. The distribution of a mosquito's lifespan across various behavioral states changes substantially as a function of this proportion (Figure 8). One implication is that, if mosquitoes were sugar feeding more frequently than usual in a resource sparse environment where behavior is dominated by long searching flights (as in 0% peri-domestic breeding example), attractive toxic sugar baits (ATSB) could potentially have a large impact. Alternatively in settings where more time is spent in and around human dwellings, traditional tools such as long-lasting insecticide treated nets (LLINs) and indoor residual spraying (IRS) may remain the best choice for vector control.

MBITES was developed as a framework for building models of sufficient complexity to examine whether the current widely used small set of entomological parameters is adequate to the task of identifying critical features of transmission and informing control. Despite the model's enormous complexity, what became obvious was that much of what was occuring during a single activity bout can be summarized by simple outcomes and their accompanying behavioral state transitions: death, failure or success to feed or oviposit, and the decision to stay or search. MBDETES is our method to grapple with the complexity of MBITES mathematically. While MBITES is a stochastic agent-based model with upwards of 40 parameters, MBDETES has 18 parameters and is expressed as a set of differential equations. One result from this rigorous mapping of detailed behavioral algorithms onto aggregate probabilities in MBDETES, was that much of the individual-level stochasticity in a bout was only important insofar as it affected aggregate transitions, though it is possible more complex models would show greater effect. Landscape details and mosquito responses to these details, on the other hand, proved to be enormously consequential for simulated outcomes. If one seeks to further reduce complexity, the result is the Ross-Macdonald model with five bionomic parameters, and the derived quantity of vectorial capacity summarizes transmission potential in a single expression.

A relevant lesson emerging from our analysis is how difficult it would have been to try and piece together estimates of mosquito bionomic parameters by measuring just directly observable aspects of mosquito behavior. The large number of parameters describing the outcome of a bout suggests the relevance of any particular direct observation of mosquitoes is only meaningful when it is measured along with all other parameters, and the importance of any particular behavior for transmission would thus probably differ by context. Our simulations have shown that it is important to challenge conventions and refine models. Estimated vectorial capacity is likely relevent for transmission only if measures of dispersion of infectious bites are taken into account [103, 140].

Despite the compelling logic and parsimony of the Ross-Macdonald model, do models of this type really capture all of the essential features of a time and place? Even if

parsimony were the only measure of quality, there must be some way to determine the appropriate level of model complexity, which implies the necessity of building at least some non-parsimonious models for comparison. The functionality that is potentiated by MBITES and MBDETES comes with a cost; their parametric complexity makes these models suboptimal for tasks that demand parsimony. As with any complex, mimetic simulation model, issues of over-parameterization and limits of available field data to provide suitable parameter values arises. One way to parameterize such models is by assuming some specific behavior has evolved optimally to some ecological context, and then back-solving for parameters which would lead to such behavior [104]. Another is *calibration*, where the model is fit to data by either statistical or more *ad hoc* approaches. However, another purpose of complex models is *sensitivity analysis* (SA). For a highly detailed model that reflects, as best as possible, existing entomological and ecological knowledge, SA methods may be employed in a variety of ways to identify non-obvious ways that mosquito populations could vary, and to help guide future empirical data collection which could best reduce uncertainty in some aspect of model output. Such knowledge can be quite relevant for planning intervention and control in natural systems, in addition to more basic scientific interests [75, 144]. SA is most powerful when used to evaluate how parameters, alone or in concert, produce qualitatively different model responses. Given a response of interest, Monte Carlo methods can help detect parameter interaction and the differing scales at which parameters wax or wane in importance, which can reveal unusual model behavior, identify possible control strategies, and improve interpretation of how models respond to perturbation [65, 143]. While extensive Monte Carlo simulations to perform SA may seem daunting, there is much active work in the field, including statistical emulation, efficient computer-based experimental design, and advanced history matching techniques [153, 124, 10].

Using individual-based models developed in MBITES, we have shown how bionomic parameters, vectorial capacity, and dispersion of mosquitoes and their bites arise from a set of mosquito behavioral algorithms in response to the distribution of resources and their spatial arrangement. Standard models lack the ability to comprehensively explore these questions, and while existing models offer compelling evidence of spatial effects [63], MBITES offers a higher level of individual and spatial resolution. In these models, search and dispersion are strongly affected by the co-distribution of resources [133], and the contextual factors affecting the frequency of search strongly affect vectorial capacity. The importance of ecological context was expressed eighty years ago by Hackett [67]:

> *Everything about malaria is so moulded by local conditions that it becomes a thousand epidemiological puzzles. Like chess, it is played with a few pieces but it is capable of an infinite variety of situations.*

This has been quoted frequently by malariologists, but it has been difficult to reconcile Hackett's view picture with the elegant concepts of VC and entomological inoculation rates, which concisely summarize the factors that are most likely to affect transmission.

VC has a virtual hegemony in mechanistic models (where EIR is a derived concept), due partly to its simplicity and sound logic [125]. If the challenges of malaria transmission dynamics and control are best understood as a collection of puzzles to be solved and not effectively summarized by VC or EIR, then what other aspects of vector biology matter? The view of malaria as a chess game has, perhaps, been most apparent in the variable responses of vector control, where small behavioral differences among species have affected the rates of contact with interventions and thus the outcome of control. Our results suggest that fine-grained heterogeneity in movement driven by the co-distribution of resources shape mosquito dispersion, and that among-individual differences in VC and its associated dispersion will also have strong affects on transmission.

In retrospect, it is remarkable that investigation of pathogen transmission by mosquitoes has been so stable since it was jump-started by an intuitive leap by Ronald Ross [128]. Entomological work that followed over the next decades iteratively refined Ross's ideas culminating in a fully fledged theory of transmission [105, 141], including field methods to measure a handful of relevant parameters. After more than a century of studying mosquito behavior, medical entomologists have assigned approximate bionomic parameter values to most of the parameters for most of the dominant vector species that transmit human infectious diseases. These have been assembled from hundreds of studies conducted in various ways over several decades. Biology and genetics constrain the behaviors giving rise to some of the differences in the average value of parameters assigned to some species. Our simulations show these bionomic parameters must also be partly determined by local resources and ecology. Consistent with Ronald Ross's original conception of *a priori* models as methods to assimilate disprate data, models like MBITES can help synthesize conclusions about transmission and control from novel sources of data, including entomological, genetic, ecological, and spatial. Despite this, existing studies do not adequately characterize a vector species across multiple settings. Studies are generally too heterogeneous in their design and implementation to be comparable across settings [64]. Few studies have identified systematic differences in mosquito bionomics looking across ecological contexts, perhaps because there has been no theory to suggest what they should look for. Neither evidence nor theory alone could provide a sufficient basis for making an educated guess about how the values of bionomic parameters vary in a different ecological setting or the effect modification of setting on vector control. These highly mimetic models of mosquito behavior can be used to set priorities in the study of pathogen transmission by mosquitoes, help shed light on the effect sizes of vector control, and explain heterogeneity in the outcome of control studies. In providing a framework for re-examining mosquito behavior and perhaps forging a new synthesis of ecology and behavior, these behavioral state models provide an *in silico* laboratory to fill some of the gaps required to understand and synthesize much of the data on mosquitoes that is not directly related to estimation of the basic bionomic parameters.

The mathematical and computational framework for simulation and analysis that is presented here can be used to investigate a broad range of questions about the interface between mosquito biology and life-history traits, the local ecology, and vector control.

This framework was designed to evaluate heterogeneity and complexity through simulation, rather than through *ad hoc* approximation. While this approach has some disadvantages over parametrically simple models, it fills an important need by providing a way of testing whether those simple models cover all the relevant phenomena. MBITES makes it possible to systematically investigate whether the behavior of individual-based models ever deviates from the behavior of parametrically simpler models of transmission, such as the Ross-Macdonald model or MBDETES. The high degree of realism can also provide other functionality, such as power calculations for randomized control trials, investigation of bias and accuracy of field methods, *in silico* investigation of the interactions among vector-based interventions, and calibration of effect sizes versus coverage for vector-based interventions.

Chapter 3

MGDrivE 2: A simulation framework for gene drive systems incorporating seasonality and epidemiological dynamics

3.1 Introduction[1]

Interest in gene drive technology has continued to grow in recent years as a range of promising new constructs have been developed in the lab and discussions have moved towards implementing field trials in some cases. Recently developed systems include a CRISPR-based homing system intended for population suppression targeting the doublesex gene in Anopheles gambiae, the main African malaria vector [97], a split gene drive system intended for confineable and transient population replacement in Aedes aegypti, the main vector of dengue, chikungunya and Zika viruses [102], and CRISPR-based homing systems intended for population replacement in *An. gambiae* [28] and Anopheles stephensi, the main malaria vector in urban India [3].

As the technology advances and potential field trials are discussed [80], models are needed that incorporate additional ecological detail, including parameters that change over time in response to environmental variables such as temperature and rainfall, as well as models linking entomological and epidemiological outcomes [81]. Many insects, including mosquitoes, display a high degree of seasonality in their population dynamics, as development time from one life stage to another, and mortality rates associated with each life stage, vary with temperature and other environmental variables [114]. For *An. gambiae* and several other mosquito disease vectors, population size varies largely in response to recent rainfall, which creates pools of standing water and hence enhanced carrying capacity of the environment for mosquito larvae [151]. Seasonal changes in tem-

[1]This chapter has been previously published [155]

perature and rainfall thus lead to seasonal changes in mosquito population density and consequent disease transmission, which must be accounted for in disease control strategies.

Models of disease transmission are also becoming increasingly relevant to models of gene drive dynamics, as: i) the readiness of a gene drive system for field trials will be determined in part by its expected (*i.e.*, modeled) epidemiological impact, and ii) initial field trials are expected to have a measured entomological outcome alongside a modeled epidemiological outcome [80]. Given the potential for a non-localized gene drive system to spread broadly, it has been acknowledged that constructs at the trial stage should be expected to cause a significant reduction in disease transmission, as even a confined trial could lead to wide-scale spread for an effective system [80]. Therefore, readiness for field trials should be determined by alignment with a target product profile (TPP) and/or list of preferred product characteristics (PPCs) that include expected impact on disease transmission [81]. Models that incorporate both gene drive and epidemiological dynamics can account for local malaria or arboviral transmission dynamics and specify gene drive construct parameters that achieve the desired level of epidemiological control.

Previously, we developed the MGDrivE 1 modeling framework to model the population dynamics of a variety of genetics-based and biological control systems and their spread through spatially-explicit populations of mosquitoes, or insects having a similar life history [130]. Here, we present MGDrivE 2, which significantly improves upon the capabilities of MGDrivE 1 by addressing the above-mentioned considerations, namely: i) the ability of parameter values to change over time, and hence to model seasonal population dynamics, and ii) the incorporation of an epidemiology module that can accommodate pathogen transmission between humans and mosquitoes. Minor additional improvements have been made to the inheritance, life history and landscape modules of the framework to reflect advances in these fields; for instance, a more resolved understanding of maternal deposition of Cas protein for CRISPR-based gene drive systems has been incorporated [33]. Models in MGDrivE 2 are represented as a stochastic Petri net (SPN), which has both computational and architectural benefits: model specification is separate from simulation, models can be efficiently stored and updated in memory, and a wealth of fast simulation algorithms from other fields can be used [60].

In this paper, we describe the key developments implemented in MGDrivE 2. We then demonstrate the application of the framework to the disease control impact of a CRISPR-based homing gene drive system intended to drive a disease-refractory gene into a population, and conclude with a discussion of future needs and applications for simulation packages in the field of gene drive modeling.

3.2 Design and Implementation

MGDrivE 2 is a significant extension of and development from MGDrivE 1, a model for the spread of gene drive systems through spatially-explicit mosquito populations. The

MGDrivE 2 model incorporates: i) an "inheritance module" that describes the distribution of offspring genotypes for given maternal and paternal genotypes, ii) a "life history module" that describes the development of mosquitoes from egg to larva to pupa to adult, iii) a "landscape module" that describes the distribution and movement of mosquitoes through a metapopulation, and iv) an "epidemiology module" that describes pathogen transmission between mosquitoes and humans (Fig 3.1). The framework is formulated as a SPN that can be mapped to a continuous-time Markov process in which model parameters may vary over time. It can also be implemented as a deterministic model via mean-field approximation of the stochastic model [21].

The core framework is developed in R (`https://www.r-project.org/`). The SPN framework enables separation of model components, allowing users to modify code on a component-by-component basis as needed for model specification or computational speed. We now describe the model extensions and developments from MGDrivE 1 to 2 in more detail. Full details of the MGDrivE 2 model framework are provided in Appendix B.

Time-dependent parameters and seasonality

The incorporation of time-dependent parameters represents a significant improvement of the MGDrivE 2 modeling framework. In MGDrivE 1, the mosquito life history module follows the lumped age-class model of [68] as adapted by [40], which describes development from egg to larva to pupa to adult using delay-difference equations. The delay framework allows development times to be modeled as fixed rather than exponentially-distributed; however, it is not compatible with time-varying parameters as these could vary during the delay. In MGDrivE 2, the discrete-time, fixed-delay framework of MGDrivE 1 is replaced by a continuous-time implementation in which each life stage is divided into a series of substages. For a single substage, the development time is exponentially-distributed; but as the number of substages increases, the distribution of development times becomes concentrated around the mean. Specifically, if a life stage with a mean development time of $1/d$ is divided into a series of n substages, the new development times are Erlang-distributed with mean, $1/d$, and variance, $1/(dn^2)$, or equivalently, with shape parameter, n, and rate parameter, d/n. The mean development time, $d(t)$, may also vary over time, t; however the number of substages, n, and hence the mean-variance relationship for development times, must remain constant within a simulation.

Most importantly, the new model implementation allows any model parameter to vary with time, enabling the framework to account for seasonal variation in development times and mortality rates due to environmental dependencies. Temperature is known to strongly influence development times for juvenile mosquito stages, and mortality rates for all mosquito life stages [17, 114], and rainfall is known to influence the carrying capacity of the environment for larvae, and therefore density-dependent larval mortality rates [151, 116]. The new model formulation allows these parameters to vary in continuous

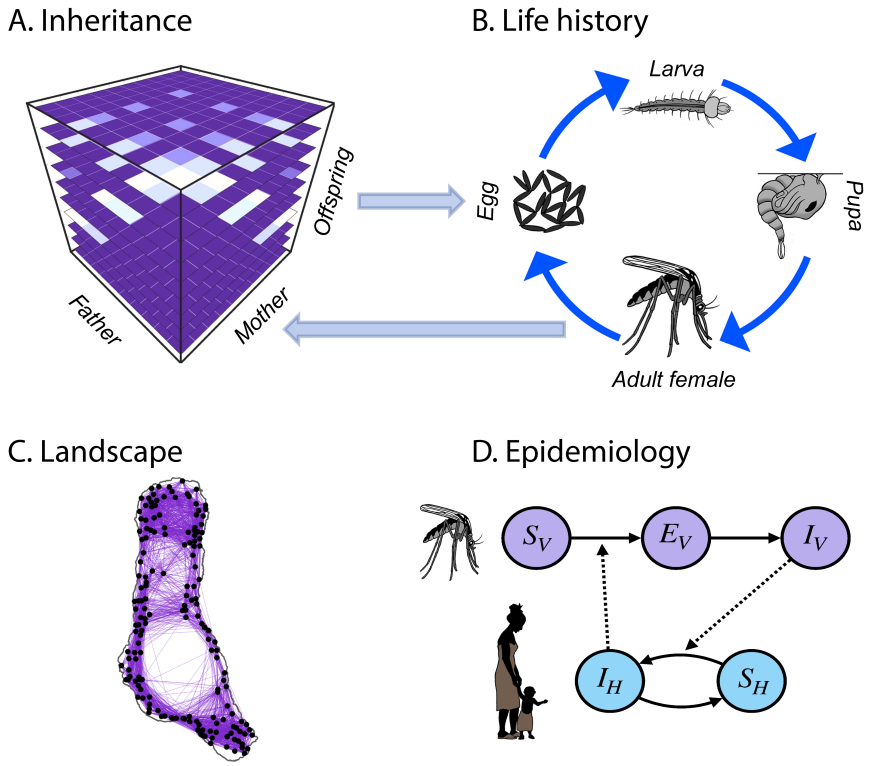

Figure 3.1: **Modules in the MGDrivE 2 framework. (A)** Genetic inheritance is embodied by a three-dimensional tensor referred to as an "inheritance cube". Maternal and paternal genotypes are depicted on the x and y-axes and offspring genotypes on the z-axis. **(B)** Mosquito life history is modeled according to an egg-larva-pupa-adult (female and male) life cycle in which density dependence occurs at the larval stage, and life cycle parameters may vary as a function of environmental variables over time. Genotypes are tracked across all life stages, and females obtain a composite genotype upon mating - their own and that of the male they mate with. Egg genotypes are determined by the inheritance cube. **(C)** The landscape represents a metapopulation in which mosquitoes are distributed across population nodes and move between them according to a dispersal kernel. Population sizes and movement rates may vary as a function of environmental variables. **(D)** The epidemiology module describes reciprocal transmission of a vector-borne pathogen between mosquitoes and humans. This requires modeling human as well as mosquito populations, and the number of individuals having each infectious state. Epidemiological parameters may vary as a function of environmental variables.

time in response to environmental data, and hence for seasonal variations in temperature and rainfall to drive seasonal variations in mosquito population density.

Parameters defining other modules of the model - inheritance, landscape and epidemiology - are also able to vary over time within the new model formulation. For instance, gene drive systems under the control of temperature-dependent promoters [160, 42] may

have time-varying homing efficiencies, mosquito movement rates may vary seasonally in response to temperature and other environmental factors [99], and epidemiological parameters such as the extrinsic incubation period (EIP) and pathogen transmission probabilities from human-to-mosquito and mosquito-to-human are all known to display seasonal variation through temperature dependence [17, 114].

Epidemiology module

The epidemiology module describes reciprocal transmission of a vector-borne pathogen between mosquitoes and humans. This requires modeling of both vector and human populations, as well as an attribute describing the number of individuals in the vector and human populations having each infectious state (Fig 3.2). To model malaria, the Ross-Macdonald model is included, which has susceptible (SV), exposed/latently infected (EV), and infectious (IV) states for mosquitoes, and susceptible (SH), and infected/infectious (IH) states for humans [129, 106]. Malaria infection in humans is described by an SIS model, in which humans become infected at a per-capita rate equal to the "force of infection" in humans, λ_H, and recover at a rate, r. Malaria infection in mosquitoes is described by an SEI model, in which adult mosquitoes emerge from pupae in the susceptible state, become exposed and latently infected at a per-capita rate equal to the force of infection in mosquitoes, λ_V, and progress to infectiousness at a rate equal to γ_V. The force of infection in humans, λ_H, is proportional to the fraction of mosquitoes that are infectious, I_V/N_V, where N_V is the adult mosquito population size, and the force of infection in mosquitoes, λ_V, is proportional to the fraction of humans that are infectious, H_H/N_H, where N_H is the human population size. Since an exponentially-distributed EIP leads to some mosquitoes having unrealistically brief incubation periods, we divide the E_V state into a series of n sub-states, as described in section 2.1, leading to the EIP being Erlang-distributed with shape parameter, n, and rate parameter, γ_V/n [137]. Finally, transmission parameters may be tied to specific mosquito genotypes - for instance, an antimalarial effector gene may be associated with a human-to-mosquito or mosquito-to-human transmission probability of zero.

To model arboviruses such as chikungunya, Zika and single serotypes of dengue virus, we include an SEIR model for human transmission, in which the human states are: susceptible (S_H), exposed/latently infected (E_H), infectious (I_H), and removed/recovered (R_H) [95, 126]. The E_H and R_H states are included because arboviruses are generally thought to be immunizing, and have latent periods that tend to be on a similar timescale to the duration of infectiousness. Humans become exposed/latently infected at a per-capita rate equal to λ_H, progress to infectiousness at rate, γ_H, and recover at rate, r. For mosquito transmission, the SEI model with an Erlang-distributed EIP is used again. Further details of the mathematical formulation of both the malaria and arbovirus models are provided in Appendix B. The extensibility of the SPN framework means that more complex epidemiological models can be developed and implemented by users.

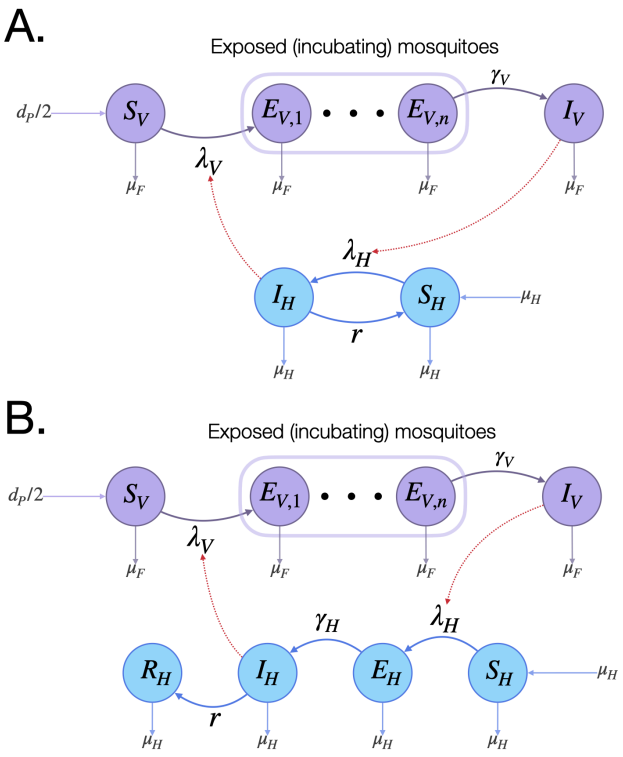

Figure 3.2: **Epidemiology module.** MGDrivE 2 includes two basic models for reciprocal pathogen transmission between mosquitoes and humans - one for malaria **(A)**, and one for arboviruses **(B)**. In both cases, female mosquitoes emerge from pupae at a rate equal to $d_P/2$ as susceptible adults (S_V), become exposed/latently infected ($E_{V,1}$) at a rate equal to the force of infection in mosquitoes, λ_V, and progress to infectiousness (I_V) through the extrinsic incubation period (EIP = $1/\gamma_V$), which is divided into n bins to give an Erlang-distributed dwell time. The mortality rate, μ_F, is the same for female mosquitoes in each of these states. For malaria **(A)**, susceptible humans (S_H) become infected/infectious (I_H) at a rate equal to the force of infection in humans, λ_H, and recover at rate r, becoming susceptible again. For arboviruses **(B)**, susceptible humans (S_H) become exposed/latently infected (EH) at a rate equal to λ_H, progress to infectiousness (I_H) at rate equal to γ_H, and recover (R_H) at rate, r. Infection dynamics couple the mosquito and human systems via the force of infection terms; λ_V is a function of I_H, and λ_H is a function of I_V, shown via red edges.

Modeling vector-borne disease transmission within a metapopulation framework generally requires each population node in the network to have both a defined mosquito and human population size. Since the mosquito vectors we are interested in are anthropophilic, they tend to coexist with humans, so human population sizes and state distributions can be attributed to the same nodes at which mosquito populations are de-

fined; however MGDrivE 2 also includes the possibility of human-only and mosquito-only nodes. Mosquito-only nodes could represent sites with only non-human animals from which mosquitoes bloodfeed, while human-only nodes could represent locations unsuitable for mosquitoes. As mosquitoes are able to move between nodes in the metapopulation, so can humans. This is an important factor to include, as human movement has been shown to drive the spatial transmission of mosquito-borne diseases such as dengue virus [146].

Other extensions to inheritance, life history and landscape modules

Additional functionality has been included in the inheritance and life history modules of the MGDrivE framework since publication of version 1.0. The inheritance module is unchanged, and inheritance "cubes", describing the distribution of offspring genotypes given maternal and paternal genotypes for a given genetic element, are usable in both versions. Several new inheritance cubes have been made available, including: a) homing-based remediation systems, including ERACR (Element for Reversing the Autocatalytic Chain Reaction) and e-CHACR (Eracing Construct Hitchhiking on the Autocatalytic Chain Reaction) [47, 158], and b) newly proposed drive systems capable of regional population replacement, including CleaveR (Cleave and Rescue) [118] and TARE (Toxin-Antidote Recessive Embryo) drive [32].

In the life history module, there are now two density-dependent functional forms to regulate population size - logistic and Lotka-Volterra - with the potential to add more. For mosquito vectors such as *Ae. aegypti* and *An. gambiae*, density-dependence is thought to act at the larval stage due to increased resource competition at higher larval densities [151, 116]. The adult population size, N, is used to determine the carrying capacity of that habitat patch for larvae, K, which determines the degree of additional density-dependent mortality experienced by larvae at that patch. For the logistic model, the per-capita larval mortality rate is given by $\mu_L + (1 + L(t)/K)$, where μ_L is the density-independent larval mortality rate, and $L(t)$ is the total larval population size for the patch at time t. For the Lotka-Volterra model, the per-capita larval mortality rate is given by $\mu_L + \alpha L(t)$, where α is the density-dependent term. Further details on these two density-dependent functions are provided in Appendix B.

In the landscape module, movement through the network of population nodes is again determined by a dispersal kernel; however, due to the continuous-time nature of MGDrivE 2, movement between patches is described by a rate rather than a probability. The mathematical mapping between the rate matrix of MGDrivE 2 and the transition probability matrix of MGDrivE 1 is provided in Appendix B.

Stochastic Petri net formulation

The most fundamental change from MGDrivE 1 to 2 is restructuring the model as a SPN [66]. Adopting a SPN framework has several benefits. First, SPNs allow the mathematical

specification of a model to be decoupled from its algorithmic implementation, allowing users to leverage extensive sampling algorithms from the physical and chemical simulation communities for efficient computation [60, 53]. Second, SPNs have a well-established and consistent formalism, allowing them to be readily understood and modified by anyone familiar with this [62]. And third, SPNs are isomorphic to continuous-time Markov chains (CTMCs), meaning that model parameters can be time-varying, including Erlang-distributed aquatic stage durations and the pathogen EIP.

A Petri net is a bipartite graph consisting of a set of places, P, and a set of transitions, T. Directed edges or "arcs" lead from places to transitions (input arcs) and from transitions to places (output arcs). The set of arcs that connect places to transitions and transitions to places can be denoted by two matrices whose entries are non-negative integers describing the weight of each arc. The places define the allowable state space of the model; however, in order to describe any particular state of the model, the Petri net must be given a marking, M, which is defined by associating each place with a non-negative integer number of tokens. In the language of CTMCs, a marking, M, is referred to as a "state." When a transition occurs, it induces a state change by "consuming" tokens in M given by the set of input arcs, and "producing" tokens in M according to the set of output arcs [152]. Each transition has a "clock process," parameterized by a "hazard function" which defines that event's current rate of occurrence. In MGDrivE 2, tokens represent an integer number of mosquitoes or humans, and the distribution of tokens (mosquitoes or humans) across states at time t defines a marking, $M(t)$. A graphical representation of a Petri net for the mosquito life history module of MGDrivE 2 is depicted in (Fig 3.3A), with a full description of the mathematical formalism provided in Appendix B.

The code that generates the Petri net is independent of the code that simulates trajectories from it. Once the Petri net is stored as a set of sparse matrices, it is passed to a simulation application program interface (API) which allows trajectories to be simulated as ordinary differential equations (ODEs), stochastic differential equations (SDEs), or CTMCs (Fig 3.2B). Each of these are referred to as "step" functions, but are not limited to discrete time steps; these functions are responsible for updating the model between time points where the user requests output to be recorded. The ODE step function provides a deterministic approximation and interfaces with the numerical routines provided in the "deSolve" R package [142]. Three stochastic numerical routines are provided that treat the model as a continuous-time Markov process and provide different levels of approximation. The most straightforward method to sample trajectories is Gillespie's direct method, which samples each event individually [57]. While statistically exact, this is prohibitively slow for medium-to-large population sizes. Two approximate stochastic methods are provided that have been widely used in the chemical physics literature: i) a second order continuous SDE approximation known as the chemical Langevin equation [54], and ii) a fixed-step tau-leaping method [55]. Both methods achieve substantial gains in computational speed at the expense of statistical accuracy. While the SDE approximation is often faster, tau-leaping retains the discrete character of the process it approximates and is usually the preferred technique. A full description of each of the nu-

merical routines is provided in Appendix B. In addition, we demonstrate how a user can write a custom simulation algorithm and incorporate it within the MGDrivE 2 codebase in the "Advanced Topics" vignette available at `https://marshalllab.github.io/MGDrivE/docs_v2/articles/advanced_topics.html`.

3.3 Results

To demonstrate how the MGDrivE 2 framework can be used to initialize and run a simulation of the spread of a gene drive system through a metapopulation with time-varying model parameters, including its implications for vector-borne pathogen transmission, we have provided vignettes with the package, available via installation from CRAN at `https://CRAN.R-project.org/package=MGDrivE2` and additional examples and information on GitHub at `https://marshalllab.github.io/MGDrivE/docs_v2/index.html`. The vignettes provide extensive examples of how to use the software, including advanced features such as implementing custom time-varying rates and numerical simulation algorithms. They consist of a set of five "core" manuals that describe how to simulate population genetics and dynamics for a mosquito-only population and metapopulation, then how to incorporate SEI-SIS Ross-Macdonald malaria transmission dynamics in a population with humans included, and finally how to incorporate SEI-SEIR arbovirus transmission dynamics. Following these are three "advanced" manuals that introduce: i) how to process and analyze output from simulations that write to CSV files, ii) how users can write custom time-varying hazard functions, and iii) how a user might implement their own numerical simulation routine, using an explicit Euler method for ODEs as an example.

Here, we describe the application of the package to model the release of a population replacement gene drive system designed to drive a malaria-refractory gene into an *An. gambiae* mosquito population with seasonal population dynamics and transmission intensity calibrated to a setting resembling the island of Grand Comore, Union of the Comoros. The gene drive system resembles one engineered in *An. stephensi* that is integrated into the kynurenine hydroxylase gene and includes a recoded copy of that gene that rescues its function [3]. This design selects against resistance alleles that interrupt its function. Four alleles are considered: an intact homing allele (denoted by "H"), a wild-type allele (denoted by "W"), a functional, cost-free resistant allele (denoted by "R"), and a non-functional or otherwise costly resistant allele (denoted by "B"). Full details of the inheritance dynamics are provided in [3] and model parameters are summarized in Table 3.1.

The life history module is parameterized with typical bionomic parameter values for *An. gambiae* (Table S1), including mean-variance relationships describing the development times of juvenile life stages [16]. The carrying capacity of the environment for larvae is a function of recent rainfall, and the adult mortality rate is a function of temperature. Remotely sensed rainfall data for Grand Comore was obtained from the ERA5 dataset

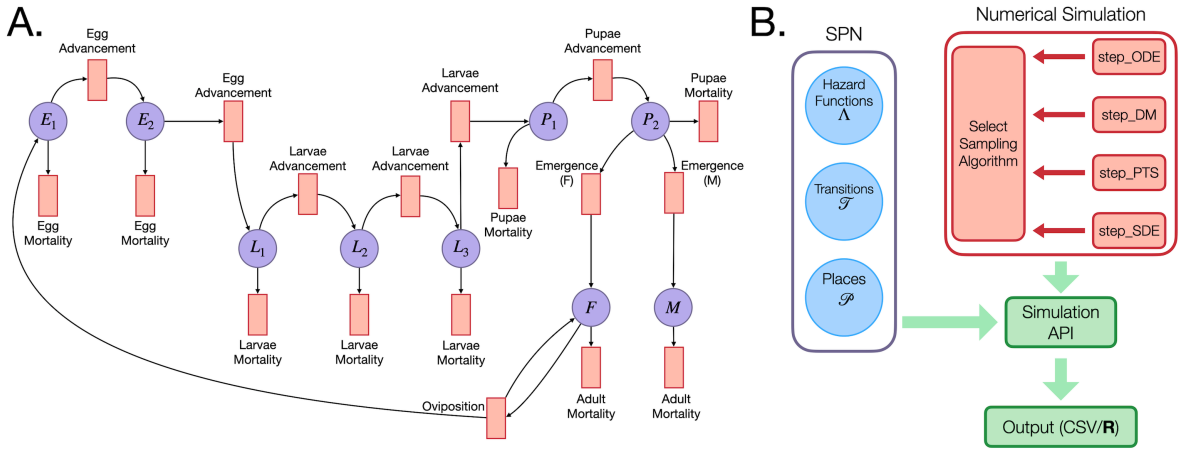

Figure 3.3: **Stochastic Petri net (SPN) implementation of MGDrivE 2. (A)** Petri net representation of the life history module. The set of purple circles corresponds to places, P, and red rectangles to transitions, T. This Petri net shows a model in which development times for the egg stage are Erlang-distributed with shape parameter $n = 2$, and for the larval stage are Erlang-distributed with shape parameter $n = 3$. Population dynamics are derived directly from this graph; *e.g.*, the transition corresponding to oviposition has one edge beginning at F, meaning at least one female mosquito must be present for oviposition to occur. When oviposition occurs, a token is added to E_1 (new eggs are laid) and a token is returned to F. **(B)** Conceptual representation of the SPN software architecture showing the separation between the model representation (blue circles) and set of sampling algorithms (red rectangles). These two components of the codebase meet at the simulation API, enabling users to match models and simulation algorithms interchangeably. Output may be returned as an array in R for exploratory work, or written to CSV files for large simulations.

(`https://www.ecmwf.int/en/forecasts/datasets/reanalysis-datasets/era5`) [1], and a mathematical relationship adapted from [151] was used to translate this to lar-

val carrying capacity, assuming that half of the island's carrying capacity was provided by permanent breeding sites (*e.g.*, large cisterns) and half was provided by recent rainfall. Temperature data for Grand Comore was also obtained from the ERA5 dataset, and adult mortality was derived using methods described by [114]. Both climatological time series covered the ten year period beginning January 1, 2010. For the purpose of this demonstration, Grand Comore was treated as a single randomly mixing population, although simulations involving a more detailed landscape module are included in the vignettes.

The epidemiology module is parameterized with typical parameter values for Plasmodium falciparum transmission (Table 3.1), human population size and life expectancy parameters from the National Institute of Statistics and Demographic Studies, Comoros [79], and is calibrated to local malaria prevalence estimates from the Malaria Atlas Project [121]. This calibration was achieved by multiplying the carrying capacity time series by a constant such that the average adult female mosquito population over a year sustained malaria transmission in the human population at the estimated local prevalence. Finally, we caution that these simulations are merely intended to demonstrate the software's capabilities and that, while the simulations are parameterized with data from Grand Comore, they are not intended to provide an accurate forecast of local gene drive mosquito dynamics, or to imply approval of the intervention by the local population and regulatory agencies.

Simulation workflow

The code for this simulation is available at `https://github.com/MarshallLab/MGDrivE/tree/master/Examples/SoftwarePaper2`. We begin by loading the MGDrivE 2 package in R, as well as the package for the original MGDrivE simulation, which provides the inheritance cubes required for simulation of genetically-stratified mosquito populations. Next, we define model parameters, including the bionomic parameters of *An. gambiae s.l.*, and demographic and epidemiological parameters specific to Grande Comore. To parameterize time-varying adult mosquito mortality (hourly) and larval carrying capacity (daily), we load CSV files containing those data as time series for the ten year simulation period. We then use the base "stepFun()" function in R to create an interpolating function of those time-series data that will return a value for any time within the simulation period, which is required for calculation of hazard functions. More sophisticated interpolating functions, such as splines, may also be used. We also specify the inheritance cube at this point, as the number of modeled genotypes and distribution of offspring genotypes for given parental genotypes will be used to build the Petri net.

Next, we use functions from MGDrivE 2 to create the "places" and "transitions" of the Petri net, which are stored as lists in R and then converted into a sparse matrix representation used in the simulation code. Epidemiological dynamics and states are coded automatically by calling the functions that create the Petri net. In this case, "spn_P_epiSIS_node()" and "spn_T_epiSIS_node()" will generate the places and transitions for a single node model with SEI-SIS mosquito and human malaria transmission dynamics. Each transition has a

tag that specifies the hazard function it requires. Following that, we write custom time-varying hazard functions for adult mosquito mortality and larval mortality (a function of carrying capacity). We provide a guided walkthrough of how a new user might write their own time-varying hazard function in the vignette "Simulation of Time-inhomogeneous Stochastic Processes." Once the vector of hazard functions has been stored (as a list), we create the data frame that stores the times, genotypes, sex, and size of each release event.

With the construction of all model components necessary for the simulation, we call the simulation API which handles the details of simulating trajectories from the model. In this case, we chose the tau-leaping algorithm to sample stochastic trajectories, and to record output on a daily basis. MGDrivE 2 allows users to choose how model output is reported back - for exploratory or smaller simulations, users may return output directly to R as an array; however for larger simulations, it is often preferable to write directly to CSV files due to memory considerations, and MGDrivE 2 has sophisticated functions to both specify CSV output and process completed simulations.

Entomological population dynamics

In (Fig 3.4), we display a potential visualization scheme produced in Python for the simulations described above. The code to produce this visualization is available at `https://github.com/Chipdelmal/MoNeT/tree/master/DataAnalysis/v2` (note that MGDrivE 2 code does not depend on Python). (Fig 3.4A) displays the climatological time-series data - temperature in magenta and rainfall in blue - which were used to calculate time-varying adult mosquito mortality rate and larval carrying capacity, respectively. The total adult female population size averaged over 100 stochastic runs is shown in green. This is relatively consistent throughout the year due to moderate seasonal changes in temperature in the tropical climate of the Comoros and the presence of permanent breeding sites such as cisterns throughout the island. (Fig 3.4B) displays allele frequencies for adult female mosquitoes over the simulation period. After eight consecutive weekly releases of 10,000 male mosquitoes homozygous for the drive allele (HH) three years into the simulation, we see the drive allele (H) spread to high frequency in the population, the wild-type allele (W) be completely lost, and the in-frame resistant allele (R) accumulate to a small but noticeable extent. This occurs due to the drive of the H allele, and because the R allele is generated at a low rate and has neither a fitness cost nor benefit relative to the H and W alleles. The out-of-frame or otherwise costly resistant allele (B) initially rises in frequency more quickly than the R allele due to its higher generation rate, but declines in frequency once there are no more W alleles to cleave due to its inherent selective disadvantage.

Epidemiological dynamics

The gene drive system we consider includes a malaria-refractory gene that results in complete inability of mosquitoes to become infected with the malaria parasite, whether present in either one or two allele copies. In (Fig 3.4C), we depict the spread of the

malaria-refractory trait through the female mosquito population, and the consequences this has for mosquito and human infection status. Prior to the release, we see that infection prevalence in humans (*P. falciparum* parasite rate, PfPR) is mildly seasonal, with the proportion of infected humans (solid red line) waxing and waning in response to the fluctuating mosquito population size (green line in Fig 3.4A). The proportion of infectious female mosquitoes (dotted dark purple line) oscillates in synchrony with the proportion of infected humans; but at a much lower proportion due to the short mosquito lifespan and the fact that most mosquitoes die before the parasite completes its EIP. Following the release of the drive system and refractory gene at year three, the proportion of refractory female mosquitoes (dotted light purple line) increases and, consequently, the proportion of infectious mosquitoes declines. As humans recover from infection and less develop new infections, the PfPR declines until it reaches near undetectable levels by year five. Lastly, (Fig 3.4D) depicts human malaria incidence, measured as the number of new infections per 1,000 humans per day. Stochastic variation in this model output is more pronounced due to the small number of incident cases relative to the total population. Incidence is halted by the beginning of year four, but PfPR takes almost a year longer to approach zero as infected humans clear parasites.

3.4 Future directions

We are continuing development of the MGDrivE 2 software package and welcome suggestions and requests from the research community regarding future directions. The field of gene drive research is moving quickly, and we intend the MGDrivE 2 framework to serve as a flexible tool to address exploratory, logistical and operational questions regarding genetics-based control systems for mosquito disease vectors. This includes exploratory modeling of novel genetic constructs, assessment of candidate constructs against TPPs and PPCs, and field trial planning as constructs progress through the development pipeline. Future functionality that we are planning includes: i) modeling of mosquito traps to address questions related to monitoring and surveillance, and ii) more detailed epidemiological models addressing phenomena important to malaria and arbovirus transmission - for instance, dengue models that incorporate multiple serotypes with temporary cross-protective immunity and complications related to antibody-dependent enhancement [150], and malaria models that incorporate age-structure, immunity, asymptomatic infection and superinfection [61].

Additionally, we are exploring numerical sampling algorithms that can increase computational efficiency and speed, facilitated by separation of model specification and simulation in the software. The complexity of models that can be developed in MGDrivE 2 means that sensitivity analyses can become extremely computationally intensive, and the ability of the SPN framework to leverage efficient algorithms in these circumstances will be highly valuable. We also continue to be interested in developing a corresponding individual-based model capable of efficient modeling when the number of possible

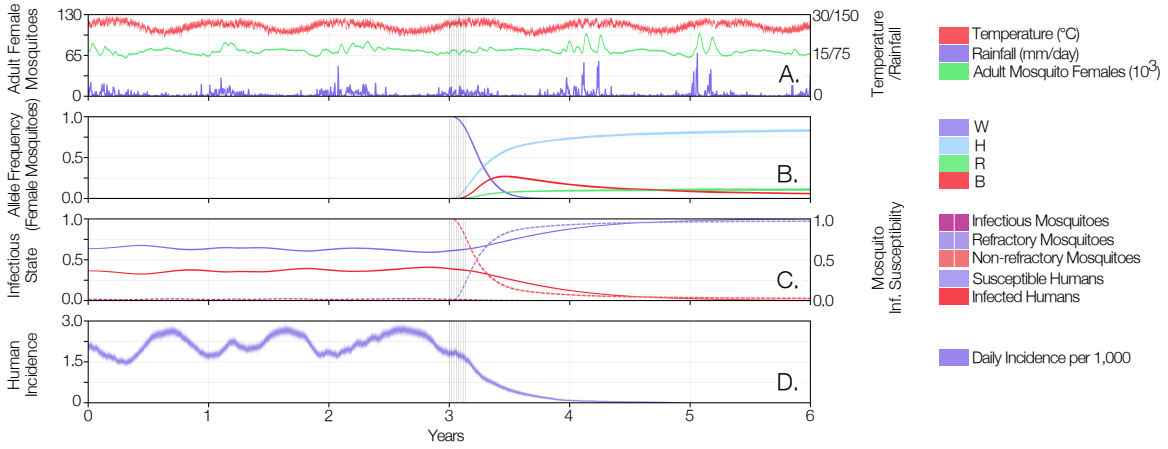

Figure 3.4: **Example MGDrivE 2 simulations.** Example MGDrivE 2 simulations for a population replacement gene drive system designed to drive a malaria-refractory gene into an *An. gambiae s.l.* mosquito population with seasonal population dynamics and transmission intensity calibrated to a setting resembling the island of Grand Comore, Union of the Comoros. The gene drive system resembles one recently engineered in *An. stephensi* [3] for which four alleles are considered: an intact homing allele and malaria-refractory gene (denoted by "H"), a wild-type allele (denoted by "W"), a functional, cost-free resistant allele (denoted by "R"), and a non-functional or otherwise costly resistant allele (denoted by "B"). Model parameters describing the construct, mosquito bionomics and malaria transmission are summarized in Table 3.1. **(A)** Climatological time-series data - temperature in red and rainfall in purple - that were used to calculate time-varying adult mosquito mortality rate and larval carrying capacity, respectively. The resulting adult female population size is shown in green. **(B)** Allele frequencies for adult female mosquitoes over the simulation period. Grey vertical bars beginning at year three denote eight consecutive weekly releases of 10,000 male mosquitoes homozygous for the drive allele (HH). **(C)** Spread of the malaria-refractory trait through the female mosquito population, and consequences for mosquito and human infection status. Following the release of the drive system at year three, the proportion of refractory female mosquitoes (dotted light purple line) increases and the proportion of infectious mosquitoes (dotted dark purple line) declines. As humans recover from infection and less develop new infections, the P. falciparum parasite rate (solid red line) declines until it reaches near undetectable levels by year five. **(D)** Human malaria incidence is halted by the beginning of year four.

states exceeds the number of individuals in the population - for instance, for multi-locus systems such as daisy-drive [117] and multiplexing schemes in which a single gene is targeted at multiple locations to reduce the rate of resistance allele formation [122], and for epidemiological models in which age structure, immunity and mosquito biting heterogeneity become prohibitive for population models [61].

Parameter:	Symbol:	Value:	Reference:
Gene drive construct:			
Cleavage rate	c_H	1	[3]
Proportion of cleaved alleles subject to accurate homology-directed repair (HDR) in females	$P_{HDR,F}$	0.99	[3]
Proportion of cleaved alleles subject to accurate (HDR) in males	$P_{HDR,M}$	1	[3]
Proportion of resistant alleles that are in-frame, functional	P_{RES}	0.17	[3]
Cleavage rate due to maternal deposition of Cas9	P_{MC}	0.937	[3]
Proportion of resistant alleles due to maternal deposition of Cas9 that are in-frame, functional	P_{MR}	0.17	[3]
Female fecundity cost due to BB genotype	$S_{BB,F}$	0.998	[3]
Mosquito bionomics:			
Egg production per adult female (day^{-1})	β	32	[39]
Mean duration of egg stage (days)	T_E	3	[159]
Mean duration of larval stage (days)	T_L	7	[159]
Mean duration of pupa stage (days)	T_E	2	[159]
Coefficient of variation (duration of egg stage)	$CV(T_E)$	0.2	[16]
Coefficient of variation (duration of larval stage)	$CV(T_L)$	0.3	[16]
Coefficient of variation (duration of pupae stage)	$CV(T_E)$	0.2	[16]
Carrying capacity of environment (larvae)	K	(time-varying)	Data: [1], Method: [151]
Mortality rate of adult mosquitoes (day^{-1})	μ_F, μ_M	(time-varying)	Data: [1], Method: [114]
Malaria transmission:			
Blood feeding index	f	1/3	[138]
Human blood index	Q	0.9	[138]
Transmission efficiency: infected mosquito to human	b	0.55	[138]
Transmission efficiency: infected human to mosquito	c	0.15	[138]
Mean duration of extrinsic incubation period (days)	EIP ($1/\gamma_V$)	10	[137]
Coefficient of variation of extrinsic incubation period	CV(EIP)	0.4	[77]
Human infectious period (days)	$1/r$	200	[138]
Human lifespan (years)	$1/\mu_H$	62	[79]
Human population size	N_H	350,998	[79]

Table 3.1: **Parameters for example simulation output.** Model parameters describing the gene drive construct, mosquito bionomics and malaria epidemiology for simulations resembling releases on Grand Comore, Union of the Comoros.)

Chapter 4

Principled simulation of agent-based models in epidemiology

4.1 Introduction

Stochastic simulation of complex mathematical models is a vital tool for understanding and describing disease transmission systems. While early efforts by probabilists Bailey and Kendall [12, 87], and the biochemist and physician-epidemiologist pair Kermack and McKendrick [89, 90] were highly mathematical in nature, they were at best, coarse approximations of natural processes. In the century hence, disease transmission models have incorporated myriad details including age structure, commuting, migration, and within-host immunology to better represent our understanding of how these systems function. Complex simulation models have been used to great effect in understanding rapidly changing epidemic situations, such as the outbreak of a novel pathogen, or events which require immediate response, such as the 2001 veterinary epidemic of hand foot and mouth disease in the UK [85]. When addressing urgent public health crises, complex models of epidemic processes can be invaluable tools, serving as platforms for data integration [145], estimation of current burden [147], forecasting trends [46], evaluation of intervention strategies and counterfactual scenarios [82], among other roles.

These models are often formulated as compartmenal models and simulated as stochastic jump processes, where a jump is a change in an individual's epidemiological state. Sample paths (trajectories) are piecewise constant, and change only due the to occurrence of discrete events that change the epidemiological state of individuals (jumps). When jumps are only allowed to occur after exponentially distributed intervals, the process is a continuous-time Markov chain (CTMC). Because the modeler is free to design the states, state transitions, and associated distribution of inter-jump intervals as they see fit, this class of models can be directly specified from the results of survival analysis [6], allowing close alignment to empirical data and standard survival models. In general, jump processes are also valued for their deep connection to deterministic models (*e.g.*, com-

partmental models) in limiting cases which can aid model verification; such results are well known for CTMC models [21, 56] and exist for some non-Markovian extensions [20]. Furthermore, these models benefit from over a half-century of rigorous mathematical and algorithmic study [88], especially in chemical kinetics, physics, and operations research communities, which has led to a plethora of publicly available algorithms to sample trajectories from such processes, as well as techniques for statistical inference and model fitting.

The complexity of these models, however, frustrates analytic approaches and can even thwart straightforward application of classic simulation techniques, making quick development and application challenging, especially in epidemic response situations. Incorporating non-Markovian dynamics is still difficult in most simulation frameworks, and because the majority of "industrial strength" simulation software is designed for relatively straightforward chemical reaction networks [131], peculiarities of epidemiological simulation such as highly nonlinear force of infection terms, age and location-based mixing, immunological dynamics, and other elaborations make direct utilization of these software difficult. While there exist some open-source software for simulation of epidemiological dynamics, many frameworks are restricted to simple compartmental models, or may have a significant enough learning curve that they are simply not an option when a model must be developed in a matter of days [72, 43]. In addition, researchers may require specific forms of model output that can be difficult for software packages to support.

Beacuse of their expressive power, agent-based models (ABM) are often the most straightforward way to turn a whiteboard description of a complex system into useable code, and are a viable alternative to other methods of representing a model. Many ABMs are developed as bespoke programs for a specific analysis, but the technical complexity of implementation means that a variety of subjective decisions may be made when writing simulation code. Not all design choices will lead to simulation algorithms that necessarily have a limiting interpretation as some stochastic jump process, valuable for both model verification and model modification based on the formal rules of the stochastic process.

Here we describe a method to construct approximate ABM representations of stochastic models in which agents with arbitrarily complex internal dynamics interact through discrete events in continuous time. Our method relies on specification of a discrete time step of size Δt, over which interactions *between* agents are approximated (dependent events); dynamics *within* an agent (internal events) are still simulated exactly in continuous time. A significant contribution in this work is presenting a generic algorithm to simulate systems that are relevant to a wide class of epidemiological models, via approximation of dependent events which can help speed up even highly complex ABMs. We also demonstrate that our algorithm approaches the true continuous time jump process as $\Delta t \to 0$. To verify our method and provide numerical comparisons to exact stochastic simulation, we use our algorithm to simulate a Markovian and non-Markovian SIR (Susceptible-Infectious-Recovered) model. We conclude with a discussion of strengths and weaknesses of our approach, as well as fruitful next steps to generalize our method. We hope that our method gives mathematical epidemiologists considerable freedom in

designing a model to fit their needs, and that by approximating dependent events, even highly complex models can be feasible to simulate. We also expect our method will be of interest to researchers in ecology, demography, and the quantitative social sciences.

4.2 Materials and methods

Hazard Rates in Stochastic Simulation

Formally, a jump process is a stochastic process, X whose trajectories (sample paths) are piecewise constant functions of time over a countable set of states, $\mathcal{S}$ so that $X(t) \in \mathcal{S}$, $t \geq 0$. Here we restrict ourselves to considering time-homogeneous processes, so that only the dwell time in the current state is relevant for the process. In order to sample trajectories from X, we must specify hazard functions $\lambda_j(\tau, s)$ associated with each event $j \in \{1, \ldots, M\}$. The hazard functions tell us the conditional probability of j occurring in the next infinitesimal time interval $[\tau, \tau + dt)$, if the process has dwelled in state $s \in \mathcal{S}$ for some time τ (in the case where there is no dependence on τ, the hazard will be a constant value and X is a CTMC). When j occurs, it is allowed to change the state X in some way. Given a set of M events, simulation consists of sampling when the next event occurs, which event was it, updating state appropriately, recalculating hazards that change, and repeating this process [52]. The state space can be defined implicitly, and can be (countably) infinite, so long as only a finite number of events have non-zero hazards at any time.

To define the process that the ABM will sample from, we let $X(t) = (s_1, ..., s_n)$ be a vector where n is the number of agents being simulated, and each s_h is the state of person h. Expanding state space in this was to achieve an agent-based representation is known as disaggregation, and may be used to study ABMs via the technical condition of lumpability [14]. Then, any events which affect person h and whose hazard function depends on more elements of X than only s_h is a dependent event; events which affect person h and whose hazard function is only allowed to depend on s_h is an internal event. Consider the recovery event in an SIR model. The recovery event for person h does not need to know about the states of anyone else in order to calculate the hazard of recovery and so is an internal event. However, the infection event for individual h *does* require knowing the state of other agents in order to compute the hazard, and therefore is a dependent event.

To draw approximate trajectories from the ABM requires a choice of time step Δt, over which hazards for each agent's dependent events may only use information from other agents at the start of the step, ignoring changes which occur *during* the time step. Put another way, agents only exchange information at the start of each time step. Then over a time step beginning at time t, a susceptible agent i is subject to infection hazard (force of infection, hereafter FOI) $\beta(u)I(t)$ for $u \in [t, t + \Delta t)$, where $\beta(u)$ is the effective contact rate [11]. Note that we allow the contact rate to possibly depend on time, and that the approximation is in setting the number of infected individuals to a constant value (the

number at time t). Dependent events can be simulated via rejection sampling. Internal events, by definition will not depend on any other individuals and therefore will not be approximated. This type of simulation is reminiscent of tau-leaping techniques [55], but whereas in standard tau-leaping *all* hazard functions are approximated as constants over the time step, our method only approximates dependent events, and internal events are simulated exactly.

We postpone a complete description of our method to section Simulation Algorithm, and first demonstrate that the accept-reject sampling we use for sampling dependent event times can draw correct times in a base case.

Approximation of Hazard Rates

Consider the a single susceptible agent who is subject to a single event, infection. Let $\tau_{S\to I}$ be a random variable giving the time at which this agent becomes infected, $tmax$ be the end of the current time step, $[tmax - \Delta t, tmax)$, and λ be the FOI which is valid over that time step.

In our model, each agent stores its current state s_h, the time at which it entered that state $tnow$, and the next scheduled event time $tnext$ and state s'_h. For all internal events, simulation is identical to classic discrete event simulation techniques. While the agent's next scheduled event time is less than $tmax$ the agent will update their state and time according to that scheduled event, and sample a new state and time. If the new event time is greater than *tmax*, the update does not occur until the time step in which that event falls.

In the case of infection, a dependent event, if we naively sampled the time of infection as $\tau_{S\to I} \sim tnow + Exp(\lambda)$, we would be ignoring future stochastic changes in FOI, which could change at $tmax$. Crucially, from the perspective of this agent, the FOI is a stochastic quantity, because it depends on the states of other agents. To develop a reasonable approximation, one needs to implement a rejection algorithm to sample $\tau_{S\to I}$.

The sampling is described graphically in Fig 4.1 A. During this time step, λ is constant (red region), and the agent samples a *putative* time to infection $\widehat{\tau}_{S\to I} \sim tnow + Exp(\lambda)$. Note that there is no restriction $tnow$ be equal to the start of the time step, because it could have been a randomly sampled quantity from previous events. If $\widehat{\tau}_{S\to I}$ falls within the remaining time for which that hazard is valid (purple region of size $tmax - tnow$, which is to say $\widehat{\tau}_{S\to I} < tmax$), then we accept the sample and infect the agent at time $\widehat{\tau}_{S\to I}$. The probability of the putative time being accepted is $1 - e^{-\lambda(tmax - tnow)}$.

If however we reject the putative time ($\widehat{\tau}_{S\to I} \geq tmax$) then we set the agents next event time to be $tmax$, and do not change the agent's state. Then, on the next time step, the agent sets their current time to the start of that time step and resamples $\widehat{\tau}_{S\to I}$ using the *newly updated* FOI λ'. The probability of acceptance is $1 - e^{-\lambda'\Delta t}$.

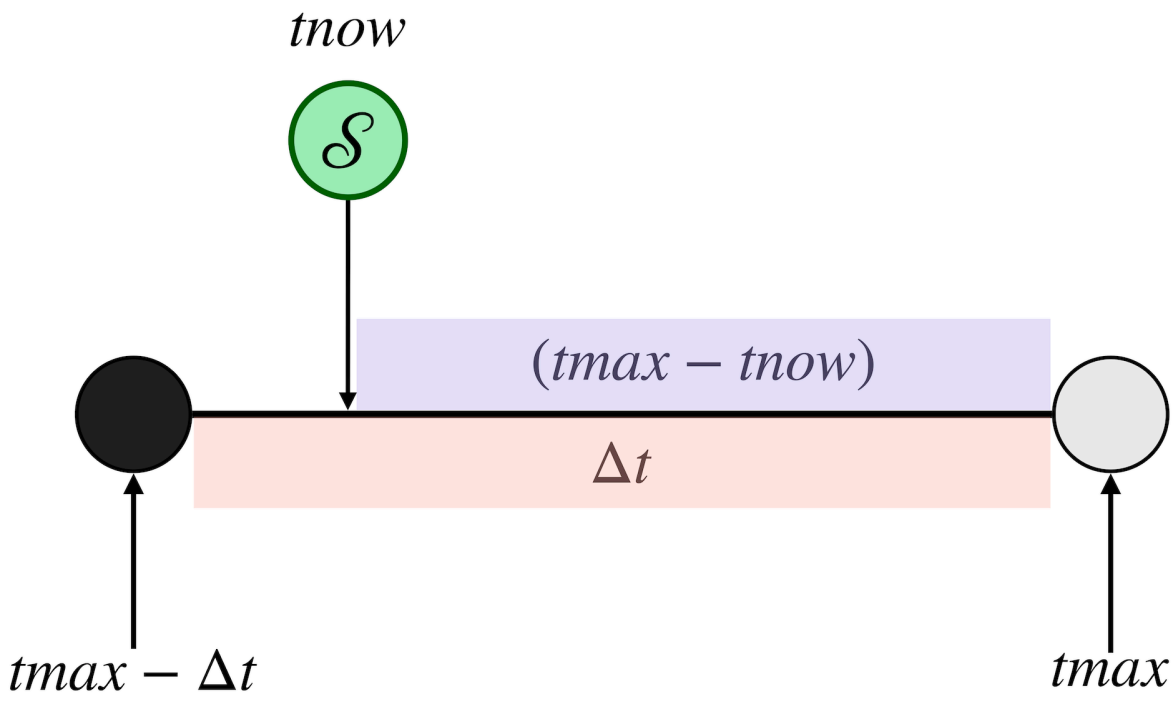

Figure 4.1: **Approximate infection hazard over a time.** The left filled circle and unfilled right circle indicate that time steps are closed on the left and open on the right.

Accept-reject Algorithm for Piecewise Constant Hazard Rates

When $\Delta t \to 0$, the accept-reject algorithm for time of infection becomes exact. To demonstrate this, first consider the case where the FOI is a deterministic quantity, and, furthermore, that it is a constant. Then the probability of acceptance on any time step of size Δt is $p = 1 - e^{-\lambda \Delta t}$. Consequently, the expected number of rejections prior to the acceptance is given as $\sum_{n=0}^{\infty} \left((1-p)^n p\right) n = \frac{1-p}{p}$. The expected number of trials including the acceptance is thus $\frac{1-p}{p} + 1 = \frac{1}{p}$, or the expectation of a Geometric random variable. Note that this is not quite the same as the expected value of the time to infection, which is $\frac{1}{\lambda}$. The value $\frac{1}{p}\Delta t = \frac{\Delta t}{1-e^{-\lambda \Delta t}}$ "overshoots" because the acceptance could have occurred at any point in the final time step, not just at the end.

Now, conditional on being accepted during trial n (that is, prior to its conclusion), the time τ at which the acceptance occurs within the time step $[(n-1)\Delta t, n\Delta t)$ is given by an upper truncated Exponential distribution (Fig E.1). This random variable has expectation $\mathbb{E}[\tau] = \int_0^{\Delta t} \frac{\lambda e^{-\lambda \tau}}{1-e^{-\lambda \Delta t}} \tau \, d\tau = \frac{\Delta t}{1-e^{\lambda \Delta t}} + \frac{1}{\lambda}$. Then the time at which the event occurs should be equal to the number of rejections, each scaled by the time step size, plus this quantity, which is: $\frac{\Delta t(1-p)}{p} + \frac{\Delta t}{1-e^{\lambda \Delta t}} + \frac{1}{\lambda} = \frac{1}{\lambda}$, so we show that the accept-reject algorithm recovers

precisely the same average waiting time as the Exponential random variate.

If instead of constant, the FOI is a deterministic piecewise constant function such that λ_n is the value of the FOI between $[n\Delta t, (n+1)\Delta t)$ similar reasoning applies but the number of trials needed no longer follows a Geometric distribution. The time of acceptance within the acceptance interval however, still follows a truncated Exponential, because it is conditioned on the infection event occurring in that time step of (piecewise) constant hazard. In this case, sampling $\tau_{S\to I}$ is equivalent to sampling the first event time of an nonhomogeneous Poisson process (NHPP) with intensity function $\lambda(t)$.

From [41], one way to sample from such a process is by inversion of the distribution of inter-event times, which has distribution function $F(\tau;\lambda) = 1 - e^{-\int_0^\tau \lambda(u)\,du}$. To sample the first event time, one should draw a uniform random number u between $[0, 1)$ and solve so that τ is the first event time: $-\log(1-u) = \int_0^\tau \lambda(u)\,du$. If the cumulative hazard function $\Lambda(\tau) = \int_0^\tau \lambda(u)\,du$ is especially easy to invert, then by the random time change (RTC) theorem, we can also sample from the distribution of t by sampling v from a unit rate Exponential distribution and then solving $\tau = \Lambda^{-1}(v)$ [100].

When FOI is piecewise constant, $\Lambda(\tau)$ will be piecewise linear so inversion of the cumulative hazard will be the most straightforward sampling method. To compare the accept-reject algorithm with inversion sampling of NHPP first event times, we discretized a continuous intensity function $\tilde{\lambda}(t) = \frac{1}{8}\sin\left(\frac{(t-6)2\pi}{24}\right) + \frac{1}{8}$. The function has a period of 24 hours, with a maximum amplitude of 0.25 (corresponding to $1/4$ events an hour) with a vertical shift so that it is non-negative and a phase shift of 6 hours such that the maximum intensity occurs each day at noon and minimum intensity at midnight (Fig E.2). The integrated continuous intensity is $\tilde{\Lambda}(\tau) = \frac{1}{8}\left(t - \frac{12\sin\left(\frac{\tau\pi}{12}\right)}{\pi}\right)$.

In Fig 4.2 we show that the accept-reject sampler for first event times of NHPPs is equivalent to exact inversion methods given in [41, 100]. In both panels the red curve is the density function of first event times calculated directly from $f(\tau) = \tilde{\lambda}(\tau)e^{-\tilde{\Lambda}(\tau)}$, and we drew 10^6 samples using each algorithm to construct the histograms. We see that both the accept-reject algorithm and integrated hazard sampling are sampling from the correct density function.

In a full model with interacting agents, each agent's FOI depends on the state of other agents, and the piecewise constant approximation means that on the $[n\Delta t, (n+1)\Delta t)$ time step that FOI is computed at $n\Delta t$ and remains constant until the next time step at time $(n+1)\Delta t$, when agents may exchange information. Let us consider what happens as we let $\Delta t \to 0$. Because the model is a set of simple counting processes in continuous time, meaning that only jumps of size 1 are allowed, the probability of two events occurring simultaneously is zero [24]. So when Δt is near zero, we expect that on each time step either 0 or 1 event will occur, regardless of how many agents are in the system. With infinitesimal time steps, after a single event occurs, the FOI for all agents will be updated *immediately* and the algorithm becomes exact.

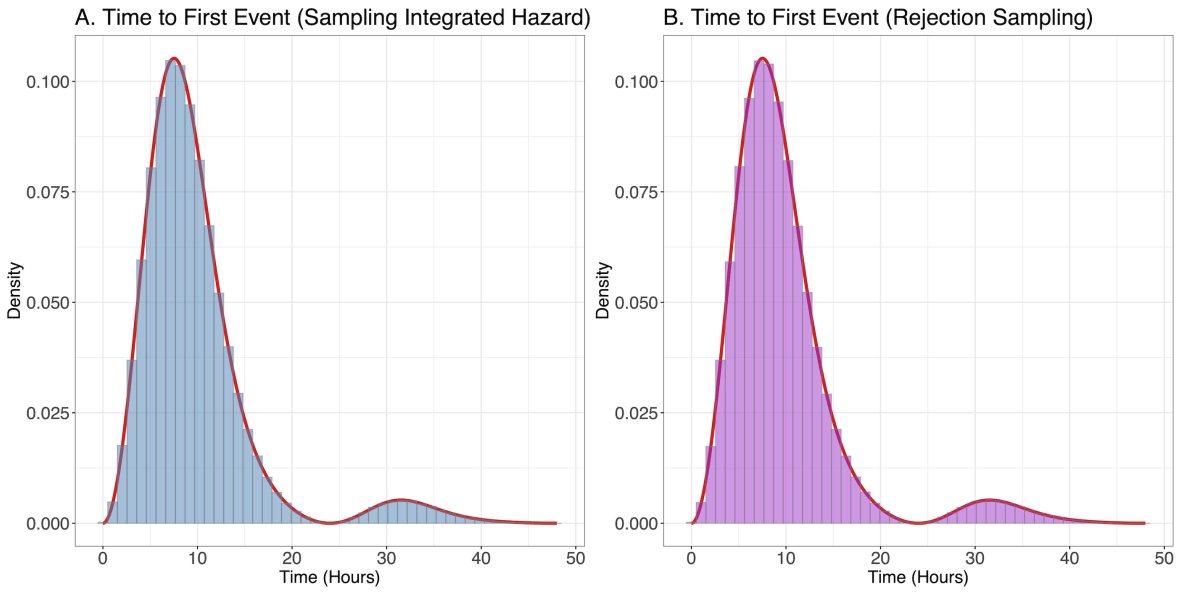

Figure 4.2: **Comparison of Rejection Sampler and Direct Inversion for sampling first event times.** Panel A: using integrated hazard to sample, Panel B: using accept-reject algorithm to sample. Red curves in both panels are the exact density, from numerical integration.

Simulation Algorithm

Our agent-based simulation algorithm for stochastic epidemic models where each agent is subject to a single dependent event, infection, is given in pseudocode below. Generalization to multiple dependent events (such as multiple strains or routes of transmission, for example) can be easily accommodated by keeping track of multiple force of infection (hazard) terms for each agent, and letting the accept-reject algorithm sample the first event time over all competing dependent events. Each agent in the population being simulated ($h \in \{1, \ldots, n\}$) stores (at minimum) the following pieces of information: their current state s_h, next state s'_h, current time $tnow_h$, and next time $tnext_h$.

1. Initialize. For each agent h, set $tnow_h = tnext_h = 0$ and set their initial state $s_h = s'_h = s_h(0) \in \mathcal{S}$. Set system time $t = 0$.
2. Set $tmax = t + \Delta t$.
3. Compute the force of infection on each agent λ_h.
4. Simulate each human's trajectory between $[tnow_h, tmax)$:
    - While $tnext_h < tmax$:
        a) $tnow_h = tnext_h$

   b) $s_h = s'_h$
   c) Run code associated with the new state s_h and sample the next state transition and time $(s'_h, tnext_h)$.

5. Set $t = tmax$.

6. Return to step 2 or quit.

When the agent is in a susceptible state and the accept-reject algorithm is being used to sample their time to infection, it is crucial that if the putative time of infection is rejected, the next time is set as $tnext_h = tmax$ so that on the next time step, a new putative infection time is drawn. Because each agent updates themselves in continuous time within the while loop on step 4, the distribution of sampled times for internal events will be exact. Additionally, because each agent stores their own next state and time, so there is no need for a complex global event queue.

How in particular each agent samples from the tuple $(s'_h, tnext_h)$ in step 4c is left unspecified. Any exact sampling method for competing hazards is valid, and choice of method will depend on the problem at hand. Additionally we did not specify how to record model output; the method which provides the most granular output, and enabling survival analysis of results to verify the model, would delegate writing output to code associated with the event which causes the transition to each new state s_h, in step 4c. If coarse-grained output is deemed sufficient, a natural place to track output is step 2, which already requires a for loop over all agents.

Fig 4.3 shows how the simulation algorithm samples from an SIR epidemic [4] with three agents over two time steps. The state space for each agent is $\mathcal{S} = \{S, I, R\}$. At time $t = (n-1)\Delta t$, there are two infectious individuals and one susceptible individual. For susceptible individual 3, we additionally show their FOI $\lambda_3(t)$ in blue. Note that while agents may experience state changes at any point in time (agent 1 recovers during the first time step and agent 2 during the second time step), the FOI is only allowed to change at each time step when agents exchange information (shown by red arrows). During the first time step, agent 3 samples a putative time to infection which exceeds time $n\Delta t$, so it is rejected. Agent 1 recovers sometime before the end of the time step, but is not allowed to update agent 3 until the start of the next step. When the next time step begins, after updating its FOI, agent 3 again samples a putative infection time, which occurs during that time step $(\widehat{\tau}_{S\to I} < (n+1)\Delta t)$, becoming infectious at that time. Additionally, agent 2 recovers sometime before the end of the time step.

While the diagram only shows a trajectory that overestimates the true FOI over each interval, if there was another S individual who transitioned to I during the time step their contribution would be left out and it would be an underestimate.

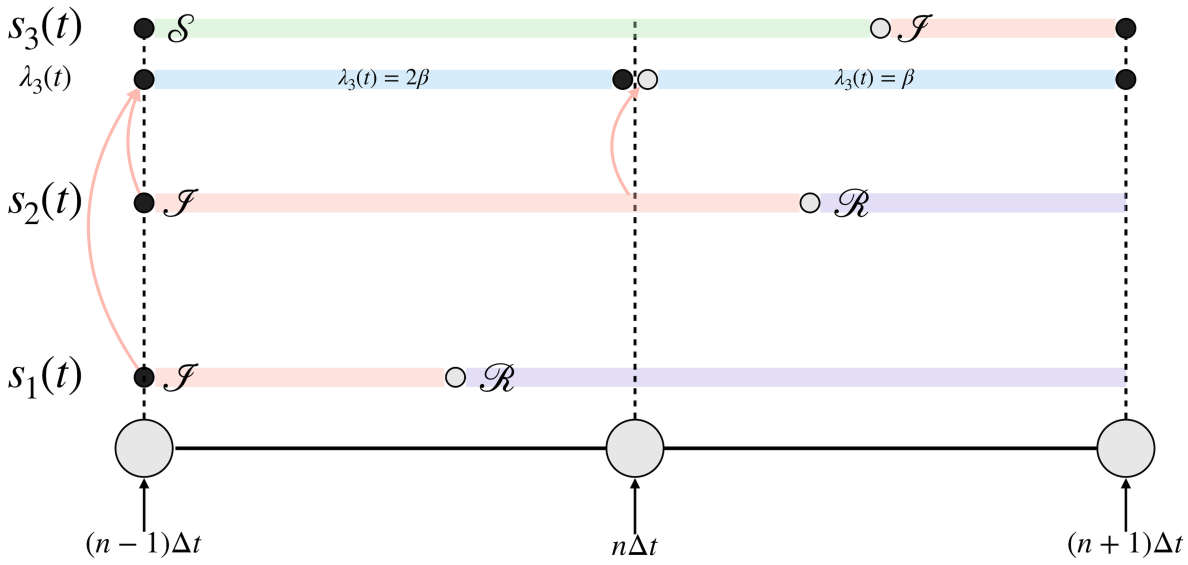

Figure 4.3: **Graphical representation of simulation algorithm with three agents.** Rows $s_1(t), s_2(t), s_3(t)$ are piecewise constant functions that give each agent's state in the state space (S, I, R) at time t; each agents' trajectory will be a piecewise constant function through state space. S (susceptible) is green, I (infectious) is blue, and R (recovered) is violet. The blue stripe $\lambda_3(t)$ gives the FOI on agent 3 (the only one to begin as susceptible).

4.3 Results

To illustrate use of our agent-based simulation method, we simulate a Markovian and non-Markovian SIR model. For both models we compare the sampled transition probability distribution from the ABM to that sampled from an exact stochastic simulation algorithm (SSA). We also compare samples from the ABM to closed form results on final epidemic size distributions, which provides exact analytic checks of algorithm accuracy. For the Markovian SIR model we can additionally compare the agent-based simulation to numerical solutions of the Kolmogorov forward equation (master equation) of the system, which gives the exact transition probabilities of the stochastic model. Because both these results provide a complete description of the probabilistic behavior of the stochastic models, they are more useful than comparing sampled trajectories (time series). However, we show some simple comparisons of sampled trajectories between exact stochastic simulation and the agent-based model in Fig E.3.

All of our code, written in R and C++ to reproduce all findings and figures in this paper is available at `https://github.com/dd-harp/euler-abm`.

Markovian SIR Model

In Eq (4.1) we present the Kolmogorov forward equations (KFE) for the Markovian SIR model, following [4]. Because much recent research into methods for solving KFEs originates in statistical physics, which, unlike probability theory or mathematical epidemiology commonly uses *step operators*, we present the equations using step operators and work out a more familiar form, as presented in [86]. A brief introduction to using step operators to simplify writing KFEs for stochastic jump processes is available in Appendix C. The term $\mathbf{P}(S, I, R, t)$ is the probability for the system to be in state (S, I, R) at time t, such that $S + I + R = N$. We consider a simple mass action force of infection term to simplify the mathematics, so that the deterministic $R_0 = \frac{\beta}{\gamma}N$, but the method is not restricted to simple mass action.

$$
\begin{aligned}
\frac{d}{dt}\mathbf{P}(S,I,R,t) = &\overbrace{(E_S^1 E_I^{-1} - 1)[\beta SI\,\mathbf{P}(S,I,R,t)]}^{\text{infection}} \\
&+ \overbrace{(E_I^1 E_R^{-1} - 1)[\gamma I\,\mathbf{P}(S,I,R,t)]}^{\text{recovery}} \\
&= (E_S^1 E_I^{-1})[\beta SI\,\mathbf{P}(S,I,R,t)] - \beta SI\,\mathbf{P}(S,I,R,t) \\
&\quad + (E_I^1 E_R^{-1})[\gamma I\,\mathbf{P}(S,I,R,t)] - \gamma I\,\mathbf{P}(S,I,R,t) \\
&= \beta(S+1)(I-1)\,\mathbf{P}(S+1,I-1,R,t) - \beta SI\,\mathbf{P}(S,I,R,t) \\
&\quad + \gamma(I+1)\,\mathbf{P}(S,I+1,R-1,t) - \gamma I\,\mathbf{P}(S,I,R,t) \\
&= -(\beta SI + \gamma I)\,\mathbf{P}(S,I,R,t) + \beta(S+1)(I-1)\,\mathbf{P}(S+1,I-1,R,t) \\
&\quad + \gamma(I+1)\,\mathbf{P}(S,I+1,R-1,t)
\end{aligned}
\tag{4.1}
$$

While solution of the KFEs via matrix exponentiation or, for small state spaces, direct numerical integration of the ODEs is possible, in order to evaluate the probability transition matrix over all possible $\frac{(N+1)(N+2)}{2}$ unique model states we use a recently developed technique based on continued fraction expansion which can calculate the state transition probability matrix directly [73, 35]. For an up to date review of methods for solving transition probabilities for common epidemic models, except the method of [35], see [76].

Solutions of Eq (4.1), computed via the continued fractions method are the "ground truth" against which we want to evaluate samples from our ABM method. For comparison to an exact SSA, we choose to implement the Modified Next Reaction Method (MNRM) of [7] to sample exact trajectories from the KFE because it is simple to code and easily extends to the non-Markovian case.

Transition Probabilities

Solutions to the KFEs for the Markovian SIR model will give the exact transition probability matrix at a future time t given an initial state. That is, given some number of

susceptible, infected, and recovered individuals at time 0, $S(0), I(0), R(0)$, the KFEs can be solved to give the probability distribution over all possible states of the system at future time $t \geq 0$, $\mathbf{P}(S, I, R, t|S(0), I(0), R(0))$. This conditional probability distribution describes the exact probability law of the stochastic process; we use the method of [73], implemented in the R package, MultiBD [74] to solve for that distribution. We compare the exact distribution from solving Eq (4.1) to Monte Carlo simulation from the MNRM and ABM.

To assess the ability of the agent-based model to sample from the correct probability distribution over future states when simulating trajectories, we initiated a simulation with initial conditions $S(0) = 60, I(0) = 10, R(0) = 0$, $\gamma = 1/3.5$, and $R_0 = 2.5$. We sampled 10^5 trajectories from the ABM, exiting the simulation when the next event time would exceed $t = 5$, and using a time step $\Delta t = 0.01$. We drew the same number of trajectories from the MNRM simulation algorithm so we could have a sense of how an exact stochastic sampler would approximate the true distribution. The results are visualized in Fig 4.4. We visualized the bivariate probability distribution over $\mathbf{P}(S, I, t = 5|S(0), I(0))$ using contours to represent curves of constant probability. Because of the constraint $N = S + I + R$, we do not lose any statistical information by disregarding R. Panel A compares the sampled MNRM (dashed contours) to the exact (solid contours), and Panel B compares the sampled ABM to the exact distribution. In both cases we observed very good equivalence between the sampled distributions and the exact distribution.

Effect of Time Step on Accuracy

We expect that as Δt increases, the accuracy of the approximate ABM will deteriorate. We therefore evaluated the distribution $\mathbf{P}(S, I, t = 5|S(0), I(0))$ using the same parameters as the previous section, for a grid of time step sizes of 0.001, 0.005, 0.01, 0.025, 0.05, 0.075, 0.1, 0.5, 1. We chose this grid to span over several orders of magnitude, from extremely small values where we expect the ABM will be essentially exact, to a time step of one day, which for this specific setting is expected to be highly inaccurate. For each value of Δt, we drew 2×10^5 samples from the ABM to generate a Monte Carlo estimate of the transition probabilities. To calculate the exact transition probabilities, we used [74] to solve Eq (4.1).

For each time Δt, we calculated absolute error as the sum of differences between the Monte Carlo estimate of the transition matrix and the exact transition matrix. Interestingly, although moving from the smallest step size of 0.001 to a more modest size of 0.1 spanned two orders of magnitude, absolute error changed little, from 0.045 to 0.059. Increasing Δt to 0.5 and 1, however, swiftly increased absolute error to intolerable levels. We show a visual comparison of the effect of various step sizes on absolute error in Fig 4.5, where we plot the absolute difference between between each element in the bivariate distribution as a heatmap, visually revealing the method is highly accurate until large time steps of 0.5 and 1.

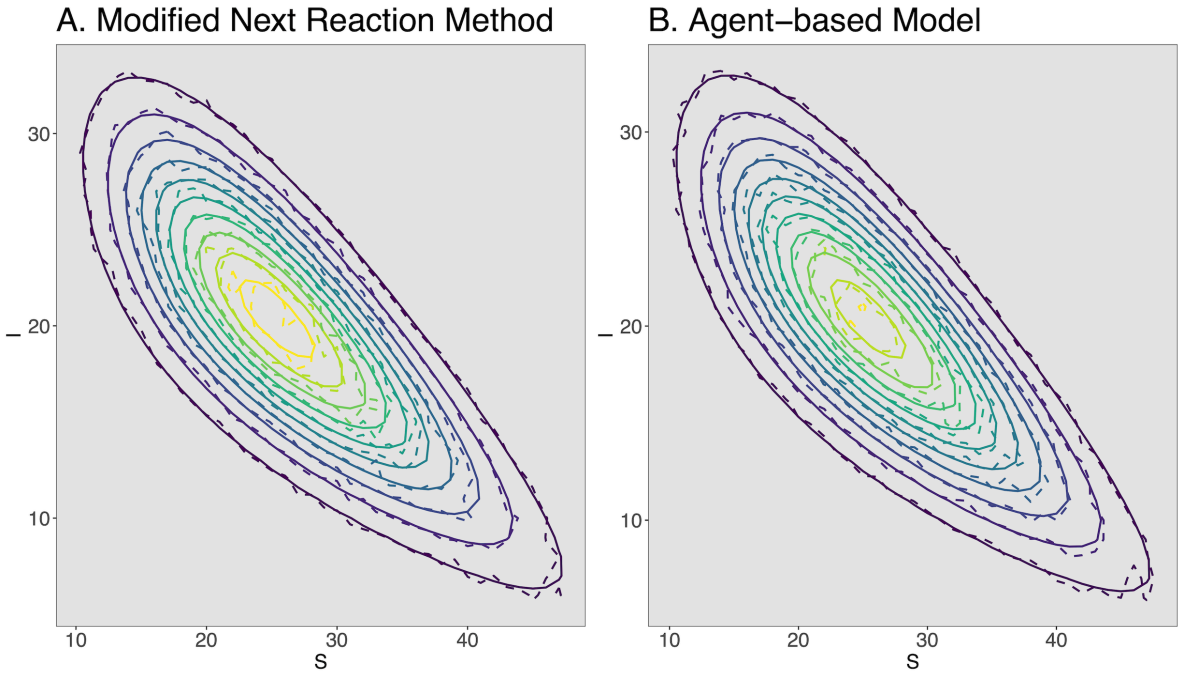

Figure 4.4: **Comparison of exact transition probabilities to MNRM and ABM transition probabilities.** Panel A: Comparison of MNRM (dashed contours) against exact probability distribution (solid contours), Panel B: Comparison of ABM (dashed contours) against exact probability distribution (solid contours). In both panels the x-axis and y-axis give the probability of having that number of susceptible and infectious individuals at $t = 5$, respectively.

Final Epidemic Size Distribution

An alternative to computing transition probabilities from Eq (4.1) for checking that our ABM is sampling from the correct process is to compare the final epidemic size distribution computed by Monte Carlo simulation to an exact analytic result. For SIR models, a closed form final epidemic size distribution was developed in [135, 13] and recently reviewed in [9]. This closed form solution for the distribution of final epidemic sizes is particularly valuable because this distribution will be affected by the distribution of duration of infectiousness, meaning it provides a complete check on the the ability of a sampling algorithm to simulate the SIR model.

If the duration of infectious period F has a moment generating function (MGF) given by $\Psi_F(t) = \mathbb{E}[e^{tF}]$ and where the initial states are given as $S(0) = N, I(0) = m$, the rate of effective contact by λ, then the final epidemic size vector is $p^{(N)} = (p_0^{(N)}, \ldots, p_N^{(N)})$ where $p_k^{(N)}$ is the probability that k of the initial N susceptible individuals are infected when the epidemic ends. The probability $p_k^{(N)}$ for any element of the vector is given in Eq (4.2) and a complete derivation is shown in Appendix D.

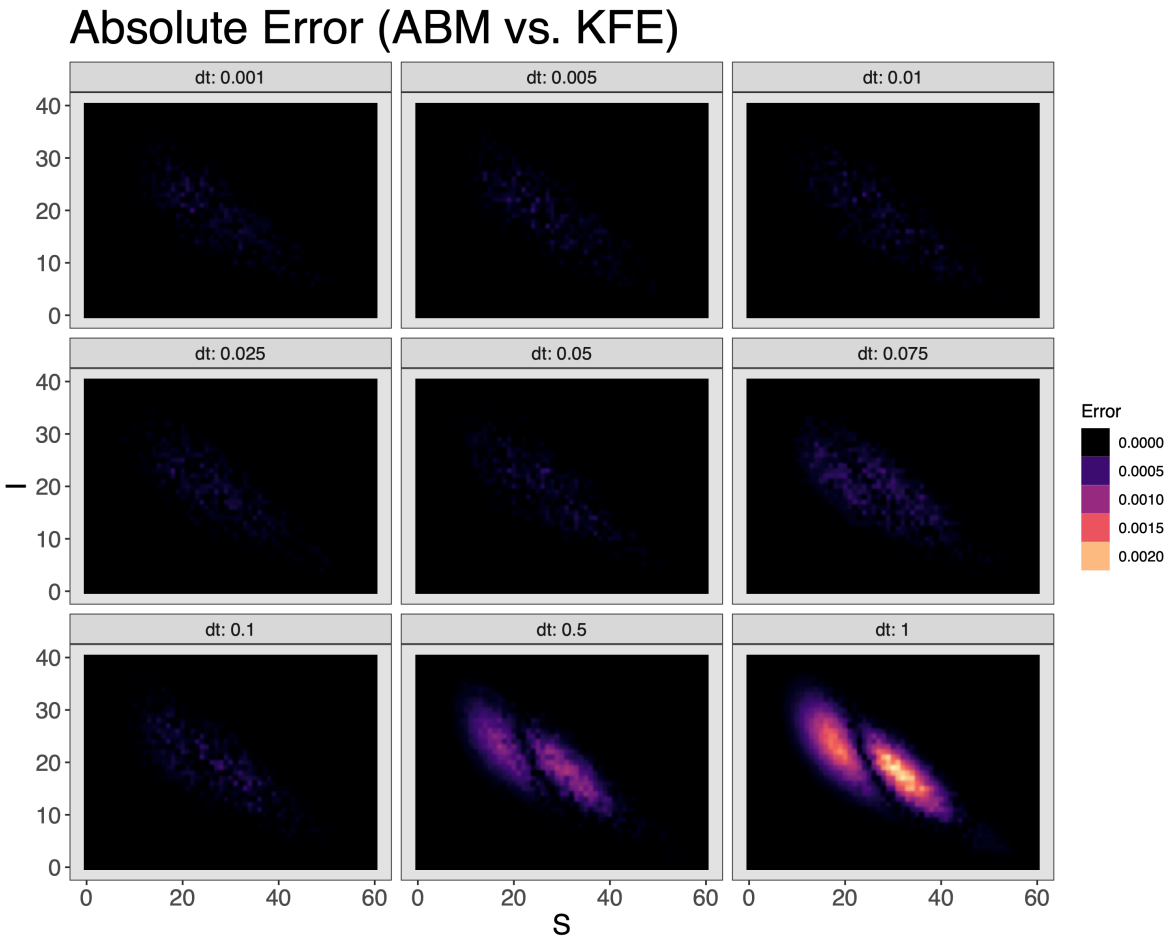

Figure 4.5: **Absolute error between ABM and exact transition probabilities for different sized time steps.** Panels show absolute error between transition probabilities calculated from the ABM versus exact distribution, from smallest time step (0.001) in the upper left to largest (1.0) in lower right. Darker areas correspond to small error while lighter regions correspond to higher error.

$$p_k^{(N)} = \binom{N}{k}\left[\Psi_F\left(-\frac{(N-k)\lambda}{N}\right)\right]^{k+m} - \sum_{i=0}^{k-1}\left[\binom{N-i}{k-i}p_i^{(N)}\left[\Psi_F\left(-\frac{(N-k)\lambda}{N}\right)\right]^{k-i}\right] \quad (4.2)$$

Because the equations use the MGF of the infectious period distribution, Eq (4.2) can compute final epidemic size distributions for both the Markovian and non-Markovian SIR model.

We compared the final epidemic size distribution sampled from the exact simulation algorithm (MNRM) and the ABM with $\Delta t = 0.01$ to the exact closed form probabilities calculated from Eq (4.2) in Fig 4.6. We used initial conditions of $N = 50$ and $m = 1$, and

sampled 10^4 epidemic sizes from each stochastic simulation. The effective contact rate was calculated to give $R_0 = 2.5$, and $\gamma = 1/5$. The exact probabilities are given by red dots, and the empirical probabilities are given by the purple horizontal lines; pointwise 95% confidence intervals were computed for each empirical probability by Wilson's score method and the coverage interval is given as the shaded rectangle around the empirical probability [134]. In both cases the empirical distribution from stochastic simulation is nearly identical to the analytic probabilities, with remaining deviations due to Monte Carlo finite sample error.

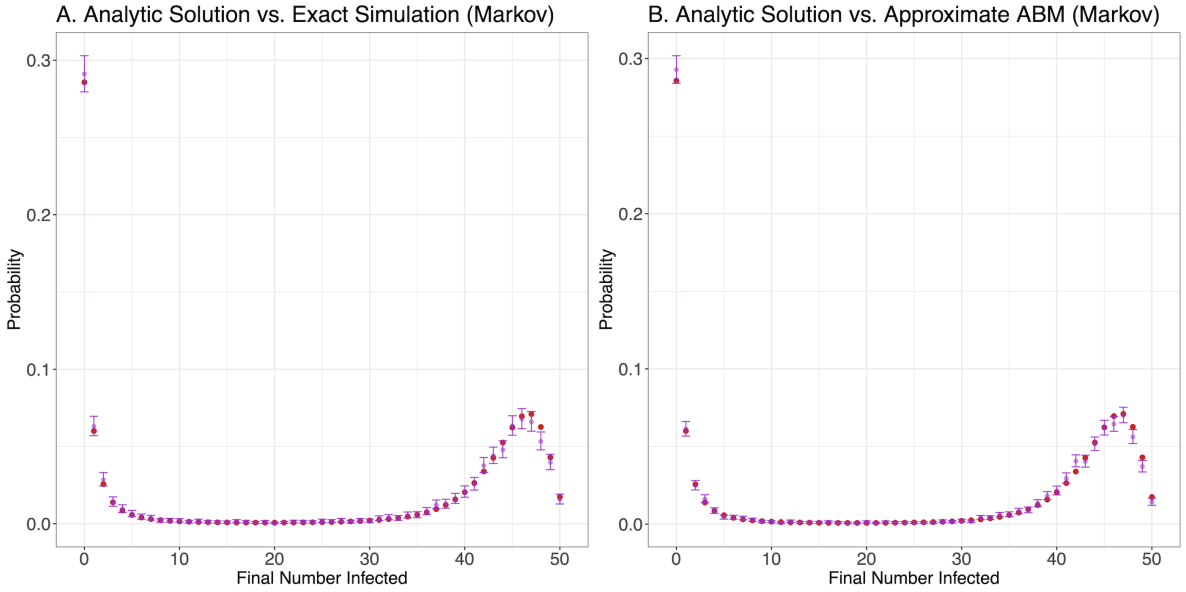

Figure 4.6: **Final epidemic size distributions for Markovian SIR model.** Panel A: Analytic final epidemic size distribution (red) versus empirical distribution (purple) from MNRM [7], Panel B: same, but empirical distribution (purple) from ABM. For each possible final size value we plotted the mean of simulation results as a purple dot with error bars indicating the pointwise 95% confidence interval from Wilson's score method.

Non-Markovian SIR Model

In Eq (4.3) we present the Kolmogorov forward equations for the non-Markovian (semi-Markov) SIR model, where the infectious period $\tau \sim F$ is a random variable that has a density function $f = \frac{d}{d\tau}F$, which may differ from an Exponential distribution. Because we assume that infection events still occur according to the points of a Poisson process, the contribution to the KFE from infection is the same as Eq (4.1).

However the contribution from the recovery term is more complicated. In particular, we need to introduce the two-time joint probability distribution $\mathbf{P}(S, I, R, t; S_{t-\tau}, I_{t-\tau}, R_{t-\tau}, t-$

$\tau)$, which is the joint probability of the system being in state $(S_{t-\tau}, I_{t-\tau}, R_{t-\tau})$ at a time $t-\tau$, and in state (S, I, R) at a later time t. In Eq (4.3), the recovery term must sum over all possible states that the process could have been in τ units of time in the past, where τ ranges from $[0, \infty)$, and is weighted by $f(\tau)d\tau$, the probability of an infectious period of duration τ. This means when a S particle becomes an I particle at time $t - \tau$ it *immediately* samples a time to recovery according to f. Those recovery events which complete at time t have probability $f(\tau)d\tau$ of requiring that amount of time to do so.

In this sense, the recovery events in the system are still controlled by the points of the Poisson process generating infection events, but represent delayed effects of that event. An excellent description of stochastic systems with delayed effects is given in [26]; another slightly different approach to these systems is described by [98].

$$
\begin{aligned}
\frac{d}{dt}\mathbf{P}(S,I,R,t) = &\overbrace{(E_S^1 E_I^{-1} - 1)[\beta SI\,\mathbf{P}(S,I,R,t)]}^{\text{infection}} \\
&+ \overbrace{(E_I^1 E_R^{-1} - 1)\left[\sum_{S',I',R'} \int_0^\infty \beta S'I'\,\mathbf{P}(S,I,R,t; S_{t-\tau}, I_{t-\tau}, R_{t-\tau}, t-\tau) f(\tau)\,d\tau\right]}^{\text{recovery}} \\
&= (E_S^1 E_I^{-1})[\beta SI\,\mathbf{P}(S,I,R,t)] \\
&\quad - \beta SI\,\mathbf{P}(S,I,R,t) \\
&\quad + (E_I^1 E_R^{-1})\left[\sum_{S',I',R'} \int_0^\infty \beta S'I'\,\mathbf{P}(S,I,R,t; S_{t-\tau}, I_{t-\tau}, R_{t-\tau}, t-\tau) f(\tau)\,d\tau\right] \\
&\quad - \sum_{S',I',R'} \int_0^\infty \beta S'I'\,\mathbf{P}(S,I,R,t; S_{t-\tau}, I_{t-\tau}, R_{t-\tau}, t-\tau) f(\tau)\,d\tau \\
&= \beta(S+1)(I-1)\,\mathbf{P}(S+1, I-1, R, t) \\
&\quad - \beta SI\,\mathbf{P}(S,I,R,t) \\
&\quad + \sum_{S',I',R'} \int_0^\infty \beta S'I'\,\mathbf{P}(S, I+1, R-1, t; S_{t-\tau}, I_{t-\tau}, R_{t-\tau}, t-\tau) f(\tau)\,d\tau \\
&\quad - \sum_{S',I',R'} \int_0^\infty \beta S'I'\,\mathbf{P}(S,I,R,t; S_{t-\tau}, I_{t-\tau}, R_{t-\tau}, t-\tau) f(\tau)\,d\tau
\end{aligned}
\tag{4.3}
$$

The final non-Markovian Kolmogorov forward equation has four terms. The first and second terms represent infection events that will push the state into, and out of (S, I, R), respectively. The third term represents infection events that fired some time τ in the past and whose delayed recovery event will push the process into state (S, I, R) at time t. Likewise the final term represents those infection events whose delayed recovery events

are just about to push the process out of that state.

To draw exact samples from the non-Markovian SIR model, we used the MNRM from [7] for arbitrarily distributed delays. We modified Algorithm 7 such that the delayed reaction channels store completion events as a priority queue implemented as binary heap, after drawing the delay, τ from the appropriate distribution.

Transition Probabilities

To assess the ability of the agent-based model to sample from the correct transition probability distribution over future states when simulating trajectories from the non-Markovian model, we initiated a simulation with conditions $S(0) = 60, I(0) = 10, R(0) = 0$, $\gamma = 1/3.5$, and $R_0 = 2.5$. We sampled 10^5 trajectories from the ABM, exiting the simulation when the next event time would exceed $t = 5$, and using a time step $\Delta t = 0.01$. We drew the same number of trajectories from the MNRM simulation algorithm in order to compare approximate transition probabilities from the ABM to an exact sampler. Unlike the Markovian SIR model, the non-Markovian KFEs in Eq (4.3) are analytically and numerically intractable, so the comparison in this section is only between the exact MNRM and ABM. The results are displayed in Figure 4.7. We visualized the bivariate probability distribution over $\mathbf{P}(S, I, t = 5|S(0), I(0))$ using contours to represent curves of constant probability. We observed a very good equivalence between the transition probabilities sampled via the approximate ABM (dashed contours) and exact sampler (solid contours).

Final Epidemic Size Distributions

As a further verification that our approximate ABM correctly sampled trajectories for the non-Markovian model, we used Eq (4.2) to compute exact final epidemic size distributions for the non-Markovian SIR and compared both the MNRM samples and ABM samples to the closed form solution. The delay distribution ($f(\tau)$ in Equation 4.3) was a Gamma distribution, with a mean of 5 days and standard deviation of 0.5 days, giving a distribution peaked near the mean with most of the probability mass concentrated between 4 and 6 days. We chose a Gamma distribution because it has an analytically tractable moment generating function, so that the closed-form final epidemic size distributions are easy to compute.

We calibrated β to give $R_0 = 1.85$, and sampled 10^4 epidemic sizes from each simulation method. The ABM used a time step size $\Delta t = 0.01$. As before, $N = 50$ and $m = 1$. The procedure used to construct pointwise confidence intervals was the same as used in the Markovian example. Fig 4.8 shows that our approximate ABM with the chosen time step is able to sample from the closed form probability distribution with high accuracy (Panel B), and its performance is indistinguishable from an exact sampler (Panel A).

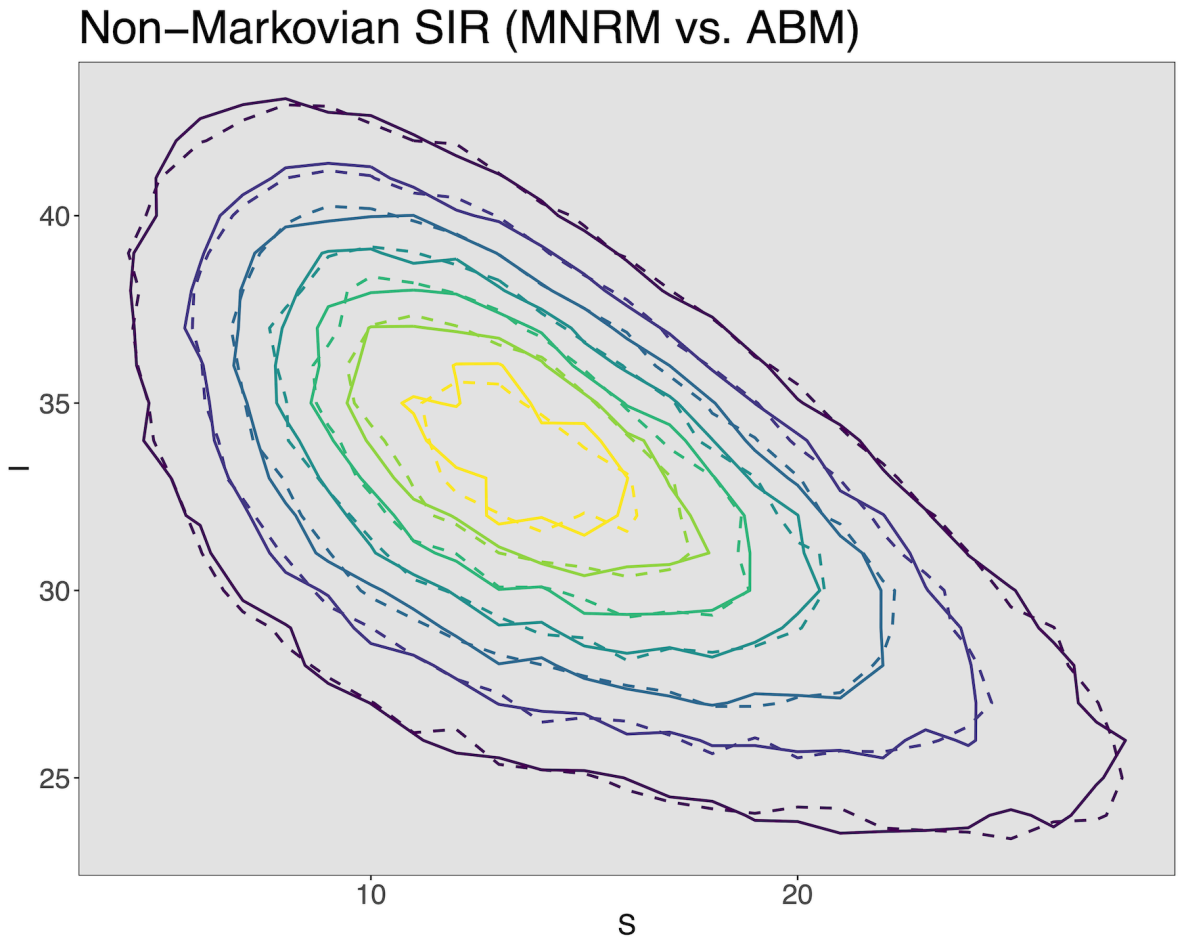

Figure 4.7: **Comparison of exact transition probabilities to MNRM and ABM transition probabilities.** Comparison of transition probability distribution sampled from MNRM (solid contours) to distribution sampled from the ABM (dashed contours). The x-axis and y-axis give the probability of having that number of susceptible and infectious individuals at $t = 5$, respectively.

4.4 Discussion

We have presented a practical approach to simulating ABMs with attractive properties. One interesting consequence of using a time step is that integration with other models becomes easier. If certain hazards depended upon, say a mosquito model with some discrete time step, that information could be exchanged between models at each step. As the model is formulated with continuous hazards, the size of a time step can vary over a simulation run, potentially widening applicability of the method. Furthermore, its generality means there are several interesting avenues for further development.

A clear next step is a method for bounding approximation error during a simula-

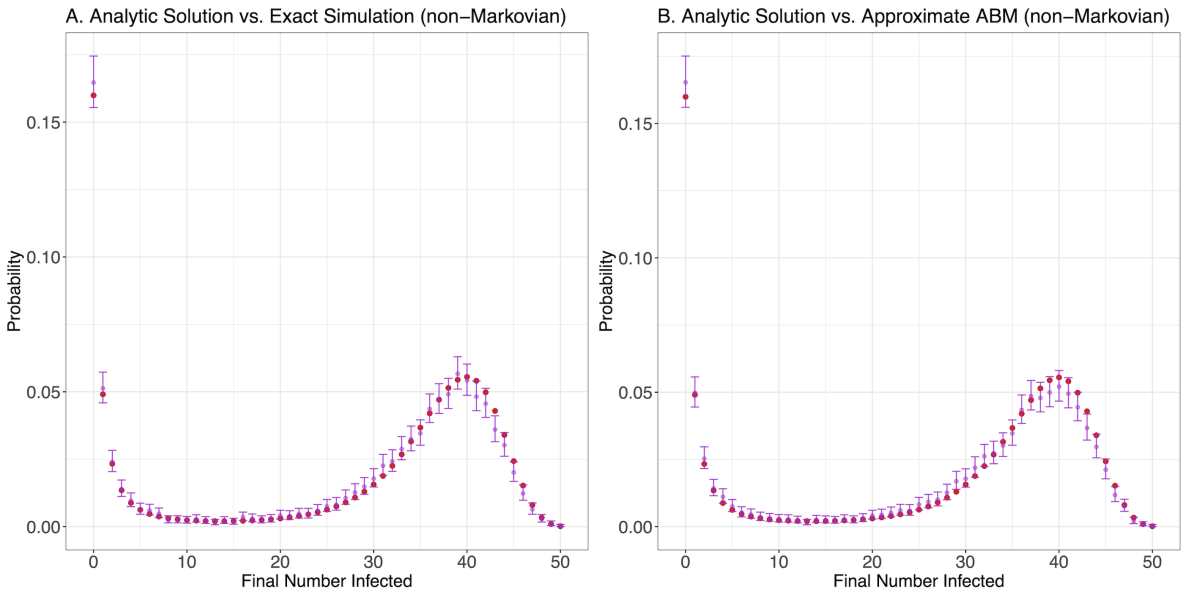

Figure 4.8: **Final epidemic size distributions for non-Markovian SIR model.** Panel A: Analytic final epidemic size distribution (red) versus empirical distribution (purple) from MNRM [7], Panel B: same, but empirical distribution (purple) from ABM. For each possible final size value we plotted the mean of simulation results as a purple dot with error bars indicating the pointwise 95% confidence interval from Wilson's score method.

tion run, which would allow for development of methods for adaptive selection of Δt. While the ABM formulation means the model's computational structure is different (disaggregated) compared to chemical kinetic simulations, hazard functions can could still be queried by looping over all individuals in the simulation. Because the discrete time step only approximates dependent events, agents without any enabled dependent events could be skipped. A first approach at adaptive selection of Δt may look somewhat similar to the straightforward methods presented in [55], and there is a wealth of citing literature that could be used for further development.

Another interesting avenue for future research is investigating how to handle multiple types of interaction which occur on different time scales. Because in the example SIR models presented here, agents only interact through a single dependent event, which is assumed to occur at the points of a Poisson process, all interactions occur on the same time scale. However, if multiple types of dependent interaction were simulated (frequent contacts between close friends versus rare meetings between acquaintances, for example), total error induced by a choice of Δt would depend on contributions from approximation error from all interaction types. While chemical kinetics has developed several methods for dealing with reactions occurring on very different characteristic time scales (see [69] for an example), it is not clear what is the best way to deal with separation of time scale in

the ABM. A naive approach would involve slower interaction terms being updated only at some integer multiple of Δt, but further work should be undertaken to characterize the best way to choose such an updating scheme suitable for multiple time-scales, with the caveat that appropriate schemes would be highly problem dependent.

Our method is not restricted to pure jump stochastic processes. One generalization of a pure jump process is to assume that the system can be described by coupling continuous state variables to the discrete variables such that between jump times, the continuous part evolves according to a differential equation. Such systems are known as piecewise deterministic Markov processes (PDMP) when the distribution of inter-event times is given by an nonhomogeneous Poisson process whose intensity may depend on the continuous variables [161]. This model representation may be natural to simulate multi-scale models, where within-host immune dynamics follow a differential equation model, like the method proposed in [51] to model host-pathogen interaction. In the case where the deterministic dynamics are fully internal to each agent the implementation simply involves solving a differential equation for each agent to sample their next state and time. More complex internal dynamics, such as allowing the continuous state to follow a stochastic differential equation, can be implemented in the same way, as long as the next jump time for each agent's discrete state is computable from the solution of the process (for example, from a first hitting time). These models can be useful to integrate results from medical survival analysis [2].

The computational methods for epidemiological problems have borrowed heavily from other computational disciplines, but some of the unique features of epidemiological systems would benefit innovation and algorithms to addressing the kinds of problems that arise. In particular, for simulation of complex epidemiological models, agent-based models are a useful alternative to other modeling techniques, and can be both flexible and extensible. In this work we have presented a generic algorithm to sample trajectories from agent based models, for agents which may experience dependent or internal events, parameterized by hazard functions. Approximation of a subset of event hazards, those that depend on multiple agents' state, speeds up simulation. A key contribution of our ABM simulation technique is that it will converge to a continuous-time stochastic jump process in the limit of small step sizes. Our intention is not to argue that models without a limiting interpretation are wrong, but that in many practical cases being able to connect the ABM to a well defined stochastic process is valuable, such as for parameterization from results of survival analysis or for verification of simulation software. Construction from continuous-time hazards means that ABMs developed in this framework can be more clearly linked to other results in stochastic simulation, easing inclusion of various elaborations relevant to epidemiological simulation, such as time-varying hazards [101, 31]. We hope that the simplicity of the method presented in this paper can help researchers respond more quickly to urgent situations where stochastic models are required.

Bibliography

[1] Copernicus Climate Change Service (C3S). "ERA5: Fifth generation of ECMWF atmospheric reanalyses of the global climate". In: (2017).

[2] Odd Aalen, Ornulf Borgan, and Hakon Gjessing. *Survival and event history analysis: a process point of view*. Springer Science & Business Media, 2008.

[3] Adriana Adolfi et al. "Efficient population modification gene-drive rescue system in the malaria mosquito Anopheles stephensi". In: *bioRxiv* (2020).

[4] Linda JS Allen. "A primer on stochastic epidemic models: Formulation, numerical simulation, and analysis". In: *Infectious Disease Modelling* 2.2 (2017), pp. 128–142.

[5] Linda JS Allen. "Some discrete-time SI, SIR, and SIS epidemic models". In: *Mathematical biosciences* 124.1 (1994), pp. 83–105.

[6] Per Kragh Andersen and Niels Keiding. "Multi-state models for event history analysis". In: *Statistical methods in medical research* 11.2 (2002), pp. 91–115.

[7] David F Anderson. "A modified next reaction method for simulating chemical systems with time dependent propensities and delays". In: *The Journal of chemical physics* 127.21 (2007), p. 214107.

[8] David F. Anderson. "Incorporating postleap checks in tau-leaping". In: *Journal of Chemical Physics* 128.5 (2008). ISSN: 00219606. DOI: 10.1063/1.2819665.

[9] Hakan Andersson and Tom Britton. *Stochastic epidemic models and their statistical analysis*. Vol. 151. Springer Science & Business Media, 2012.

[10] Ioannis Andrianakis et al. "Bayesian history matching of complex infectious disease models using emulation: a tutorial and a case study on HIV in Uganda". In: *PLoS Comput Biol* 11.1 (2015), e1003968.

[11] Janis Antonovics. "Transmission dynamics: critical questions and challenges". In: *Philosophical Transactions of the Royal Society B: Biological Sciences* 372.1719 (2017), p. 20160087.

[12] Norman TJ Bailey. "A simple stochastic epidemic". In: *Biometrika* (1950), pp. 193–202.

[13] Frank Ball. "A unified approach to the distribution of total size and total area under the trajectory of infectives in epidemic models". In: *Advances in Applied Probability* 18.2 (1986), pp. 289–310.

[14] Sven Banisch. *Markov chain aggregation for agent-based models*. Springer, 2015.

[15] Douglas Bates and Martin Maechler. *Matrix: Sparse and Dense Matrix Classes and Methods*. R package version 1.2-17. 2019. URL: https://CRAN.R-project.org/package=Matrix.

[16] M N Bayoh and S W Lindsay. "Effect of temperature on the development of the aquatic stages of Anopheles gambiae sensu stricto (Diptera: Culicidae)". en. In: *Bull. Entomol. Res.* 93.5 (Oct. 2003), pp. 375–381.

[17] Lindsay M Beck-Johnson et al. "The importance of temperature fluctuations in understanding mosquito population dynamics and malaria risk". en. In: *R Soc Open Sci* 4.3 (Mar. 2017), p. 160969.

[18] W L Bidlingmayer. "The measurement of adult mosquito population changes–some considerations." In: *J Am Mosq Control Assoc* (1985).

[19] Mogens Bladt and Bo Friis Nielsen. *Matrix-Exponential Distributions in Applied Probability*. Vol. 81. 2017. ISBN: 978-1-4939-7047-6. DOI: 10.1007/978-1-4939-7049-0. URL: http://link.springer.com/10.1007/978-1-4939-7049-0.

[20] Luca Bortolussi and Jane Hillston. "Fluid approximation of CTMC with deterministic delays". In: *Proceedings - 2012 9th International Conference on Quantitative Evaluation of Systems, QEST 2012* (2012), pp. 53–62. DOI: 10.1109/QEST.2012.13.

[21] Luca Bortolussi et al. "Continuous approximation of collective system behaviour: A tutorial". In: *Performance Evaluation* 70.5 (May 2013), pp. 317–349. ISSN: 01665316. DOI: 10.1016/j.peva.2013.01.001. URL: http://linkinghub.elsevier.com/retrieve/pii/S0166531613000023.

[22] Oliver J Brady et al. "Vectorial capacity and vector control: reconsidering sensitivity to parameters for malaria elimination." In: *Transactions of the Royal Society of Tropical Medicine and Hygiene* (2016).

[23] Paul Bratley, Bennet Fox, and Linus Schrage. *A guide to simulation*. Springer Science & Business Media, 2011.

[24] Pierre Brémaud. *Markov chains : Gibbs fields, Monte Carlo simulation, and queues*. 1999. ISBN: 0387985093 (acid-free paper).

[25] Carles Bretó et al. "Time series analysis via mechanistic models". In: *The Annals of Applied Statistics* 3.1 (2009), pp. 319–348.

[26] Tobias Brett and Tobias Galla. "Gaussian approximations for stochastic systems with delay: Chemical Langevin equation and application to a Brusselator system". In: *Journal of Chemical Physics* 140.12 (2014). ISSN: 00219606. DOI: 10.1063/1.4867786.

[27] Peter Buchholz, Jan Kriege, and Iryna Felko. *Input Modeling with Phase-Type Distributions and Markov Models*. 2014. ISBN: 978-3-319-06673-8. DOI: 10.1007/978-3-319-06674-5. URL: http://link.springer.com/10.1007/978-3-319-06674-5.

[28] Rebeca Carballar-Lejarazú et al. "Next-generation gene drive for population modification of the malaria vector mosquito," en. In: *Proc. Natl. Acad. Sci. U. S. A.* 117.37 (Sept. 2020), pp. 22805–22814.

[29] Richard Carter. "Spatial simulation of malaria transmission and its control by malaria transmission blocking vaccination". In: *International Journal for Parasitology* (2002).

[30] Richard Carter, K N Mendis, and D Roberts. "Spatial targeting of interventions against malaria." In: *Bull World Health Organ* (2000).

[31] Bernard Cazelles, Clara Champagne, and Joseph Dureau. "Accounting for non-stationarity in epidemiology by embedding time-varying parameters in stochastic models". In: *PLoS computational biology* 14.8 (2018), e1006211.

[32] Jackson Champer et al. "A toxin-antidote CRISPR gene drive system for regional population modification". en. In: *Nat. Commun.* 11.1 (Feb. 2020), p. 1082.

[33] Jackson Champer et al. "Reducing resistance allele formation in CRISPR gene drive". en. In: *Proc. Natl. Acad. Sci. U. S. A.* 115.21 (May 2018), pp. 5522–5527.

[34] Laura Cooper et al. "Pareto rules for malaria super-spreaders and super-spreading". en. In: *Nat. Commun.* 10.1 (Sept. 2019), p. 3939.

[35] Forrest W. Crawford, Lam Si Tung Ho, and Marc A. Suchard. "Computational methods for birth-death processes". In: *Wiley Interdisciplinary Reviews: Computational Statistics* 10.2 (2018), pp. 1–22. ISSN: 19390068. DOI: 10.1002/wics.1423.

[36] John N Darroch and Eugene Seneta. "On quasi-stationary distributions in absorbing continuous-time finite Markov chains". In: *Journal of Applied Probability* (1967).

[37] John N Darroch and Eugene Seneta. "On quasi-stationary distributions in absorbing discrete-time finite Markov chains". In: *Journal of Applied Probability* 2.1 (1965), pp. 88–100.

[38] T H Davey and R M Gordon. "The estimation of the density of infective anophelines as a method of calculating the relative risk of inoculation with malaria from different species or in different localities". In: *Ann Trop Med Parasitol* (1933).

[39] Jean-Marc O Depinay et al. "A simulation model of African Anopheles ecology and population dynamics for the analysis of malaria transmission". en. In: *Malar. J.* 3 (July 2004), p. 29.

[40] Anne Deredec, H Charles J Godfray, and Austin Burt. "Requirements for effective malaria control with homing endonuclease genes". In: *Proceedings of the National Academy of Sciences* 108.43 (2011), E874–E880.

[41] Luc Devroye. "Nonuniform random variate generation". In: *Handbooks in operations research and management science* 13 (2006), pp. 83–121.

[42] Nico Dissmeyer. "Conditional Modulation of Biological Processes by Low-Temperature Degrons". en. In: *Methods Mol. Biol.* 1669 (2017), pp. 407–416.

[43] Philip A Eckhoff and Edward A Wenger. "The EMOD Individual-Based Model". In: *Spatial Agent-Based Simulation Modeling in Public Health: Design, Implementation, and Applications for Malaria Epidemiology* (2016), pp. 185–208.

[44] Peter G Fennell, Sergey Melnik, and James P Gleeson. "Limitations of discrete-time approaches to continuous-time contagion dynamics". In: *Physical Review E* 94.5 (2016), p. 052125.

[45] Woodbridge A Foster. "Mosquito sugar feeding and reproductive energetics". In: *Annual review of entomology* 40.1 (1995), pp. 443–474.

[46] Sylvain Gandon et al. "Forecasting epidemiological and evolutionary dynamics of infectious diseases". In: *Trends in ecology & evolution* 31.10 (2016), pp. 776–788.

[47] Valentino M Gantz and Ethan Bier. "The dawn of active genetics". en. In: *Bioessays* 38.1 (Jan. 2016), pp. 50–63.

[48] C Garrett-Jones. "Prognosis for interruption of malaria transmission through assessment of the mosquito's vectorial capacity." In: *Nature* (1964).

[49] C Garrett-Jones. "The human blood index of malaria vectors in relation to epidemiological assessment." In: *Bull World Health Organ* (1964).

[50] Michelle L Gatton et al. "The importance of mosquito behavioural adaptations to malaria control in Africa." In: *Evolution* (2013).

[51] Michael A Gilchrist and Akira Sasaki. "Modeling host-parasite coevolution: a nested approach based on mechanistic models". In: *Journal of Theoretical Biology* 218.3 (2002), pp. 289–308.

[52] Daniel T Gillespie. "Monte Carlo simulation of random walks with residence time dependent transition probability rates". In: *Journal of Computational Physics* 28.3 (1978), pp. 395–407.

[53] Daniel T Gillespie. "Stochastic simulation of chemical kinetics". In: *Annu. Rev. Phys. Chem.* 58 (2007), pp. 35–55.

[54] Daniel T Gillespie. *The multivariate Langevin and Fokker–Planck equations*. 1996.

[55] Daniel T. Gillespie. "Approximate accelerated stochastic simulation of chemically reacting systems". In: *The Journal of chemical physics* 115.4 (2001), pp. 1716–1733.

[56] Daniel T. Gillespie. "Deterministic limit of stochastic chemical kinetics". In: *The Journal of Physical Chemistry B* 113.6 (2009), pp. 1640–1644.

[57] Daniel T. Gillespie. "Exact stochastic simulation of coupled chemical reactions". In: *The journal of physical chemistry* 81.25 (1977), pp. 2340–2361.

[58] Daniel T. Gillespie. "The multivariate Langevin and Fokker–Planck equations". In: *American Journal of Physics* 64.10 (2005), pp. 1246–1257. ISSN: 0002-9505. DOI: 10.1119/1.18387.

[59] Peter W. Glynn. "A GSMP Formalism for Discrete Event Systems". In: *Proceedings of the IEEE* (1989). ISSN: 15582256. DOI: 10.1109/5.21067.

[60] P J Goss and J Peccoud. "Quantitative modeling of stochastic systems in molecular biology by using stochastic Petri nets". en. In: *Proc. Natl. Acad. Sci. U. S. A.* 95.12 (June 1998), pp. 6750–6755.

[61] Jamie T Griffin et al. *Reducing Plasmodium falciparum Malaria Transmission in Africa: A Model-Based Evaluation of Intervention Strategies*. 2010.

[62] Anja Gronewold and Michael Sonnenschein. *Event-based modelling of ecological systems with asynchronous cellular automata*. 1998.

[63] Weidong Gu et al. "Source reduction of mosquito larval habitats has unexpected consequences on malaria transmission". In: *Proceedings of the National Academy of Sciences* 103.46 (2006), pp. 17560–17563.

[64] Carlos A Guerra et al. "A global assembly of adult female mosquito mark-release-recapture data to inform the control of mosquito-borne pathogens." In: *Parasites & Vectors* (2014).

[65] Hoshin V Gupta and Saman Razavi. "Revisiting the basis of sensitivity analysis for dynamical earth system models". In: *Water Resources Research* 54.11 (2018), pp. 8692–8717.

[66] Peter J Haas. *Stochastic Petri Nets: Modelling, Stability, Simulation*. en. Springer Science & Business Media, Apr. 2006.

[67] Lewis Wendell Hackett. *Malaria in Europe*. London, Oxford University Press, 1937.

[68] Penny A Hancock and H Charles J Godfray. "Application of the lumped age-class technique to studying the dynamics of malaria-mosquito-human interactions". In: *Malaria journal* 6.1 (2007), p. 98.

[69] Eric L Haseltine and James B Rawlings. "Approximate simulation of coupled fast and slow reactions for stochastic chemical kinetics". In: *The Journal of chemical physics* 117.15 (2002), pp. 6959–6969.

[70] Simon I Hay et al. "Global, regional, and national disability-adjusted life-years (DALYs) for 333 diseases and injuries and healthy life expectancy (HALE) for 195 countries and territories, 1990-2016: a systematic analysis for the Global Burden of Disease Study 2016". In: *The Lancet* 390.10100 (Sept. 2017), pp. 1260–1344.

[71] Eva Herrmann and Martin Maechler. *lokern: Kernel Regression Smoothing with Local or Global Plug-in Bandwidth*. 2016. URL: https://cran.r-project.org/web/packages/lokern/index.html.

[72] Thomas Hladish et al. "EpiFire: An open source C++ library and application for contact network epidemiology". In: *BMC bioinformatics* 13.1 (2012), pp. 1–12.

[73] Lam Si Tung Ho et al. "Birth/birth-death processes and their computable transition probabilities with biological applications". In: *Journal of Mathematical Biology* 76.4 (2018), pp. 911–944. ISSN: 14321416. DOI: 10.1007/s00285-017-1160-3. arXiv: 1603.03819.

[74] Lam Si Tung Ho et al. *MultiBD: Multivariate Birth-Death Processes*. R package version 0.2.0. 2016. URL: https://CRAN.R-project.org/package=MultiBD.

[75] GM Hornberger and Robert C Spear. "Eutrophication in Peel Inlet—I. The problem-defining behavior and a mathematical model for the phosphorus scenario". In: *Water Research* 14.1 (1980), pp. 29–42.

[76] Thomas House, Joshua V. Ross, and David Sirl. "How big is an outbreak likely to be? Methods for epidemic final-size calculation". In: *Proceedings of the Royal Society A: Mathematical, Physical and Engineering Sciences* 469.2150 (2013). ISSN: 14712946. DOI: 10.1098/rspa.2012.0436.

[77] John H Huber et al. "Quantitative, model-based estimates of variability in the generation and serial intervals of Plasmodium falciparum malaria". In: *Malaria journal* 15.1 (2016), pp. 1–12.

[78] Paul J Hurtado and Adam S Kirosingh. "Generalizations of the 'Linear Chain Trick': incorporating more flexible dwell time distributions into mean field ODE models". In: *Journal of mathematical biology* 79.5 (2019), pp. 1831–1883.

[79] INSEED. *Annuaire Statistique des Comores. Moroni, Union of the Comoros*. National Institute of Statistics, Economic, and Demographic Studies (INSEED), 2015.

[80] Stephanie L James et al. *Pathway to Deployment of Gene Drive Mosquitoes as a Potential Biocontrol Tool for Elimination of Malaria in Sub-Saharan Africa: Recommendations of a Scientific Working Group †*. 2018.

[81] Stephanie L James et al. "Toward the Definition of Efficacy and Safety Criteria for Advancing Gene Drive-Modified Mosquitoes to Field Testing". en. In: *Vector Borne Zoonotic Dis.* 20.4 (Apr. 2020), pp. 237–251.

[82] Joshua Kaminsky et al. "Perfect counterfactuals for epidemic simulations". In: *Philosophical Transactions of the Royal Society B* 374.1776 (2019), p. 20180279.

[83] Nikolay P Kandul et al. "Transforming insect population control with precision guided sterile males with demonstration in flies". In: *Nature communications* 10.1 (2019), p. 84.

[84] Su Yun Kang et al. "Heterogeneous exposure and hotspots for malaria vectors at three study sites in Uganda". In: *Gates Open Research* (2018).

[85] Matt J Keeling et al. "Dynamics of the 2001 UK foot and mouth epidemic: stochastic dispersal in a heterogeneous landscape". In: *Science* 294.5543 (2001), pp. 813–817.

[86] Matthew J Keeling and Joshua V Ross. "On methods for studying stochastic disease dynamics". In: *Journal of the Royal Society Interface* 5.19 (2008), pp. 171–181.

[87] David G Kendall. "Deterministic and stochastic epidemics in closed populations". In: *Proc. 3rd Berkeley Symp. Math. Statist. Prob*. Vol. 4. 1956, pp. 149–165.

[88] David G. Kendall. "An Artificial Realization of a Simple "Birth-And-Death" Process". In: *Journal of the Royal Statistical Society: Series B (Methodological)* 12.1 (1950), pp. 116–119. ISSN: 0035-9246. DOI: 10.1111/j.2517-6161.1950.tb00048.x.

[89] William Ogilvy Kermack and Anderson G McKendrick. "Contributions to the mathematical theory of epidemics—I". In: *Philosophical Transactions of the Royal Society A: Mathematical, Physical and Engineering Sciences* 115.772 (1927), pp. 700–721.

[90] William Ogilvy Kermack and Anderson G McKendrick. "Contributions to the mathematical theory of epidemics. II.—The problem of endemicity". In: *Philosophical Transactions of the Royal Society A: Mathematical, Physical and Engineering Sciences* 138.834 (1932), pp. 55–83.

[91] Gerry F Killeen et al. "A simplified model for predicting malaria entomologic inoculation rates based on entomologic and parasitologic parameters relevant to control". In: *American Journal of Tropical Medicine and Hygiene* (2000).

[92] Gerry F Killeen et al. "Made-to-measure malaria vector control strategies: rational design based on insecticide properties and coverage of blood resources for mosquitoes". In: *Malaria journal* 13.1 (2014), pp. 1–9.

[93] John F.C. Kingman. "Markov Population Processes". In: *J. Appl. Probab.* 6.1 (1969), pp. 1–18. ISSN: 0021-9002. URL: http://www.jstor.org/stable/3212273.

[94] Samson S Kiware et al. "Attacking the mosquito on multiple fronts: Insights from the Vector Control Optimization Model (VCOM) for malaria elimination." In: *PLoS ONE* (2017).

[95] Adam J Kucharski et al. "Transmission dynamics of Zika virus in island populations: a modelling analysis of the 2013–14 French Polynesia outbreak". In: *PLoS neglected tropical diseases* 10.5 (2016), e0004726.

[96] Thomas G. Kurtz. "Solutions of Ordinary Differential Equations as Limits of Pure Jump Markov Processes". In: *Journal of Applied Probability* 7.1 (1970), p. 49. ISSN: 00219002. DOI: 10.2307/3212147. URL: http://www.jstor.org/stable/3212147?origin=crossref.

[97] Kyros Kyrou et al. "A CRISPR-Cas9 gene drive targeting doublesex causes complete population suppression in caged Anopheles gambiae mosquitoes". en. In: *Nat. Biotechnol.* 36.11 (Dec. 2018), pp. 1062–1066.

[98] L. F. Lafuerza and R. Toral. "Stochastic description of delayed systems". In: *Philosophical Transactions of the Royal Society A: Mathematical, Physical and Engineering Sciences* 371.1999 (2013). ISSN: 1364503X. DOI: 10.1098/rsta.2012.0458.

[99] Gilbert Le Goff et al. "Field evaluation of seasonal trends in relative population sizes and dispersal pattern of Aedes albopictus males in support of the design of a sterile male release strategy". en. In: *Parasit. Vectors* 12.1 (Feb. 2019), p. 81.

[100] Lawrence M Leemis and Stephen Keith Park. *Discrete-event simulation: A first course*. Pearson Prentice Hall Upper Saddle River, NJ, 2006.

[101] Geoffrey Legault and Brett A. Melbourne. "Accounting for environmental change in continuous-time stochastic population models". In: *Theoretical Ecology* 12.1 (2019), pp. 31–48. ISSN: 18741746. DOI: 10.1007/s12080-018-0386-z.

[102] Ming Li et al. "Development of a confinable gene drive system in the human disease vector". en. In: *Elife* 9 (Jan. 2020).

[103] Alun L Lloyd, J Zhang, and A M Root. "Stochasticity and heterogeneity in host-vector models". In: *Journal of The Royal Society Interface* (2007).

[104] Brian O Ma and Bernard D Roitberg. "The role of resource availability and state-dependence in the foraging strategy of blood-feeding mosquitoes". In: *Evolutionary Ecology Research* 10.8 (2008), pp. 1111–1130.

[105] George Macdonald. "The analysis of the sporozoite rate". In: *Trop Dis Bull* (1952).

[106] George Macdonald. *The Epidemiology and Control of Malaria*. en. 1957.

[107] Luca Marchetti, Corrado Priami, and Vo Hong Thanh. *Simulation algorithms for computational systems biology*. Springer, 2017.

[108] John M Marshall, Anna Buchman, Omar S Akbari, et al. "Overcoming evolved resistance to population-suppressing homing-based gene drives". In: *Scientific reports* 7.1 (2017), p. 3776.

[109] Maia Martcheva. *An introduction to mathematical epidemiology*. Vol. 61. Springer, 2015.

[110] Deborah G Mayo. *Statistical inference as severe testing*. Cambridge: Cambridge University Press, 2018.

[111] F Ellis McKenzie et al. "Strain theory of malaria: the first 50 years". In: *Advances in parasitology* 66 (2008), pp. 1–46.

[112] Arnaud Le Menach et al. "The unexpected importance of mosquito oviposition behaviour for malaria: non-productive larval habitats can be sources for malaria transmission". In: *Malaria Journal* (2005).

[113] Scott Meyers. *Effective modern C++: 42 specific ways to improve your use of C++ 11 and C++ 14*. O'Reilly Media, Inc., 2014.

[114] Erin A Mordecai et al. "Thermal biology of mosquito-borne disease". en. In: *Ecol. Lett.* 22.10 (Oct. 2019), pp. 1690–1708.

[115] Stephen Munga et al. "Effects of larval competitors and predators on oviposition site selection of Anopheles gambiae sensu stricto." In: *Journal of medical entomology* (2006). ISSN: 0022-2585.

[116] Simon M Muriu et al. "Larval density dependence in Anopheles gambiae s.s., the major African vector of malaria". en. In: *J. Anim. Ecol.* 82.1 (Jan. 2013), pp. 166–174.

[117] Charleston Noble et al. "Daisy-chain gene drives for the alteration of local populations". en. In: *Proc. Natl. Acad. Sci. U. S. A.* 116.17 (Apr. 2019), pp. 8275–8282.

[118] Georg Oberhofer, Tobin Ivy, and Bruce A Hay. "Cleave and Rescue, a novel selfish genetic element and general strategy for gene drive". en. In: *Proc. Natl. Acad. Sci. U. S. A.* 116.13 (Mar. 2019), pp. 6250–6259.

[119] E Onori and B Grab. "Indicators for the Forecasting of Malaria Epidemics". In: *Bulletin of the World Health Organization* (1980).

[120] T Alex Perkins et al. "Heterogeneity, mixing, and the spatial scales of mosquito-borne pathogen transmission." In: *PLoS Computational Biology* (2013).

[121] Daniel A Pfeffer et al. *malariaAtlas: an R interface to global malariometric data hosted by the Malaria Atlas Project*. 2018.

[122] Thomas A A Prowse et al. "Dodging silver bullets: good CRISPR gene-drive design is critical for eradicating exotic vertebrates". en. In: *Proc. Biol. Sci.* 284.1860 (Aug. 2017).

[123] R Core Team. *R: A Language and Environment for Statistical Computing*. R Foundation for Statistical Computing. Vienna, Austria, 2018. URL: `https://www.R-project.org/`.

[124] Saman Razavi and Hoshin V Gupta. "A new framework for comprehensive, robust, and efficient global sensitivity analysis: 1. Theory". In: *Water Resources Research* 52.1 (2016), pp. 423–439.

[125] Robert C Reiner Jr et al. "A systematic review of mathematical models of mosquito-borne pathogen transmission: 1970–2010". In: *Journal of The Royal Society Interface* 10.81 (2013), p. 20120921.

[126] Marguerite Robinson et al. *A Model for a Chikungunya Outbreak in a Rural Cambodian Setting: Implications for Disease Control in Uninfected Areas*. 2014.

[127] Bernard D. Roitberg, Edward B. Mondor, and Jabus G A Tyerman. "Pouncing spider, flying mosquito: Blood acquisition increases predation risk in mosquitoes". In: *Behavioral Ecology* (2003). ISSN: 10452249. DOI: 10.1093/beheco/arg055.

[128] Ronald Ross. *Report on the Prevention of Malaria in Mauritius*. Waterlow & Sons Limited, 1908.

[129] Sir Ronald Ross. *The Prevention of Malaria*. en. 1910.

[130] Héctor M Sánchez C et al. "MGDrivE: A modular simulation framework for the spread of gene drives through spatially explicit mosquito populations". In: *Methods in Ecology and Evolution* 11.2 (2020), pp. 229–239.

[131] Kevin R Sanft et al. "StochKit2: software for discrete stochastic simulation of biochemical systems with events". In: *Bioinformatics* 27.17 (2011), pp. 2457–2458.

[132] Simo Särkkä and Arno Solin. *Applied stochastic differential equations*. Vol. 10. Cambridge University Press, 2019.

[133] Allan Saul. "Zooprophylaxis or zoopotentiation: the outcome of introducing animals on vector transmission is highly dependent on the mosquito mortality while searching". In: *Malaria Journal* 2.1 (2003), p. 32.

[134] Ralph Scherer. *PropCIs: Various Confidence Interval Methods for Proportions*. R package version 0.3-0. 2018. URL: https://CRAN.R-project.org/package=PropCIs.

[135] Thomas Sellke. "On the asymptotic distribution of the size of a stochastic epidemic". In: *Journal of Applied Probability* 20.2 (1983), pp. 390–394.

[136] John B Silver. *Mosquito Ecology: Field Sampling Methods*. Springer, 2008.

[137] David L Smith, Jonathan Dushoff, and F Ellis McKenzie. "The risk of a mosquito-borne infectionin a heterogeneous environment". In: *PLoS Biol* 2.11 (2004), e368.

[138] David L Smith and F Ellis McKenzie. "Statics and dynamics of malaria infection in Anopheles mosquitoes". In: *Malaria journal* 3.1 (2004), p. 13.

[139] David L Smith et al. "Recasting the theory of mosquito-borne pathogen transmission dynamics and control". In: *Transactions of the Royal Society of Tropical Medicine and Hygiene* 108.4 (2014), pp. 185–197.

[140] David L Smith et al. "Revisiting the basic reproductive number for malaria and its implications for malaria control." In: *PLoS Biology* (2007).

[141] David L Smith et al. "Ross, Macdonald, and a theory for the dynamics and control of mosquito-transmitted pathogens". In: *PLoS pathogens* 8.4 (2012), e1002588.

[142] Karline Soetaert, Thomas Petzoldt, and R. Woodrow Setzer. "Solving Differential Equations in R : Package deSolve". In: *Journal of Statistical Software* (2010). ISSN: 1548-7660. DOI: 10.18637/jss.v033.i09.

[143] Robert C Spear, Thomas M Grieb, and Nong Shang. "Parameter uncertainty and interaction in complex environmental models". In: *Water Resources Research* 30.11 (1994), pp. 3159–3169.

[144] Robert C Spear and GM Hornberger. "Eutrophication in peel inlet—II. Identification of critical uncertainties via generalized sensitivity analysis". In: *Water research* 14.1 (1980), pp. 43–49.

[145] Robert C Spear et al. "Disease transmission models for public health decision making: toward an approach for designing intervention strategies for Schistosomiasis japonica." In: *Environmental health perspectives* 110.9 (2002), pp. 907–915.

[146] Steven T Stoddard et al. "House-to-house human movement drives dengue virus transmission". en. In: *Proc. Natl. Acad. Sci. U. S. A.* 110.3 (Jan. 2013), pp. 994–999.

[147] Erin M Stuckey, Thomas A Smith, and Nakul Chitnis. "Estimating malaria transmission through mathematical models". In: *Trends in parasitology* 29.10 (2013), pp. 477–482.

[148] Vo Hong Thanh et al. "Incorporating extrinsic noise into the stochastic simulation of biochemical reactions: A comparison of approaches". In: *Journal of Chemical Physics* 148.6 (2018). ISSN: 00219606. DOI: 10.1063/1.5016338. URL: http://dx.doi.org/10.1063/1.5016338.

[149] Raúl Toral and Pere Colet. *Stochastic numerical methods: an introduction for students and scientists*. John Wiley & Sons, 2014.

[150] Helen J Wearing and Pejman Rohani. "Ecological and immunological determinants of dengue epidemics". en. In: *Proc. Natl. Acad. Sci. U. S. A.* 103.31 (Aug. 2006), pp. 11802–11807.

[151] Michael T White et al. "Modelling the impact of vector control interventions on Anopheles gambiae population dynamics". en. In: *Parasit. Vectors* 4 (July 2011), p. 153.

[152] Darren J Wilkinson. *Stochastic Modelling for Systems Biology, Third Edition*. 2018.

[153] Daniel Williamson. "Exploratory ensemble designs for environmental models using k-extended Latin Hypercubes". In: *Environmetrics* 26.4 (2015), pp. 268–283.

[154] Simon N Wood. "Statistical inference for noisy nonlinear ecological dynamic systems". In: *Nature* 466.7310 (2010), pp. 1102–1104.

[155] Sean L Wu et al. "MGDrivE 2: A simulation framework for gene drive systems incorporating seasonality and epidemiological dynamics". In: *bioRxiv* (2020).

[156] Sean L Wu et al. *MGDrivE2: Mosquito Gene Drive Explorer 2*. R package version 1.0.1. 2020. URL: https://CRAN.R-project.org/package=MGDrivE2.

[157] Sean L Wu et al. "Vector bionomics and vectorial capacity as emergent properties of mosquito behaviors and ecology". In: *PLoS computational biology* 16.4 (2020), e1007446.

[158] Xiang-Ru Shannon Xu et al. "Active Genetic Neutralizing Elements for Halting or Deleting Gene Drives". en. In: *Mol. Cell* (Sept. 2020).

[159] Alpha S Yaro et al. "The distribution of hatching time in Anopheles gambiae". en. In: *Malar. J.* 5 (Mar. 2006), p. 19.

[160] Martin P Zeidler et al. "Temperature-sensitive control of protein activity by conditionally splicing inteins". en. In: *Nat. Biotechnol.* 22.7 (July 2004), pp. 871–876.

[161] S. Zeiser et al. "Simulation of genetic networks modelled by piecewise deterministic Markov processes". In: *IET Systems Biology* 2.3 (2008), pp. 113–135. ISSN: 17518849. DOI: 10.1049/iet-syb:20070045.

Appendix A

MBDETES: Duration of Feeding Cycle

To compute the probability distribution of the duration of a feeding cycle, we reformulated the MBDETES cohort differential equation model as a model of possible behavioral state transitions taken between an initial post-prandial resting state R_1, and a second post-prandial resting state R_2, accounting for state-dependent mortality in between (Equation A.1). The state notation is the same as used in the main text, F is searching for blood host, B is bloodfeeding, L is searching for oviposition site, and O is oviposition. The model follows all possible histories of a mosquito as it leaves R_1, to either of two absorbing states, R_2, or death D.

Because we assume that mosquitoes blood feed and oviposit only once per gonotrophic cycle, the distribution of the length of time needed for surviving mosquitoes to transition between R_1 and R_2 is equal to the distribution for the duration of a feeding cycle.

The state vector $\{R_1(t), L(t), O(t), F(t), B(t), R_2(t), D(t)\}$ is a probability mass function (PMF) describing the probability for a mosquito to belong to each state at any time $t \geq 0$. The set of differential equations below (also in Figure A.1) describes the flow of probability (Kolmogorov forwards equations) between the states as time passes. The trajectories from solving the equations over time thus gives the time-dependent PMF of a mosquito to be in each state.

To solve the equations we set $\{R_1(0) = 1, L(0) = 0, O(0) = 0, F(0) = 0, B(0) = 0, R_2(0) = 0, D(0) = 0\}$. Because dead mosquitoes go to compartment D, probability mass is conserved. Mosquitoes dwell in R_1 on average for some time t_R prior to leaving; but if the delay was fixed rather than exponentially distributed one could partition the probability instead across $\{L(0) = R_1(0)P_{RL}, O = R_1(0)P_{RO}, F = R_1(0)P_{RF}, B = R_1(0)P_{RB}, D = R_1(0)P_{RD}\}$, and simply add the fixed delay time to the solution output. To get the probability density function for the time to complete a feeding cycle, conditional on survival, simply renormalize such that the density at time t is $\frac{R_2(t)}{1-\int_0^\infty D(\tau)d\tau} = \frac{R_2(t)}{R_2(\infty)}$. Because R_2 and D are the only two absorbing states, $1 - R_2(\infty) = D(\infty)$.

$$\begin{bmatrix} dR_1/dt \\ dL/dt \\ dO/dt \\ dF/dt \\ dB/dt \\ dR_2/dt \\ dD/dt \end{bmatrix} = \begin{bmatrix} -1 & 0 & 0 & 0 & 0 & 0 & 0 \\ P_{RL} & (P_{LL}-1) & P_{OL} & 0 & 0 & 0 & 0 \\ P_{RO} & P_{LO} & (P_{OO}-1) & 0 & 0 & 0 & 0 \\ P_{RF} & 0 & P_{OF} & (P_{FF}-1) & P_{BF} & 0 & 0 \\ P_{RB} & 0 & P_{OB} & P_{FB} & (P_{BB}-1) & 0 & 0 \\ 0 & 0 & 0 & 0 & P_{BR} & 0 & 0 \\ P_{RD} & P_{LD} & P_{OD} & P_{FD} & P_{BD} & 0 & 0 \end{bmatrix} \begin{bmatrix} R_1/t_R \\ L/t_L \\ O/t_O \\ F/t_F \\ B/t_B \\ R_2 \\ D \end{bmatrix} \tag{A.1}$$

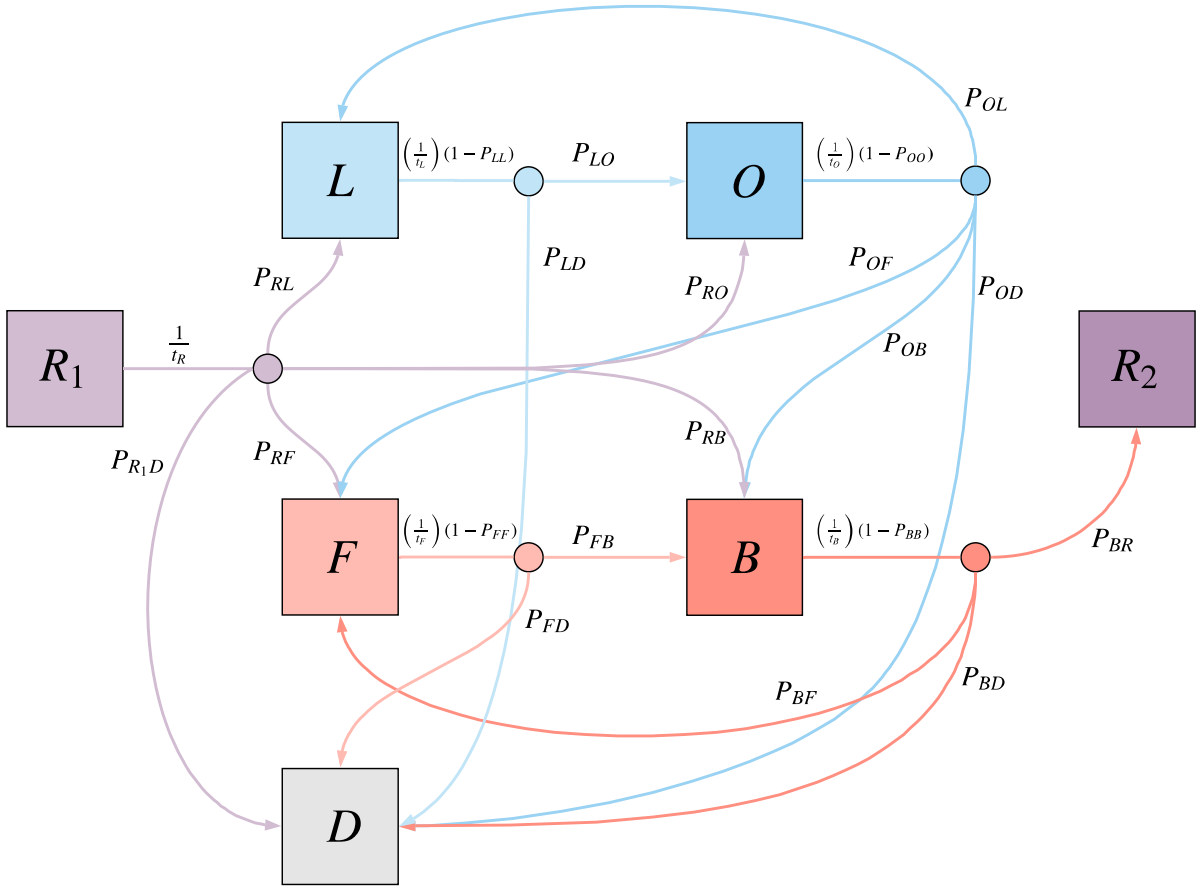

Figure A.1: Graphical representation of Equation A.1, edges are colored by their origin compartment, and correspond to elements in the matrix ODE.

Appendix B

MGDrivE 2: Description of the Modeling Framework

B.1 Lifecycle Model

The lifecycle model is similar to the discrete time ecology module used in **MGDrivE** [130]. Major differences include the switch to continuous time and replacement of fixed, constant delays with Erlang distributed delays in aquatic life stages. This change means that, whereas **MGDrivE**'s deterministic model was formulated as a set of delay difference equations, **MGDrivE 2**'s deterministic model is a set of ordinary differential equations (ODEs) (using the "linear chain trick" to simulate Erlang-distributed delays, [78]).

Similar to **MGDrivE**, the lifecycle model includes egg (E), larval (L), and pupal (P) aquatic stages. Upon emergence from P, adult mosquitoes are assigned a sex, the probability of which may depend on genotype. Upon emergence, females (F) become mated in the presence of male mosquitoes (M), and oviposit at an age-independent (though possibly time-dependent) rate until they die. If there are no adult males, newly emerging females transfer to an unmated adult female (U) compartment, where they remain until death or successful mating if males become available.

The system of ODEs describing the deterministic lifecycle model are solved at their non-trivial equilbrium to provide initial conditions for simulations in **MGDrivE 2**. These ODEs are a limiting case of the stochastic continuous-time Markov chain (CTMC) model, when populations are large (for technical conditions, see [96]). In our presentation of the ODEs and their equilibrium solutions, we ignore indexing by genotype because, for most simulations, the equilibrium solution corresponds to a baseline scenario prior to releases of modified mosquitoes, where mosquito populations are composed solely of wild-types. These equations also ignore indexing by node. We use (n_E, n_L, n_P) to denote the number of sub-stages in each aquatic stage (the Erlang shape parameter). Subscript i refers to any particular sub-stage, such that eggs are denoted E_i, larvae as L_i, pupae as P_i, and N_F, N_M the mated adult female and male populations, respectively. Because the non-

trivial equilibrium will have zero unmated females, there is no N_U compartment.

Shape and rate parameters for the Erlang-distributed delays can be constructed as follows. Consider a random delay with mean $\frac{1}{q}$ and variance $\frac{1}{nq^2}$, where n is an integer. Such a random delay can be assumed to follow an Erlang distribution, and one way to construct a model of this system is to build a linear system of n bins, where the rate of transfer from the $i-1^{th}$ to i^{th} bin is given by qn. In a deterministic model, this will be a linear system of ODEs and, for a stochastic model, a CTMC.

We present the life history model with two different parameterizations of larval density dependence, which we call the "Lotka-Volterra" and "Logistic" versions, in reference to ecological theory. Both sets of equations are available in the code, and are provided as an example of how to use different functional forms of rate equations with the same Petri net structure.

Lotka-Volterra Density-Dependent Equations

This set of equations uses a linear form of per-capita density-dependent mortality for the larval instar stages that corresponds to the functional form assumed by [68].

$$
\begin{aligned}
\frac{d}{dt}E_1 &= (\beta N_F) - (\mu_E + q_E n_E)\, E_1 \\
\frac{d}{dt}E_i &= q_E n_E E_{i-1} - (\mu_E + q_E n_E)\, E_i; \, i = (2, ..., n_E) \\
\frac{d}{dt}L_1 &= q_E n_E E_{n_E} - \left(\mu_L + \alpha \sum_j L_j + q_L n_L\right) L_1 \\
\frac{d}{dt}L_i &= q_L n_L L_{i-1} - \left(\mu_L + \alpha \sum_j L_j + q_L n_L\right) L_i; \, i = (2, ..., n_L) \\
\frac{d}{dt}P_1 &= q_L n_L L_{n_L} - (\mu_P + q_P n_P)\, P_1 \\
\frac{d}{dt}P_i &= q_P n_P P_{i-1} - (\mu_P + q_P n_P)\, P_i; \, i = (2, ..., n_P) \\
\frac{d}{dt}N_F &= \phi q_P n_P P_{n_P} - \mu_F N_F \\
\frac{d}{dt}N_M &= (1-\phi) q_P n_P P_{n_P} - \mu_M N_M
\end{aligned}
\tag{B.1}
$$

In this set of equations, the parameter α represents increased mortality rates that occur as a function of crowding, and has units of time^{-1}area^2.

To solve the model with linear density-dependence at equilibrium, we assume that the equilibrium number of adult female mosquitoes, $\overline{N_F}$ is known, and that all rate constants, with the exception of α are also fixed; we then solve for all remaining state variables plus α, giving a system of $2 + n_E + n_L + n_P$ equations and the same number of unknowns.

$$
\begin{aligned}
\overline{P_{n_P}} &= \frac{\overline{N_F}\mu_F}{n_P q_P \phi} \\
\overline{N_M} &= \frac{(1-\phi) n_P q_P \overline{P_{n_P}}}{\mu_M} \\
\overline{P_i} &= \left(\frac{\mu_P + q_P n_P}{q_P n_P}\right) \overline{P_{i+1}};\, i = (n_P - 1, ..., 1) \\
\overline{E_1} &= \frac{\beta \overline{N_F}}{\mu_E + q_E n_E} \\
\overline{E_i} &= \left(\frac{q_E n_E}{\mu_E + q_E n_E}\right) \overline{E_{i-1}};\, i = (2, ..., n_E) \\
\overline{L_{n_L}} &= \left(\frac{\mu_P + q_P n_P}{q_L n_L}\right) \overline{P_1} \\
\overline{L_1} &= \frac{\overline{E_{nE}}^{\left(\frac{n_L-1}{n_L}\right)} \overline{L_{nL}}^{\left(\frac{1}{n_L}\right)} n_E^{\left(\frac{n_L-1}{n_L}\right)} q_E^{\left(\frac{n_L-1}{n_L}\right)}}{n_L^{\left(\frac{n_L-1}{n_L}\right)} q_L^{\left(\frac{n_L-1}{n_L}\right)}} \\
\overline{L_i} &= \overline{L_1}^{\,i} \left(\frac{n_L q_L}{\overline{E_{nE}} n_E q_E}\right)^{i-1};\, i = (2, ..., n_L - 1) \\
\alpha &= \frac{\frac{\overline{E_{nE}} n_E q_E}{\overline{L_1}} - (\mu_L + n_L q_L)}{\sum_j \overline{L_j}}
\end{aligned}
\tag{B.2}
$$

Logistic Density-Dependent Equations

This set of equations uses a rational form of per-capita density-dependent mortality for the larval instar stages that uses a carrying capacity K parameterization (equivalent to the logistic model in ecology).

$$
\begin{aligned}
\frac{d}{dt}E_1 &= (\beta N_F) - (\mu_E + q_E n_E)\, E_1 \\
\frac{d}{dt}E_i &= q_E n_E E_{i-1} - (\mu_E + q_E n_E)\, E_i;\, i = (2, ..., n_E) \\
\frac{d}{dt}L_1 &= q_E n_E E_{n_E} - \left(\mu_L \left(1 + \frac{\sum_j L_j}{K}\right) + q_L n_L\right) L_1 \\
\frac{d}{dt}L_i &= q_L n_L L_{i-1} - \left(\mu_L \left(1 + \frac{\sum_j L_j}{K}\right) + q_L n_L\right) L_i;\, i = (2, ..., n_L) \\
\frac{d}{dt}P_1 &= q_L n_L L_{n_L} - (\mu_P + q_P n_P)\, P_1 \\
\frac{d}{dt}P_i &= q_P n_P P_{i-1} - (\mu_P + q_P n_P)\, P_i;\, i = (2, ..., n_P) \\
\frac{d}{dt}N_F &= \phi q_P n_P P_{n_P} - \mu_F N_F \\
\frac{d}{dt}N_M &= (1-\phi) q_P n_P P_{n_P} - \mu_M N_M
\end{aligned}
\tag{B.3}
$$

In this parameterization of density-dependent mortality, μ_L is the natural mortality rate of larvae without any effects of resource depletion or competition (because when $\sum_j L_j$ is small, the mortality is approximately μ_L).

To solve the model at equilibrium, we assume that the equilibrium number of adult female mosquitoes, $\overline{N_F}$ is known, and that all rate constants, with the exception of K, are also fixed; we then solve for all remaining state variables plus K, giving a system of $2 + n_E + n_L + n_P$ equations and the same number of unknowns.

$$
\begin{aligned}
\overline{P_{n_P}} &= \frac{\overline{N_F}\mu_F}{n_P q_P \phi} \\
\overline{N_M} &= \frac{(1-\phi) n_P q_P \overline{P_{n_P}}}{\mu_M} \\
\overline{P_i} &= \left(\frac{\mu_P + q_P n_P}{q_P n_P}\right) \overline{P_{i+1}}; i = (n_P - 1, ..., 1) \\
\overline{E_1} &= \frac{\beta \overline{N_F}}{\mu_E + q_E n_E} \\
\overline{E_i} &= \left(\frac{q_E n_E}{\mu_E + q_E n_E}\right) \overline{E_{i-1}}; i = (2, ..., n_E) \\
\overline{L_{n_L}} &= \left(\frac{\mu_P + q_P n_P}{q_L n_L}\right) \overline{P_1} \\
\overline{L_1} &= \frac{\overline{E_{nE}}^{\left(\frac{n_L-1}{n_L}\right)} \overline{L_{nL}}^{\left(\frac{1}{n_L}\right)} n_E^{\left(\frac{n_L-1}{n_L}\right)} q_E^{\left(\frac{n_L-1}{n_L}\right)}}{n_L^{\left(\frac{n_L-1}{n_L}\right)} q_L^{\left(\frac{n_L-1}{n_L}\right)}} \\
\overline{L_i} &= \frac{\overline{L_{n_L}}^{(\frac{i}{n_L})} \overline{E_{n_E}}^{(\frac{n_L-i}{n_L})} n_E^{(\frac{n_L-i}{n_L})} q_E^{(\frac{n_L-i}{n_L})}}{n_L^{(\frac{n_L-i}{n_L})} q_L^{(\frac{n_L-i}{n_L})}}; i = (1, ..., n_L - 1) \\
K &= \frac{\sum_j \overline{L_j}}{\left(\frac{q_E n_E \overline{E_{n_E}}}{\mu_L \overline{L_1}} - \frac{q_L n_L}{\mu_L} - 1\right)}
\end{aligned}
\tag{B.4}
$$

In fact, because both of these per-capita density dependent rates of mortality are linear functions in the number of larvae present (such that the overall mortality is quadratic in the number of larvae), at equilibrium the parameters α and K are related by the simple expression:

$$
\frac{\mu_L}{K} = \alpha \tag{B.5}
$$

Parameters

Due to the continuous-time model structure as well as reformulating the fixed delays of **MGDrivE** as Erlang-distributed random delays, parameters used in **MGDrivE** cannot be directly "plugged-in" to **MGDrivE 2** simulations. In this section we discuss how to parameterize **MGDrivE 2**, and discuss similarities and differences with those in [108, 130]. We note that there will be certain mathematical artifacts which prevent a one-to-one mapping between the two models due to the change between a lagged discrete-time

Markov chain (DTMC) to continuous-time Markov chain (CTMC) model formulation. For more details on how these arise and their effects, please consult [44, 5].

Aquatic Survival

Let the probability to survive any aquatic state $x \in \{E, L, P\}$ be θ_x. In **MGDrivE**, these were given as:

$$\theta_x = (1 - \mu_x)^{T_x} \tag{B.6}$$

In **MGDrivE 2**, the aquatic state is broken in n_x substages to produce an overall Erlang-distributed dwell time, τ. The Erlang distribution has shape parameter n_x and rate parameter $n_x q_x$, where $q_x = \frac{1}{T_x}$; therefore $\mathbb{E}[\tau] = \frac{1}{q_x} = T_x$ and $\mathrm{Var}[\tau] = \frac{1}{n_x q_x^2}$. Because the dwell time τ is a random variable the probability of survival is expressed :

$$\begin{aligned}
\theta_x &= \int_0^\infty e^{-\mu_x \tau} \ \mathrm{Erlang}(\tau; n_x, q_x n_x) d\tau \\
\theta_x &= \int_0^\infty e^{-\mu_x \tau} \frac{q_x n_x^{n_x}}{(n_x - 1)!} \tau^{n_x - 1} e^{-q_x n_x \tau} d\tau \\
&= \left(\frac{q_x n_x}{q_x n_x + \mu_x} \right)^{n_x}
\end{aligned} \tag{B.7}$$

If we wanted to match survival probabilities between the two models, we just consider μ_x in equation B.7 to be an unknown and solve for it:

$$\mu_x = \frac{q_x n_x}{\sqrt[n_x]{\theta_x}} - q_x n_x \tag{B.8}$$

Note that we can arrive at the solution from equation B.7 by considering not a single random variable τ but rather the random variables X, Y, where the latter is the time to death, if death were to occur, and the former is time to advancement out of stage x, were advancement to occur. Then we want the probability that $X < Y$:

$$\begin{aligned}
P(X < Y) &= \int_0^\infty \int_0^\tau \mu_x e^{-\mu_x \tau} \ \mathrm{Erlang}(\tau'; n_x, q_x n_x) \ d\tau d\tau' \\
&= \left(\frac{q_x n_x}{q_x n_x + \mu_x} \right)^{n_x}
\end{aligned} \tag{B.9}$$

Intuition behind the solution may be acquired if we take literally the interpretation of the Erlang distribution as being used in the "linear chain trick"; in this case at each substage the overall probability of survival is $\left(\frac{q_x n_x}{q_x n_x + \mu_x} \right)$. Because there are n_x substages, the total survival probability is the product of the n_x stages.

Population Growth Rate

In **MGDrivE**, the intrinsic population growth rate R_m was defined as "equal to the rate of female egg production multiplied by the life expectancy of an adult mosquito multiplied by the proportion of eggs that will survive through all of the juvenile life stages in the absence of density-dependence" [108].

In **MGDrivE** it had units of $\mathrm{mosquito}^{-1}\mathrm{day}^{-1}$:

$$R_M = \left(\frac{\beta}{\mu}\right)\left(\theta_E\theta_L\theta_P(1-\mu)\left(\frac{1}{2}\right)\right) \tag{B.10}$$

It is essentially the same in **MGDrivE 2**, using the form of θ_x from equation B.6:

$$R_M = \left(\frac{\beta}{\mu}\right)(\theta_E\theta_L\theta_P\phi) \tag{B.11}$$

Note however, the absence of the $1-\mu$ term; this is because equation B.11 is a continuous time rate; adults are available to oviposit immediately upon emergence, so there is no need extra mortality between emergence and adulthood [40].

Parameterization from Growth Rates

In **MGDrivE** the model was typically parameterized such that equilibrium solutions were available in closed form. The assumptions, outlined in the supplemental information of [108] and based on the model of [40], are that $\mu_E = \mu_L = \mu_P$; that is, the density-independent mortality of each aquatic stage is the same. In the absence of density-dependent effects, the total probability of surviving the aquatic stages was $(1-\mu_L)^{(T_E+T_L+T_P)}$. Combined with knowledge of the generation time g, the daily population (geometric) growth rate r_M, and the per-generation geometric growth $R_M = (r_M)^g$, μ_L could be found in closed form, and from that the remaining unknowns, α and L_{eq} (strength of density dependence and equilibrium larval population) could also be solved in closed form. The relevant equations were S51-S55 in [130].

In **MGDrivE 2** we want to be able to solve for equilibria under similar assumptions of equal density-independent mortality across aquatic stages. Let us define $\mu_A = \mu_E = \mu_L = \mu_P$ so we seek a solution to the unknown constant aquatic stage mortality μ_A. We first expand Equation B.11 in terms of Equation B.7:

$$R_M = \left(\frac{\beta}{\mu}\right)\left(\frac{q_E n_E}{q_E n_E + \mu_A}\right)^{n_E}\left(\frac{q_L n_L}{q_L n_L + \mu_A}\right)^{n_L}\left(\frac{q_P n_P}{q_P n_P + \mu_A}\right)^{n_P}\phi \tag{B.12}$$

Here, R_M is the per-generation growth rate; in **MGDrivE** it was $(r_M)^g$. However, because **MGDrivE 2** is a continuous time model, the equations for geometric growth are not appropriate. The equivalent infinitesimal rate of growth is $\log(r_M)$ such that $R_M = e^{g\log(r_M)}$, which is the left hand side of Equation B.12.

Finding closed form solutions to this equation is difficult because of the additional terms introduced by the Erlang delays. Therefore we use Newton's method in R (with `uniroot`) to numerically solve for μ_A. The input to the function is the daily growth rate r_M and biological parameters $\beta, \mu, q_E, n_E, q_L, n_L, q_P, n_P, \phi$, and it returns the value of μ_A such that the following equation holds:

$$\left(e^{\log(r_M)g}\right) - \left[\phi\left(\frac{\beta}{\mu}\right)\left(\frac{q_E n_E}{q_E n_E + \mu_A}\right)^{n_E}\left(\frac{q_L n_L}{q_L n_L + \mu_A}\right)^{n_L}\left(\frac{q_P n_P}{q_P n_P + \mu_A}\right)^{n_P}\right] = 0 \qquad \text{(B.13)}$$

Lifespan Modification

In **MGDrivE**, the genotype-specific parameter ω was used to reduce lifespans of non wild-type organisms due to fitness costs associated with the homing cassette, or intentional fitness reduction. However, for **MGDrivE 2** we generalize this to modify lifespans in either direction, relative to wildtype, because experimental data showed evidence of in some cases substantial lifespan *increases* from driving certain genetic material in model organisms [83].

Because wildtype lifespans (x) were geometrically distributed random variables, and daily survival was given by $(1-\mu)\omega$, one could solve for a reduced lifespan, $y < x$, by noting the daily mortality probability can be written $p = 1 - ((1-\mu)\omega) = 1 - \omega + \mu\omega$. Then note that the mean lifespan is $y = \frac{1}{1-\omega+\mu\omega}$. Thus to solve for ω, we solve for the root of the equation $\frac{1}{1-\omega+\mu\omega} - y = 0$, where only ω is unknown.

In **MGDrivE 2** adult lifespans are exponentially distributed random variables. To change the lifespan y (no longer restricted to $y < x$, y may be any positive number), consider modifying the mortality hazard by the factor ω. To find ω we just solve the following equation:

$$\begin{aligned} y &= \int_0^\infty \tau\ \mu\omega e^{-(\mu\omega)\tau} d\tau \\ \omega &= \frac{1}{y\mu} \end{aligned} \qquad \text{(B.14)}$$

Movement

In the continuous time model, mosquito movement is given by a rate of movement from each node i to all other nodes $j \neq i$. When parameterizing these rates, we need to take into account that they will be a function of the total probability of a mosquito to leave its natal habitat i over its lifetime, P. Given that adult mosquitoes are subject to mortality with rate μ, one can solve for the rate of movement out of node i to anywhere (δ) as follows:

$$
\begin{aligned}
P &= \int_0^\infty \delta e^{-(\delta+\mu)\tau} d\tau \\
\delta &= \frac{\mu P}{1-P}
\end{aligned}
\tag{B.15}
$$

Then, if from node i, we have some vector of movement probabilities $\{\pi_{ij}\}_{j\neq i}$ which give the probability to move from i to j conditional on leaving i, we can set the movement hazard between to be $\delta\pi_{ij}$ so we get the right lifetime leaving probability. The new vector of movement *hazards* is $\{\delta\pi_{ij}\}_{j\neq i}$.

Genetic Inheritance & Modification

Because **MGDrivE 2** builds upon our previous work [130], the data structure used in **MGDrivE** to store all probabilities, fitness costs, etc. related to genotypes (the "inheritance cube") is compatible with **MGDrivE 2**. In fact, we use the same cubes developed in that model and do not introduce any new cubes in this text.

While data structures can be reused, the fitness modifiers that describe the effect of inherited genotype on the life-history have a slightly different interpretation. In **MGDrivE**, genotype specific multipliers applied to daily probabilities, they had to be bounded in order to prevent nonsensical parameter values. If P represents a wild-type daily survival probability, for example, the modifier ω must be $0 < \omega < \frac{1}{P}$. Because **MGDrivE 2** is parameterized directly in terms of hazards, the genotype-specific effects can be any positive real number. This has the added benefit of making them amenable to parameterization directly from survival analysis routinely preformed on biological lab experiments which often estimate relative hazards [83].

B.2 Epidemiological Dynamics

To introduce epidemiological dynamics in **MGDrivE 2**, we use the SEI-SIS coupled model of mosquito and human infection dynamics as the basic model (Figure B.1), as more complex vector-host models tend to be modifications of the basic form. This type of model is known as the Ross-Macdonald model in mathematical epidemiology [109, 138]. **MGDrivE 2** also supports SEI-SEIR models, which we introduce briefly later.

Here S_H refers to susceptible humans, I_H to infected/infectious humans, S_V to susceptible mosquitoes, $(E_{V,1}, ..., E_{V,n})$ to incubating mosquitoes, and I_V to infectious mosquitoes. Because only mated adult females undergo gonotrophic cycles which require bloodfeeding, infection dynamics are only present in F.

To investigate the dynamics of the model, it is important to focus on events (transitions) that change state, and the rate at which they occur. For epidemiological dynamics, the two primary events are mosquito to human transmission and human to mosquito

transmission, each driven by a Poisson process. Computation of the rate with which each process occurs in time depends on the per-capita force of infection (FOI) terms: λ_H and λ_V, the rates at which any particular susceptible human gets infected and moves to the infected class, and the rate at which any particular susceptible mosquito gets infected and moves to the incubating class, respectively. When multiplied by the total numbers of susceptible humans or susceptible mosquitoes, respectively, we arrive at the correct rate for the Poisson processes.

Figure B.1: SEI-SIS pathogen transmission system; orange arrows denote the contribution of each species to the force of infection term on the other.

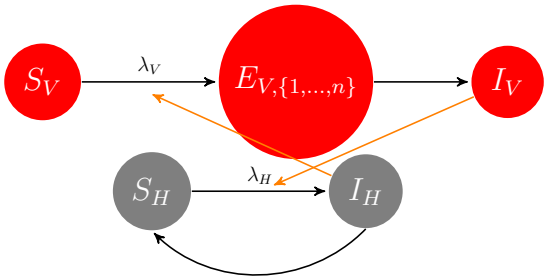

Transmission Terms

The function λ_H is the per-capita FOI on susceptible humans, such that $\lambda_H S_H$ is the total rate at which infection in the human population occurs in the deterministic model, or the intensity of the Poisson process for human infections in the stochastic model. Using Ross-Macdonald parameters as in [138], $\lambda_H = abI_V\left(\frac{1}{N_H}\right)$. This is because, if a is the human biting rate, b mosquito-human transmission efficiency, then the total number of infectious bites produced by the mosquito population is abI_V. Assuming uniform biting on humans, any particular person has probability $\frac{1}{N_H}$ of being bitten, so $abI_V\left(\frac{1}{N_H}\right)$ is the per-capita FOI. Multiplication by S_H, the total number of humans, gives the total rate of infection in the human population.

The per-capita FOI in the mosquito population is $\lambda_V S_V$. The FOI on susceptible mosquitoes is written as $\lambda_V = ac\left(\frac{I_H}{N_H}\right)$. Again, a is the human biting rate, c is the human-mosquito transmission efficiency, and $\frac{I_H}{N_H}$ is the probability that a bite lands on an infectious human. Multiplying by the total susceptible vector population, S_V, gives the total rate of infection in the mosquito population.

Deterministic Approximation

In this section we describe how to develop a mean-field approximation given by a system of ODEs to the stochastic SEI-SIS system.

Mean-field Approximation of Human Stochastic Dynamics

Here we describe in detail the method used to approximate the stochastic CTMC model of infection dynamics in the human population, as its state space is smaller and the same methods can be used for the larger mosquito dynamics. The methods follow those presented in [152]. Because we are only considering the human population, we drop the H superscript on state variables.

If we consider the mosquito population to be constant, as it would be at dynamic equilibrium for the deterministic model, then λ_H will be a constant and we can decouple the human SIS dynamics from the mosquito SEI system. We show a diagram of the human only dynamics in Figure B.2.

Figure B.2: Susceptible-infected-susceptible (SIS) human infection dynamics

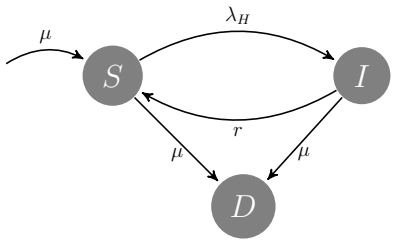

One way to analyze a CTMC is to derive the *Chapman-Kolmogorov equations* of the process. These equations give the conditional probabilities to transition to any ending state from a given starting state, over some time interval. For example if at time $t \leq t'$ the process (represented by $X(t)$) is in a state x, then the probability to jump to any state x' is $\mathbf{P}\left(X(t+t') = x' | X(t) = x\right)$, where $\mathbf{P}$ is a distribution over future states. It is often easier to work with the differential form of these equations, where the derivative is taken with respect to time, giving a system of differential equations that describes the time evolution of the Markov transition kernel over state space. Taking the derivative of these equations will involve expanding $\mathbf{P}(t+\delta t)$, which if expanded as $\mathbf{P}(t)\mathbf{P}(\delta t)$, leads to the linear system of ODEs known as the Kolmogorov forward equations (KFE).

The CTMC is a process which jumps between points in state space $(S, I) \rightarrow (S', I')$. Put another way, the joint density must be understood as giving the probability to transition between all unique pairs of ways a number of people can be either susceptible or infectious, when birth, death, infection, and recovery can change state. Taking into ac-

count all events that can cause the system state at time t to change, we can derive the KFE as:

$$\begin{aligned}\frac{d}{dt}\mathbf{P}(S,I;t) = &-\big(\mu(S+I)+\mu S+\mu I+\lambda_H S - rI\big)\,\mathbf{P}(S,I;t)\\ &+\mu\big((S-1)+I\big)\,\mathbf{P}(S-1,I;t)\\ &+\mu(S+1)\,\mathbf{P}(S+1,I;t)\\ &+\mu(I+1)\,\mathbf{P}(S,I+1;t)\\ &+\lambda_H(S+1\,)\mathbf{P}(S+1,I-1;t)\\ &+r(I+1)\,\mathbf{P}(S-1,I+1;t)\end{aligned} \tag{B.16}$$

The KFE can be manipulated to derive the deterministic approximation to the CTMC. Because we assume constant λ_H, the hazard/rate functions for each event are all first order in the state variables, the deterministic approximation will accurately describe the expected value of the stochastic model.

To go about this, we first construct the *stoichiometry matrix* $\mathbf{S}_{u\times v}$, where u is dimension of the state space, and v is the number of unique events in the process. As the dimension of both state and event spaces are small, we can easily write this as:

$$\mathbf{S} = \begin{array}{c} \\ S \\ I \end{array}\!\!\begin{array}{c} \begin{array}{ccccc} \scriptstyle\to S & \scriptstyle S\to D & \scriptstyle I\to D & \scriptstyle S\to I & \scriptstyle I\to S \end{array} \\ \begin{bmatrix} 1 & -1 & 0 & -1 & 1 \\ 0 & 0 & -1 & 1 & -1 \end{bmatrix} \end{array} \tag{B.17}$$

To begin developing our deterministic approximation, we take the time-derivative of the expectation of our state vector at time t, denoted as $X(t)$ (full derivation in [152]). We also define $h(X(t))$ as a v-dimensional column vector of rates/intensities of each event at that point x in state space.

$$\begin{aligned}\frac{d}{dt}\mathbb{E}\left[X(t)\right] &= \frac{d}{dt}\sum_{x\in\mathcal{M}} x\,\mathbf{P}(x;t), \text{ where } \mathcal{M} \text{ is the set of all allowed model states}\\ &= \sum_{x\in\mathcal{M}} x\,\frac{d}{dt}\mathbf{P}(x;t)\\ &= \sum_{x\in\mathcal{M}} x\sum_{i=1}^{v}\left[h_i(x-\mathbf{S}^{(i)})\mathbf{P}(x-\mathbf{S}^{i};t) + h_i(x)\mathbf{P}(x;t)\right]\\ &\;\;\vdots\\ &= \sum_{i=1}^{v}\mathbb{E}\left[\mathbf{S}^{(i)}h_i\left(X(t)\right)\right]\\ &= \sum_{i=1}^{v}\mathbf{S}^{(i)}\mathbb{E}\left[h_i\left(X(t)\right)\right]\end{aligned} \tag{B.18}$$

After making the substitution $y(t) = \mathbb{E}(X(t))$, the above equation can be recognized as a matrix ODE giving the deterministic approximation of the system.

$$\begin{aligned}\frac{d}{dt}y(t) = &\sum_{i=1}^{v} \mathbf{S}^i h_i(y(t)) \\ =&\mathbf{S}\big(h(y(t))\big)\end{aligned} \tag{B.19}$$

Substituting in our stoichiometry matrix $\mathbf{S}$ and SIS hazard functions, we derive the following matrix ODE (writing out the column vector $y(t)$ explicitly in terms of our two state variables):

$$\frac{d}{dt}\begin{vmatrix} S(t) \\ I(t) \end{vmatrix} = \begin{vmatrix} 1 & -1 & 0 & -1 & 1 \\ 0 & 0 & -1 & 1 & -1 \end{vmatrix} \begin{vmatrix} \mu\big(S(t)+I(t)\big) \\ \mu S(t) \\ \mu I(t) \\ \lambda_H S(t) \\ rI(t) \end{vmatrix} \tag{B.20}$$

Separating the variables and completing the matrix vector multiplication leads to the familiar ODE form of the SIS model with demography. We defer the equilibrium solution until later, when we can solve for the mosquito equilibrium jointly.

$$\begin{aligned}\frac{d}{dt}S(t) &= \mu\big(S(t)+I(t)\big) - \mu S(t) - \lambda_H S(t) + rI(t) \\ \frac{d}{dt}I(t) &= -\mu I(t) + \lambda_H S(t) - rI(t)\end{aligned} \tag{B.21}$$

Mean-field Approximation of Mosquito Stochastic Dynamics

Similar as we did for humans, we consider λ_V to be a constant and decouple the mosquito SEI dynamics from the human SIS dyanmics. A flow graph of the mosquito dynamics is shown in Figure B.3, which shows the possible states a adult female mosquito may exist in during its life, with death (D) as an absorbing state. As described in the main text, we partition the exposure (extrinsic incubation period, EIP) into n compartments such that the overall dwell time is Erlang distributed. As before, because we are purely focused on the mosquito model, we drop the V superscript for state variables.

For a single adult female mosquito, the transition rates on the edges of the graph specify the hazard rates of leaving the current state; the aggregated process for a population of mosquitoes sums the individual hazards by the number of mosquitoes in that state.

Upon emergence, the mosquito enters the susceptible S state, subject to force of infection λ_V. Susceptible mosquitoes are also subject to a mortality rate, μ, which is constant across all compartments, leading to an exponentially distributed lifespan with mean $\frac{1}{\mu}$. If the mosquito becomes infected, which occurs at rate λ_V, it will advance through the extrinsic incubation period (EIP) prior to becoming infectious.

Figure B.3: Susceptible-exposed-infected (SEI) mosquito infection dynamics

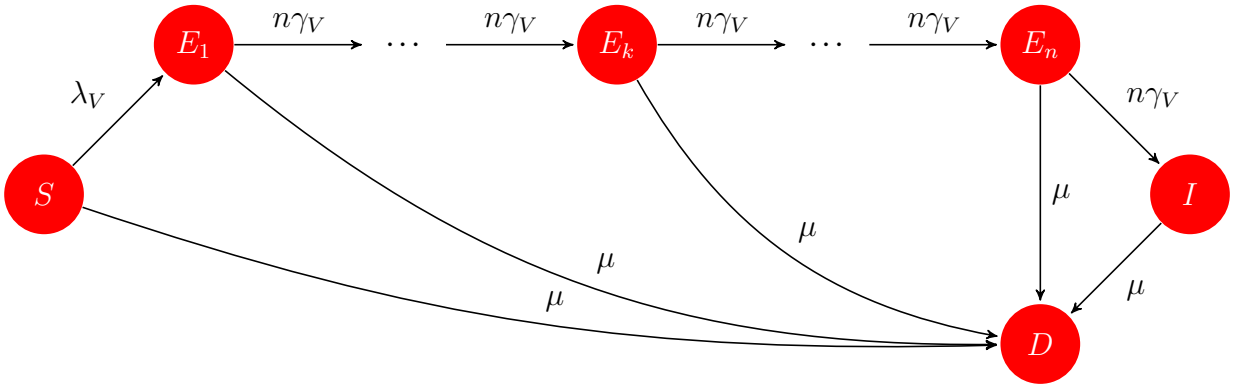

The EIP is broken into n bins, with transition from the k^{th} to $k+1^{\text{th}}$ occurring at a rate nq. This specification allows an Erlang (Gamma with integer shape parameter) distributed duration of EIP, with mean $\frac{1}{\gamma_V}$ and variance $\frac{1}{n\gamma_V^2}$. A mosquito survives the EIP with probability $\lim_{n\to\infty}(\frac{n\gamma_V}{n\gamma_V+\mu})^n = e^{-\frac{\mu}{\gamma_V}}$. Conditional on survival, the proportion of mosquitoes that become infectious t days after becoming infected is distributed as $\text{Gamma}(t; n, \frac{1}{n\gamma_V}) = \frac{(n\gamma_V)^n}{(n-1)!}t^{n-1}e^{-tn\gamma_V}$ (using shape/scale parameterization).

Written in matrix form, the infinitesimal generator matrix for a single adult female mosquito, or a cohort emerging at the same time has the following form:

$$\mathbf{Q} = \begin{array}{c} \\ S \\ E_1 \\ \vdots \\ E_k \\ \vdots \\ E_n \\ I \\ D \end{array} \begin{array}{c} \begin{array}{ccccccccc} S & E_1 & \dots & E_k & \dots & E_n & I & D \end{array} \\ \begin{bmatrix} -(\lambda_V+\mu) & \lambda_V & \dots & 0 & \dots & 0 & 0 & \mu \\ 0 & -(n\gamma_V+\mu) & n\gamma_V & 0 & \dots & 0 & 0 & \mu \\ & & & & & & & \\ 0 & 0 & \dots & -(n\gamma_V+\mu) & n\gamma_V & 0 & 0 & \mu \\ & & & & & & & \\ 0 & 0 & \dots & 0 & \dots & -(n\gamma_V+\mu) & n\gamma_V & \mu \\ 0 & 0 & \dots & 0 & \dots & 0 & -\mu & \mu \\ 0 & 0 & \dots & 0 & \dots & 0 & 0 & 0 \end{bmatrix} \end{array} \tag{B.22}$$

For the model of a single adult female mosquito, or a cohort that emerged at the same time, the infinitesimal generator (Equation B.22), the KFE is:

$$
\begin{aligned}
\frac{d}{dt}\mathbf{P}(S;t) &= -\lambda_V S\mathbf{P}(S;t) - \mu\mathbf{P}(S;t)\\
\frac{d}{dt}\mathbf{P}(E_1;t) &= \lambda_V S\mathbf{P}(S;t) - n\gamma_V\mathbf{P}(E_1;t) - \mu\mathbf{P}(E_1;t)\\
&\vdots\\
\frac{d}{dt}\mathbf{P}(E_k;t) &= n\gamma_V\mathbf{P}(E_{k-1};t) - n\gamma_V\mathbf{P}(E_k;t) - \mu\mathbf{P}(E_k;t)\\
&\vdots\\
\frac{d}{dt}\mathbf{P}(E_n;t) &= n\gamma_V\mathbf{P}(E_{n-1};t) - n\gamma_V\mathbf{P}(E_n;t) - \mu\mathbf{P}(E_n;t)\\
\frac{d}{dt}\mathbf{P}(I;t) &= n\gamma_V\mathbf{P}(E_n;t) - \mu\mathbf{P}(I;t)\\
\frac{d}{dt}\mathbf{P}(D;t) &= \mu\big(\mathbf{P}(S;t) + \mathbf{P}(E_1;t) + \ldots + \mathbf{P}(E_n;t) + \mathbf{P}(I;t)\big)
\end{aligned}
\tag{B.23}
$$

While Equation B.23 describes how the probability distribution over states for a cohort of mosquitoes changes over time, to account for emergence (which we will need for the deterministic approximation), we let ϵ give the rate at which females emerge into S from pupae. For brevity, $\mathbf{P}(\ldots;t)$ appearing in the joint density function means that those elements of the random vector do not change.

$$
\begin{aligned}
\frac{d}{dt}\mathbf{P}(S, E_1, \ldots, E_n, I;t) = \epsilon\ &\mathbf{P}(S-1,\ldots;t) - \epsilon\ \mathbf{P}(\ldots;t)\\
&- \lambda_V S\mathbf{P}(\ldots;t) + \lambda_V(S+1)\mathbf{P}(S+1, E-1, \ldots;t)\\
&- (2+n)\mu\mathbf{P}(\ldots;t)\\
&+ \mu\mathbf{P}(S+1,\ldots;t) + \mu\mathbf{P}(\ldots, E_1+1,\ldots;t) + \ldots + \mu\mathbf{P}(\ldots, I+1;t)\\
&- (n\gamma_V)n\mathbf{P}(\ldots;t)\\
&+ qn\mathbf{P}(\ldots, E_1+1, E_2-1,\ldots;t) + \ldots + n\gamma_V\mathbf{P}(\ldots, E_n+1, I-1;t)
\end{aligned}
\tag{B.24}
$$

As we did for deriving the deterministic approximation of human infection dynamics, we write out the stoichiometry matrix $\mathbf{S}_{u\times v}$ of dimensions $(2+n)\times(2n+4)$. Because each column in $\mathbf{S}$ describes an allowable jump in state space, the total number of terms in the KFEs should be equal to $2(2n+4) = 4n+8$; checking this with the derivation in the previous section allows us to confirm that the equations are correct. Once we have $\mathbf{S}$, the mean-field approximation follows the same method as in Section B.2.

$$\mathbf{S} = \begin{array}{c} \\ S \\ E_1 \\ \vdots \\ E_i \\ \vdots \\ E_n \\ I \end{array} \begin{array}{c} \begin{array}{ccccccccccccc} \rightarrow S & S \rightarrow E_1 & S \rightarrow D & E_1 \rightarrow E_2 & E_1 \rightarrow D & \dots & E_i \rightarrow E_{i+1} & E_i \rightarrow D & \dots & E_n \rightarrow I & E_n \rightarrow D & I \rightarrow D \end{array} \\ \begin{bmatrix} 1 & -1 & 0 & 0 & 0 & \dots & 0 & 0 & \dots & 0 & 0 & 0 \\ 0 & 1 & -1 & -1 & -1 & \dots & 0 & 0 & \dots & 0 & 0 & 0 \\ \vdots & \vdots & \vdots & \vdots & \vdots & \vdots & \vdots & \vdots & \vdots & \vdots & \vdots & \vdots \\ 0 & 0 & 0 & 0 & 0 & \dots & -1 & -1 & \dots & 0 & 0 & 0 \\ \vdots & \vdots & \vdots & \vdots & \vdots & \vdots & \vdots & \vdots & \vdots & \vdots & \vdots & \vdots \\ 0 & 0 & 0 & 0 & 0 & \dots & 0 & 0 & \dots & -1 & -1 & 0 \\ 0 & 0 & 0 & 0 & 0 & \dots & 0 & 0 & \dots & 1 & 0 & -1 \end{bmatrix} \end{array} \tag{B.25}$$

Using the stoichiometry and the KFEs we write down the approximating equations in matrix ODE form:

$$\frac{d}{dt}\begin{vmatrix} S(t) \\ E_1(t) \\ \vdots \\ E_n(t) \\ I(t) \end{vmatrix} = \mathbf{S}\begin{vmatrix} \epsilon \\ \lambda_V S(t) \\ \mu S(t) \\ \vdots \\ n\gamma_V E_n(t) \\ \mu E_n(t) \\ \mu I(t) \end{vmatrix} \tag{B.26}$$

Because the emergence rate ϵ and the force of infection on mosquitoes λ_V are considered a constants, all jump terms are of zero or first order and the deterministic approximation will correctly approximate the mean behavior of the stochastic system. For clarity, we write the system of linear ODEs component-wise:

$$\begin{aligned} \frac{d}{dt}S(t) &= \epsilon - \lambda_V S(t) - \mu S(t) \\ \frac{d}{dt}E_1(t) &= \lambda_V S(t) - n\gamma_V E_1(t) - \mu E_1(t) \\ &\vdots \\ \frac{d}{dt}E_n(t) &= n\gamma_V E_{n-1}(t) - n\gamma_V E_n(t) - \mu E_n(t) \\ \frac{d}{dt}I(t) &= n\gamma_V E_n(t) - \mu I(t) \end{aligned} \tag{B.27}$$

Quasi-stationary distribution for mosquito infection dynamics

In order to solve the coupled mosquito SEI - human SIS model at equilibrium, we need to be able to solve for the distribution of adult female mosquitoes across states $(S, E_1, ..., E_n, I)$. This is because, given an endemic equilibrium prevalence in humans, we can compute

the number of infectious mosquitoes I required to sustain that prevalence of disease. From that, we can use the quasi-stationary solution of the CTMC model given in Equation B.22 to compute the total adult female mosquito population and their distribution across stages, which can then be plugged into the life history equilibrium Equation B.2 or Equation B.4 to solve the entire model's endemic equilibrium. We note that for the stochastic model, this is not a stationary distribution, but a quasi-stationary distribution (QSD), as there exist absorbing states in the model.

To compute the QSD, note death (D) is an absorbing state and the set of transient states is $\mathcal{T} = (S, E_1, ..., E_n, I)$. Then the random variable representing time to absorption (death) as a phase-type distribution. The QSD over $\mathcal{T}$ will arise by conditioning on survival. This distribution allows us to distribute mosquitoes across the transient states properly at equilibrium. We partition $\mathbf{Q}$ as [19, 27]:

$$\widetilde{\mathbf{Q}} = \begin{pmatrix} \mathbf{T} & t \\ \mathbf{0} & 0 \end{pmatrix} \tag{B.28}$$

Here, $\mathbf{T}_{|\mathcal{T}|\times|\mathcal{T}|}$ is a subintensity matrix of transition rates between transient states, and $t_{|\mathcal{T}|\times 1}$ is a column vector of exit rates to the absorbing state. We denote the random variable following a continuous phase-type distribution describing time until absorption as $\tau \sim \mathrm{PH}(\pi, \mathbf{T})$ with density function $f_\tau(u) = \pi e^{\mathbf{T}u} t$, where $\pi_{1\times|\mathcal{T}|}$ is a row vector specifying the initial distribution over transient states.

Let $\mathbf{U} = (-\mathbf{T})^{-1}$ be the matrix containing the means of random variables u_{ij} denoting time spent in state j starting from i, prior to absorption. We can use this matrix to define the QSD over $\mathcal{T}$, denoted as $\tilde{\pi}$. The j^{th} element of the quasi-stationary distribution is [36, 37]:

$$\widetilde{\pi}_j = \frac{\pi^\top \mathbf{U} f_j}{\pi^\top \mathbf{U} e} \tag{B.29}$$

In Equation B.29, f_j is a column vector with 1 in the j^{th} row and 0 elsewhere, and e is a column vector of 1's. In our specific case, π places all mass on state S because the mosquito cannot emerge from the pupa stage already infected (there is no vertical transmission of pathogen), so the quasi-stationary distribution can be directly obtained from $\mathbf{U}$.

Coupled SEI-SIS Equilibrium Solutions

In order to solve for the mosquito population required to produce some equilibrium prevalence in humans, let N_V be the total adult female population, summing over infection states. Writing the SIS human dynamics (Equation B.21) with the expanded form of λ_H, we have:

$$\begin{aligned}
\frac{d}{dt}S_H(t) &= \mu\big(S_H(t) + I_H(t)\big) - \mu S_H(t) - \left(abI_V\left(\frac{1}{S_H(t) + I_H(t)}\right)\right) S_H(t) + rI_H(t) \\
\frac{d}{dt}I_H(t) &= -\mu I_H(t) + \left(abI_V\left(\frac{1}{S_H(t) + I_H(t)}\right)\right) S_H(t) - rI_H(t)
\end{aligned} \tag{B.30}$$

Because we consider both the human population size $N_H = S_H + I_H$ and equilibrium prevalence $x = \frac{I_H}{N_H}$ known constants, we can solve the model at equilibrium in terms of the number of infected mosquitoes, such that:

$$I_V = \frac{I_H(S_H + I_H)(r + \mu)}{abS_H} \tag{B.31}$$

After we have solved for the number of infected mosquitoes I_V, we can derive the total female mosquito population this implies:

$$\begin{aligned}
I_V &= N_V\left(\frac{(n\gamma_V)^n\lambda_V}{(n\gamma_V + \mu_V)(\lambda_V + \mu_V)}\right) \\
N_V &= I_V\left(\frac{(n\gamma_V + \mu_V)(\lambda_V + \mu_V)}{(n\gamma_V)^n\lambda_V}\right)
\end{aligned} \tag{B.32}$$

This total size N_V can be spread across the EIP stages via Equation B.29. Given N_V, we can calculate equilibrium solutions for the full lifecycle model by plugging in this number of adult females into either Equation B.2 or B.4.

SEIR Model

We also present results for an SEIR style model of human dynamics. An additional parameter, γ_H, is the rate of progression from $E_H \rightarrow I_H$, that is, the inverse of the duration of latency in humans.

$$\begin{aligned}
\frac{d}{dt}S_H &= \mu N_H - \lambda_H S_H - \mu S_H \\
\frac{d}{dt}E_H &= \lambda_H S_H - \gamma_H E_H - \mu E_H \\
\frac{d}{dt}I_H &= \gamma_H - rI_H - \mu I_H \\
\frac{d}{dt}R_H &= rI_H - \mu R_H
\end{aligned} \tag{B.33}$$

Where N_H is the total human population and the force of infection on humans follows the Ross-Macdonald form $\lambda_H = abI_V\left(\frac{1}{N^H}\right)$. We consider that the total population size N_H and the number of infected and infectious humans I_H are known, allowing us to solve

for R_H and E_H at equilibrium. It should be noted that for realistic parameter values, this model only has a non-trivial equilibrium when $\mu < \frac{\mu N_H - r I_H}{I_H}$, which results in extremely unrealistic (short) lifespans. The other two equilibrium points are the trivial disease free equilibrium when $\lambda_H = 0$ and the normal ($\lambda_H > 0$) case when $R_H(\infty) \to N_H$, that is, for realistic values of parameters, all surviving individuals will become infected subsequently recover. For that reason we do not explicitly calculate the endemic equilibrium. In general the SEIR human model should be used to evaluate the impact of gene drive interventions on one-off *epidemic* situations (eg; does releasing large numbers of modified mosquitoes 10 days after initial cases appear make a significant difference in final outcome), rather than for investigating *endemic* diseases, which require more complex models with waning immunity.

B.3 Stochastic Petri Net

Here we provide an introduction to the stochastic Petri net modeling formalism used in **MGDrivE 2**. Notation in this introduction is borrowed from [152].

Properties of SPN

SPN is a mathematical modeling language to describe discrete event systems, that is, a system which has a countable set of events (although only a finite number may enabled at any given time), each of which changes state in some way when it occurs. When events are assumed to happen after Exponentially-distributed intervals (alternatively, each event occurs at a constant, age-independent rate), the SPN is isomorphic to a CTMC, and can be extended to provide a modeling semantics for generalized semi-Markov processes [59]. For practical application, a benefit of adopting the SPN modeling language is that model representation is separate from numerical simulation. This can allow both for highly efficient simulation, as the model can be represented via vectors and sparse matrices, and also utilization of model-agnostic simulation algorithms that take as input a generic SPN model and output sampled trajectories.

A Petri net is, formally, a bipartite graph, consisting of a set of *places*, $\mathcal{P}$, and a set of *transitions*, $\mathcal{T}$. Directed edges, often called *arcs*, lead from places to transitions and from transitions to places. Arcs are allowed to have a positive integer weight. Therefore, if $u = |\mathcal{P}|$ and $v = |\mathcal{T}|$, the set of arcs that connect places to transitions can be denoted by a non-negative integer matrix $\mathbf{Pre}_{v \times u}$, and the set of arcs connecting transitions to places by $\mathbf{Post}_{v \times u}$.

This bipartite graph so far defines the *structural* properties of the model. When translating conceptual models to the language of Petri nets, the places define the allowable state space of the model. However, in order to describe any particular state of the model, the Petri net must be given a *marking*, M, which is given by associating with each place a non-negative integer number of *tokens*, such that $M \in \mathbb{N}^u$. Put more concretely, we

can imagine taking some number of indistinguishable tokens and assigning each one to a place in the set $\mathcal{P}$; the resulting vector in $\mathbb{N}^u$ is a valid state of the model. In the language of CTMCs the marking M is referred to as the *state*, and we use the terms interchangeably.

Each transition $k \in \mathcal{T}$ is allowed to change state when it occurs (fires). A transition k is *enabled* in some marking M and may fire when there are tokens on the place corresponding to each input arc (k^{th} row of $\mathbf{Pre}$) greater than or equal to the arc weight. When the transition fires, M is updated by removing tokens from M given by the set of input arcs and weights, that is, according to $\mathbf{Pre}$. It then adds tokens in M according to its output arcs and weights in $\mathbf{Post}$. This can be represented succinctly if we let $\mathbf{A} = \mathbf{Post} - \mathbf{Pre}$, then if r_k is a column vector of zeros with a one at place k, the state can be updated as $M' = M + \mathbf{S}r_k$, where $\mathbf{S} = \mathbf{A}^\intercal$. $\mathbf{S}$ has dimensions $u \times v$, so it maps vectors in the space of events to vectors in the space of marking updates.

So far we have described a deterministic Petri net. However, associate with each transition a clock that tells us when k will fire, if it were the first of all enabled transitions to fire and let the process associated with k be a Poisson process Y_k with intensity λ_k which may depend on the current time t, and current marking $M(t)$. Finally, if we let all enabled processes Y_k compete under a race condition by sampling the next firing time for each clock, τ_k, such that $k' = \arg\min_k\{\tau_k\}$, then k' is the event that fires. In that case the system time is updated to $t' = t + \tau_{k'}$ and the state as $M(t') = M(t) + \mathbf{S}r_{k'}$. It can be rigorously proven that such a construction is a continuous-time Markov chain [24].

An advantage of this construction of a Markov process rather than the more traditional presentation via the infinitesimal generator matrix is that processes with infinite state spaces can be compactly represented, because only a finite number of clock processes compete at any given time. In this way, infinite birth death processes, for example, can be succinctly represented graphically and simulated. Additionally, because most transitions only have a few input and output arcs, the matrices $\mathbf{Pre}$ and $\mathbf{Post}$, which define the bipartite graph, will be highly sparse.

SPN Architecture

We have developed algorithms to construct Petri nets for arbitrary genetic inheritance cubes [130], metapopulation structure, Erlang-distributed aquatic stages, infection dynamics, and human populations. Once built, and augmented with parameters for hazard functions in $\mathcal{T}$, the resulting SPN model can be numerically evaluated via a variety of sampling algorithms. We describe the SPN architecture without considering epidemiological dynamics, as those are considered in a later section.

MGDrivE 2 has been designed with consideration for computational efficiency. We store the matrices defining the SPN in sparse matrix format using the Matrix R package [15]. In addition, when constructing $\mathcal{T}$, we check the input inheritance cube. If the viability mask ($\underline{\underline{\underline{\Lambda}}}$) indicates a certain cross will never produce viable offspring, or if the probability of offspring for a cross is zero ($\underline{\underline{\underline{Ih}}}$), that transition is not instantiated in the

SPN.

Generation of the set of places $\mathcal{P}$ for a single node is simple, and requires the user to pass the inheritance cube $\overline{\overline{\overline{Ih}}}$, and the shape parameters for Erlang dwell distributions associated with egg, larval, and pupal aquatic stages to the function. The function returns the named set of places, along with an indexing data structure containing the indices of places stratified by life stage and genotype, both for easy debugging and the construction of arcs when the set of transitions is made. We note that SPN defines no particular order on the set $\mathcal{P}$ but we "unroll" the set hierarchically into a vector first by node, life-stage, and genotype, for easier comprehension and testing.

After $\mathcal{P}$ is constructed, we can construct transitions $\mathcal{T}$, using $\mathcal{P}$ as input, as well as the aforementioned shape parameters of aquatic dwell times and $\overline{\overline{\overline{Ih}}}$. While not strictly necessary for SPN, we adopted several conventions here which simplify later generation of hazard functions. We first defined "classes", K, of transitions, such that, for example, all transitions related to oviposition were grouped together. Each class K then is a proper subset of all transitions, $K \subset \mathcal{T}$, and $\bigcup_i K_i = \mathcal{T}$. Each individual transition in a set $k_j \in K_i$ has an associated R function which returns a data structure containing, at minimum, an index `vix`, indicating where in $\mathcal{T}$, k_j can be found, a `label`, a character string giving the name of the transition, `s` and `s_w`, indices of input arcs (the places they originate at), and weights respectively, `o` and `o_w`, the same for output arcs from this transition back to places, and `class`, giving the name of the class K_i as a character string this transition belongs to. To make $\mathcal{T}$, we iterate through classes K_i, and k_j within classes, storing each transition's packet of information in the vector $\mathcal{T}$. Because each transition "knows" its input and output arcs, as well as their weights, adding new classes of transitions is simple, as a single function merely needs to be written that takes in places and perhaps genetic information, and returns this minimal packet of information.

Once $\mathcal{P}$ and $\mathcal{T}$ are constructed, the SPN is formally constructed. However for computation, we prefer to store a more compact representation of the net. It is at this point we build the sparse matrices $\mathbf{Pre}$ and $\mathbf{Post}$. To do so, we simply allocate two $v \times u$ sparse integer matrices, then iterate through $k \in \mathcal{T}$. We use the information packet described earlier, specifically `s`, `s_w` and `o`, `o_w`, to fill in the non-zero entries of $\mathbf{Pre}$ and $\mathbf{Post}$ respectively. Because we have already induced ordering on $\mathcal{P}$ and $\mathcal{T}$, the matrices have the right sorting of rows and columns.

Hazard Functions

To build a CTMC model from the Petri net (SPN), each transition must have a hazard function $\lambda_k\left(t, M(t)\right)$. In the code implementation of **MGDrivE 2**, each hazard first checks if that transition is enabled, if not it immediately returns zero and else computes the hazard rate. We allow λ_k to be a function of time for simulation of inhomogeneous processes. Because in this manuscript we consider only Markovian systems, hazards only depend on

the current system state $M(t)$ and time t. Unless otherwise noted, we use λ_k to generically denote the joint hazard and enabling function for process Y_k.

This use of CTMC is known as a Markov population process, and has been used to model stochastic population models for some time now [93]. However, it can be useful to include exogeneous stochastic processes into the model, which may affect hazard rates. These processes could represent, for example, environmental processes such as temperature or rainfall. Knowledge of these processes would be necessary to evaluate the hazard functions. Consider the situation in which process Y_k is affected by environmental stochasticity represented by z so that the hazard is $\lambda_k\left(t, M(t), z\right)$; for concreteness, consider z to be temperature and k to be larval mortality. We must also consider a specific function of interest (f) to be computed from trajectories of **MGDrivE 2**, which we would like to estimate via Monte Carlo, to average over uncertainty in z. Again for concreteness, we could consider functions like time required for a specific gene to fixate, or time required for pathogen extinction in a specific node. To propagate uncertainty from arbitrary exogenous processes, we simply draw many samples from z and then run Monte Carlo simulation of **MGDrivE 2** on each realized exogenous trajectory; we can imagine an "outer" loop sampling a trajectory $\tilde{z}$ from z and an "inner" loop computing Monte Carlo estimates of f, conditioning on $\tilde{z}$ as deterministic input to $\lambda_k\left(t, M(t), \tilde{z}\right)$. Because z is by definition an exogeneous source of stochastic variation, the probability factorizes such that this method properly propagates uncertainty into our estimation of f. For specific functions, more efficient methods than naive Monte Carlo may exist, and we refer to the panoply of variance-reduction methods covered in [23].

In **MGDrivE 2**, once the Petri net $(\mathcal{P}, \mathcal{T})$ is constructed (and we have parameters θ and inheritance cube $\overline{\overline{\overline{Ih}}}$), we can construct the v-dimensional column vector of hazard functions Λ. Specifically, we store the individual λ_k functions as function closures within the vector Λ, as functions are first class objects in R. We note that this can be easily adapted to other programming languages, for example in C++98, functors could be used in lieu of closures, and in C++11/14, lambda functions could achieve the same effect [113]. Each closure stores only the elements of θ and $\overline{\overline{\overline{Ih}}}$ necessary for computation of the hazard. We note that the function closure based storage of hazard functions means that it is easy to include additional computational state for specialized algorithms or more complex processes, such as enabling times or integrated hazards.

So far we have described what the fully constructed object Λ is, but not yet how we implemented it in code, which we do now. Much like the construction of $\mathcal{T}$, we rely heavily on our assignment of transitions into classes; after allocating memory for a v-length vector, we begin iterating through $k \in \mathcal{T}$. First, we scan the `class` of the transition; this tells us the appropriate function factory to call that will return λ_k, the function closure that computes the hazard. We pass the packet k to the function factory, along with parameters θ. The packet provides all the necessary information to set up the enabling rule, and the function factory pulls out the necessary components of θ to compute that specific hazard, which are stored in the function closure. All returned hazard functions λ_k accept

only two arguments, t time, and M, the state (marking).

We allow the option for users to select if the vector of hazard functions shall be "exact" or "approximate". Exact hazards are required for both sampling algorithms that simulate integer numbers of tokens, in which case enabling rules make sense. In this case evaluation of λ_k proceeds as described above. If however a continuous-state approximation is desired, either from a deterministic interpretation of the hazard functions as rate functions for mean-field approximation, or from a drift-diffusion stochastic differential equation, we ignore the check for sufficient tokens on input arcs, as the model no longer has an integer state space.

Numerical Simulation

One key feature of the SPN representation of **MGDrivE 2** is the convenient decoupling of model specification and sampling method, allowing model-independent development of fast algorithms. This lets us benefit from extensive work into optimized stochastic sampling algorithms from the chemical kinetics and physical simulation communities, many of which can be used nearly "off the shelf" with a place/transition model representation. We refer to the encyclopedic book by [107] as one of many resources for fast simulation routines.

Currently we do not support exact simulation of inhomogeneous processes, although approximate simulation is best done via the Poisson time-step method, where inhomogeneous terms are discretized to a piecewise constant step function with the same Δt as used in the approximate time-step. Exact simulation of inhomogeneous processes is difficult, although an algorithm based on random time change was presented by [7], and [148] investigate exact and approximate rejection-based methods. We leave the incorporation of these or similar sampling methods into the **MGDrivE 2** framework for future development.

We provide example code to numerically integrate deterministic trajectories, based on the deSolve R package of ODE solvers [142], using a mean-field approximation to the stochastic system [21]. We also provide several stochastic samplers for both exact and approximate trajectories, inspired by the smfsb R package [152].

In certain situations, when populations are large (that is, no places have a small number of tokens) and hazard functions are close to linear (guaranteed when using mass-action forms), it may be the case that stochastic fluctuations can be safely neglected. [96] made rigorous the conditions under which CTMCs may converge to ODEs. Such an approach essentially simplifies to considering the hazard functions as rate functions, and the state $M(t)$ as a continuous quantity (motivating the ability for the user to select generation of "approximate" Λ) [53]. Even when stochastic fluctuations are non-negligible such that deterministic approximation is not valid, it may be useful to provide the option for deterministic integration of the SPN model for quick visualization of transient behavior, or for sensitivity analysis.

At present we only offer Gillespie's "direct-method" to sample statistically exact trajectories, a well known method to sample from stochastic models [57]. Being an exact sampler, it samples integer-valued trajectories, and thus uses exact hazards and enabling functions. Briefly, the method works via a simple update step where first the vector of hazard functions is evaluated, $h(t) = \Lambda\left(t, M(t)\right)$. The Markov transition kernel to the next state can be factored such that the sampler first samples the random variable τ describing *when* the jump occurs, relative to t, $\tau \sim \text{Exp}\left(\sum_k h_k(t)\right)$. Next it samples *which* process caused the jump, and updates the system accordingly, that is, it selects the process causing the jump, k' with probability $\frac{h_{k'}(t+\tau)}{\sum_k h_k(t+\tau)}$. Then update the marking according to matrix equation $M'(t+\tau) = M(t) + \mathbf{S}r_{k'}$. In general, large populations of mosquitoes and/or large numbers of nodes would render exact simulation practically impossible, if, for example many tens of thousands of individual events needed to fire each day, each requiring a system update and resampling of random variables for each event, both of which are computationally expensive tasks.

In addition, there are two approximate stochastic sampling algorithms that have been implemented for use in **MGDrivE 2**, and we anticipate future algorithmic development focusing on implementation of improved approximate samplers. The first of these is a simple fixed size tau-leaping method, the Poisson time-step (PTS), reviewed in [152] and first introduced by [55]. The basic concept behind the PTS algorithm is that if none of the hazard functions change significantly over a small time step, say $[t, t + \Delta t)$, then one can approximate the state change by sampling a Poisson distributed random variable for enabled each $k \in \mathcal{T}$, such that the elements of the r vector indicating how many times each event fired are each independent Poisson random variates with rate parameter $\lambda_k\left(t, M(t)\right)\Delta t$. Then the matrix update can be preformed with those sampled Poisson variates in the vector r, system time updated, and another iteration preformed. The extent to which the assumption that hazards do not change significantly over the interval determines the quality of the approximation. The original tau-leaping algorithm has spawned many variations on the theme, including some with strong probabilistic guarantees of approximation quality [8], which may be incorporated for **MGDrivE 2**.

The second approximate stochastic sampling algorithm is based on a continuous state stochastic differential equation (SDE), known as the diffusion approximation. We offer a brief heuristic explanation of the algorithm but a detailed derivation can be found in [58]. If one starts with the integer valued Markov jump process, it will have a set of differential equations known as Kolmogorov's forward equations (KFE), sometimes referred to as (chemical) Master equation. The KFE gives the complete time-evolution of the probability mass function across allowable system states, and is usually intractable. It is possible (see [149] for a brief overview) to generate a partial differential equation (PDE) second-order approximation to the KFE known as the Fokker-Planck equation, which approximates the probability mass function with a probability density function evolving according to first order drift and second order diffusion coefficients. Considering the marking M as a continuous state, the Fokker-Planck equation can be interpreted as a u-dimensional SDE

driven by independent Wiener processes. While advanced techniques for simulation of SDEs exist [132], we implement the simple Euler-Maruyama method in **MGDrivE 2**.

Appendix C

Brief Description of Step Operators

Step operators are a convenient way to simplify the expression of Kolmogorov forward equations (master equations; henceforth KFE) for jump processes. We introduce them here in the context of continuous-time Markov chains, following the exposition of [149]. Mathematically, the step operator E is a linear operator on a function $f(n)$ where $n \in \mathbb{Z}$. Because the probability flux on the right hand side of the differential KFE has contributions from all states with nonzero transition probabilities, and states are expressed as vectors of integers, the step operator E can be used to write KFEs. The main advantage of using step operators to write the KFE is that one no longer needs to keep track of what specific elements of the probability distribution the flux is flowing in and out of, one simply needs to keep note of how many "particles" of each type (corresponding to specific positions in the state vector) are being created and destroyed for each event that is allowed to change system state.

The step operator E is defined as below; for events which may cause the creation or destruction of more than one particle, note that E is defined for powers l. Most important for actually writing KFEs is the final relation, $(E^l - 1)$, which simplifies the inbound and outbound probability fluxes into a single term.

$$\begin{aligned} E[f(n)] &= f(n+1) \\ E^l[f(n)] &= f(n+l) \\ E^{-1}[f(n)] &= f(n-1) \\ \left(E^l - 1\right)[f(n)] &= E^l[f(n)] - f(n) \end{aligned} \tag{C.1}$$

When writing KFEs with the step operator defined in Equation C.1, note that to represent an event which creates l particles, one would use $\left(E^{-l} - 1\right)[f(n)]$. This is because the probability flux will include an incoming component from the state with l fewer particles, and the outbound flux from the current state.

Finally, for systems with more than one type of particle (the state space is a vector with more than one element), we can compose step operators to represent events which simultaneously change multiple particle counts simultaneously. Examples include pre-

dation in the stochastic Lotka-Volterra model, where predation simultaneously increases the count of predators and decreases the count of prey, or infection in simple epidemic models, which decrease the count of susceptibles and increases the count of infecteds. For an event which changes the count of type 1 and 2 particles by l_1 and l_2, one would use Equation C.2. To evaluate $E_1^{l_1} E_2^{l_2}[f(n)]$, one applies the operators on $f(n)$ one after the other.

$$\left(E_1^{l_1} E_2^{l_2} - 1\right)[f(n)] = E_1^{l_1} E_2^{l_2}[f(n)] - f(n) \tag{C.2}$$

To illustrate use of the step operator E, we demonstrate their use on a Lotka-Volterra model. In this model there are two types of particles, prey X and predators Y. There are three events, which can be written using notation from chemical kinetics as follows:

$$\begin{aligned} X &\to X + X \\ X + Y &\to Y + Y \\ Y &\to \emptyset \end{aligned} \tag{C.3}$$

These correspond to reproduction of prey, predation, and death of predators. At any point in time, the probability of the state n_1 prey (X) and n_2 predators (Y) at time t is denoted as $P(n_1, n_2; t)$. Reproduction of prey has per-capita rate β. Predation occurs according to simple mass-action with reaction constant γ. Finally, death of predators occurs with per-capita rate μ.

Now we write out the KFE and repeatedly apply the step operator until we get back to the familiar component-wise form.

$$
\begin{aligned}
\frac{d}{dt}P(n;t) =& \overbrace{(E_1^{-1}-1)[\beta n_1 P(n_1,n_2;t)]}^{\text{prey reproduce}} \\
&+ \overbrace{(E_2-1)[\mu n_2 P(n_1,n_2;t)]}^{\text{predator dies}} \\
&+ \overbrace{(E_1E_2^{-1}-1)[\gamma n_1 n_2 P(n_1,n_2;t)]}^{\text{predation}} \\
&= E_1^{-1}[\beta n_1 P(n_1,n_2;t)] - \beta n_1 P(n_1,n_2;t) \\
&+ E_2[\mu n_2 P(n_1,n_2;t)] - \mu n_2 P(n_1,n_2;t) \\
&+ E_1E_2^{-1}[\gamma n_1 n_2 P(n_1,n_2;t)] - \gamma n_1 n_2 P(n_1,n_2;t) \\
&= \beta(n_1-1)P(n_1-1,n_2;t) - \beta n_1 P(n_1,n_2;t) \\
&+ \mu(n_2+1)P(n_1,n_2+1;t) - \mu n_2 P(n_1,n_2;t) \\
&+ \gamma(n_{1+1})(n_2-1)P(n_1+1,n_2-1;t) - \mu n_1 n_2 P(n_1,n_2;t) \\
&= (n_1-1)\beta P(n_1-1,n_2;t) - n_1\beta P(n_1,n_2;t) \\
&+ (n_2+1)\mu P(n_1,n_2+1;t) - n_2\mu P(n_1,n_2;t) \\
&+ (n_1+1)(n_2-1)\gamma P(n_1+1,n_2-1;t) - n_1 n_2 \gamma P(n_1,n_2;t) \\
&= \overbrace{-(n_1\beta + n_2\mu + n_1 n_2\gamma)P(n_1,n_2;t)}^{\text{outbound probability flux}} \\
&+ \overbrace{(n_1-1)\beta P(n_1-1,n_2;t)}^{\text{inbound (prey reproduce)}} + \overbrace{(n_2+1)\mu P(n_1,n_2+1;t)}^{\text{inbound (predator dies)}} \\
&+ \overbrace{(n_1+1)(n_2-1)\gamma P(n_1+1,n_2-1;t)}^{\text{inbound (predation)}}
\end{aligned}
\tag{C.4}
$$

Appendix D

Derivation of Final Epidemic Size Distributions

Another metric to check that our ABM is sampling from the correct process is to compare the final epidemic size distribution computed by Monte Carlo simulation of the ABM to an exact analytic result. We rely on the method presented in [135] and well described in [9] to compute final size distributions for SIR epidemic models with general distributions of infectious periods.

For a SIR epidemic where infectious periods F have a moment generating function (MGF) which is $\Psi_F(t) = \mathbb{E}[e^{tF}]$ and where the initial states are given as $S(0) = N, I(0) = m$, the rate of effective contact by λ, then the final epidemic size vector is $p^{(N)} = (p_0^{(N)}, \ldots, p_N^{(N)})$ where $p^{(N)})_k$ is the probability that k of the initial N susceptibles are infected when the epidemic ends. From [13], these probabilities are related by the recursive equation:

$$\sum_{i=0}^{k} \left[\frac{\binom{k}{i} p_i^{(N)}}{\binom{N}{i} \left[\Psi_F \left(-\frac{(N-k)\lambda}{N} \right) \right]^{i+m}} \right] = 1 \tag{D.1}$$

Using Equation D.1, we calculate an explicit recursive formula for the probabilities $p_k^{(N)}, k = 0, \ldots, N$. We begin by using $\binom{k}{i}/\binom{N}{i} = \binom{N-i}{k-i}/\binom{N}{k}$ to get:

$$\sum_{i=0}^{k} \left[\frac{\binom{N-i}{k-i} p_i^{(N)}}{\binom{N}{k} \left[\Psi_F \left(-\frac{(N-k)\lambda}{N} \right) \right]^{i+m}} \right] = 1 \tag{D.2}$$

Then pull $1/\binom{N}{k}$ out of the sum and multiply both sides by $\binom{N}{k}$:

$$\sum_{i=0}^{k} \left[\frac{\binom{N-i}{k-i} p_i^{(N)}}{\left[\Psi_F \left(-\frac{(N-k)\lambda}{N} \right) \right]^{i+m}} \right] = \binom{N}{k} \tag{D.3}$$

Next pull out the final summation of the left hand side:

$$\sum_{i=0}^{k-1}\left[\frac{\binom{N-i}{k-i}p_i^{(N)}}{\left[\Psi_F\left(-\frac{(N-k)\lambda}{N}\right)\right]^{i+m}}\right]+\frac{p_k^{(N)}}{\left[\Psi_F\left(-\frac{(N-k)\lambda}{N}\right)\right]^{k+m}}=\binom{N}{k} \tag{D.4}$$

Now multiply all terms through by $\left[\Psi_F\left(-\frac{(N-k)\lambda}{N}\right)\right]^{k+m}$, noting that we can move the power in the denominator up to the numerator by adjusting the power by $(k+m)-(i+m)=k-i$:

$$\sum_{i=0}^{k-1}\left[\binom{N-i}{k-i}p_i^{(N)}\left[\Psi_F\left(-\frac{(N-k)\lambda}{N}\right)\right]^{k-i}\right]+p_k^{(N)}=\binom{N}{k}\left[\Psi_F\left(-\frac{(N-k)\lambda}{N}\right)\right]^{k+m} \tag{D.5}$$

Finally, solve for $p_k^{(N)}$, the desired probability:

$$p_k^{(N)}=\binom{N}{k}\left[\Psi_F\left(-\frac{(N-k)\lambda}{N}\right)\right]^{k+m}-\sum_{i=0}^{k-1}\left[\binom{N-i}{k-i}p_i^{(N)}\left[\Psi_F\left(-\frac{(N-k)\lambda}{N}\right)\right]^{k-i}\right] \tag{D.6}$$

In order to turn Equation D.6 into an algorithm, we note that when $k=0$ the sum drops out and the equation simplifies to:

$$p_0^{(N)}=\Psi_F\left(-\lambda\right)^m \tag{D.7}$$

Probabilities for $k=1,\ldots,N$ can then be solved for recursively. It should be noted that for N much larger than 100, the algorithm given by Equation D.6 suffers from numerical instability, and so should only be used for small populations. Because the equations are defined solely in terms of the MGF of the infectious period distribution, the probabilities from Equation D.6 can be used for both the Markovian and non-Markovian SIR model.

Appendix E

Principled simulation of agent-based models in epidemiology: supplemental figures

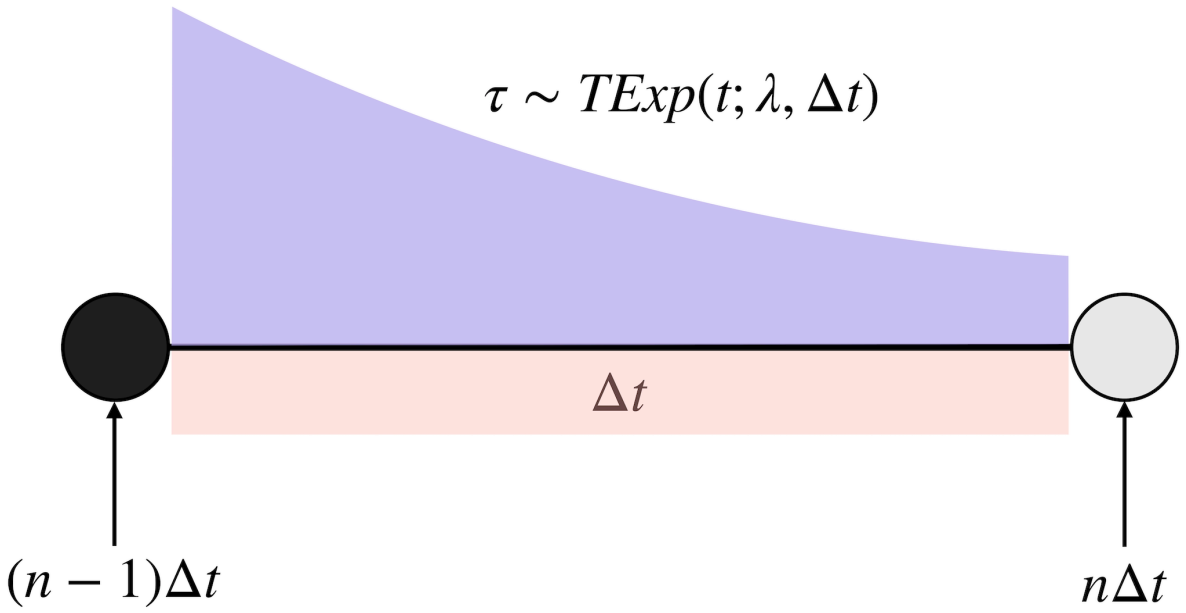

Figure E.1: **Truncated Exponential distribution of infection time on time step where the $\widehat{\tau}_{S \to I}$ is accepted.** An Exponential distribution truncated at Δt with rate parameter λ has the density $f(\tau; \lambda, \Delta t) = \frac{\lambda e^{-\lambda \tau}}{1 - e^{-\lambda \Delta t}}$.

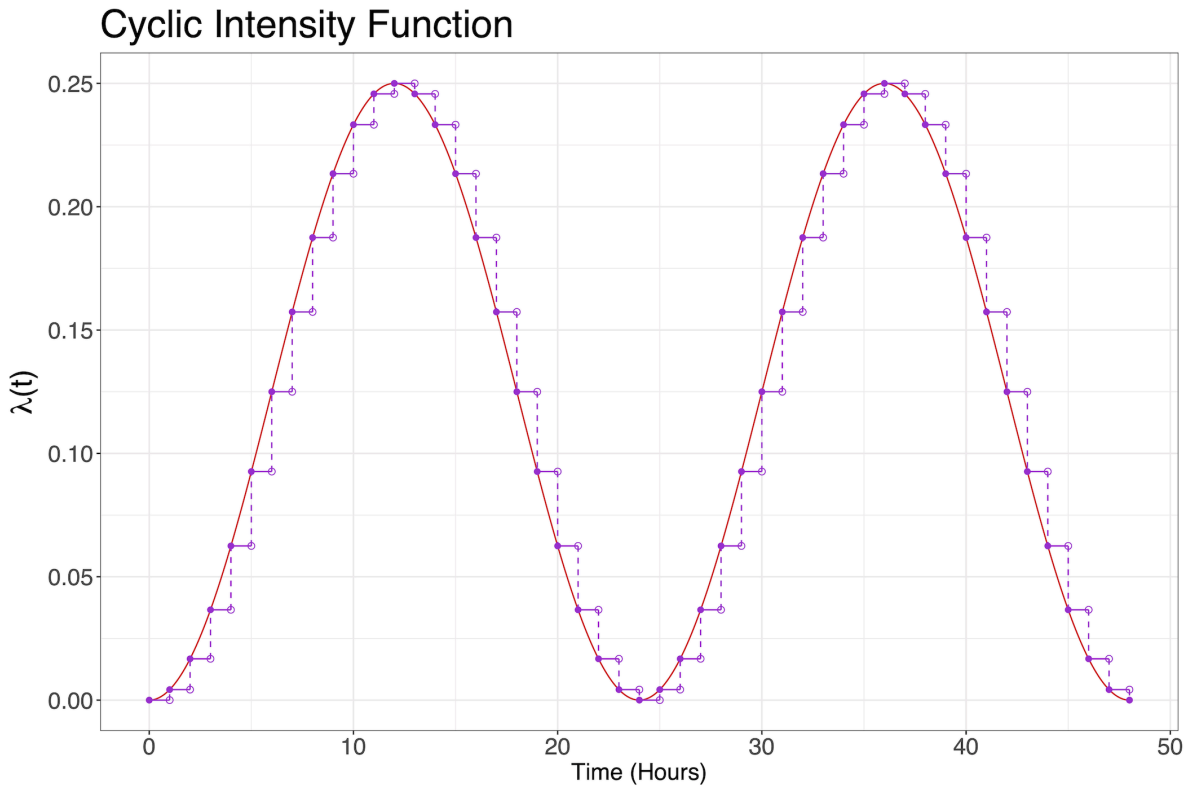

Figure E.2: **Nonhomogeneous diurnal intensity function.** Continuous intensity function $\tilde{\lambda}(t)$ (red solid line) and piecewise approximation $\lambda(t)$ (purple step function; approximation used for simulation is on much finer time-step, coarse approximation is purely for visual effect).

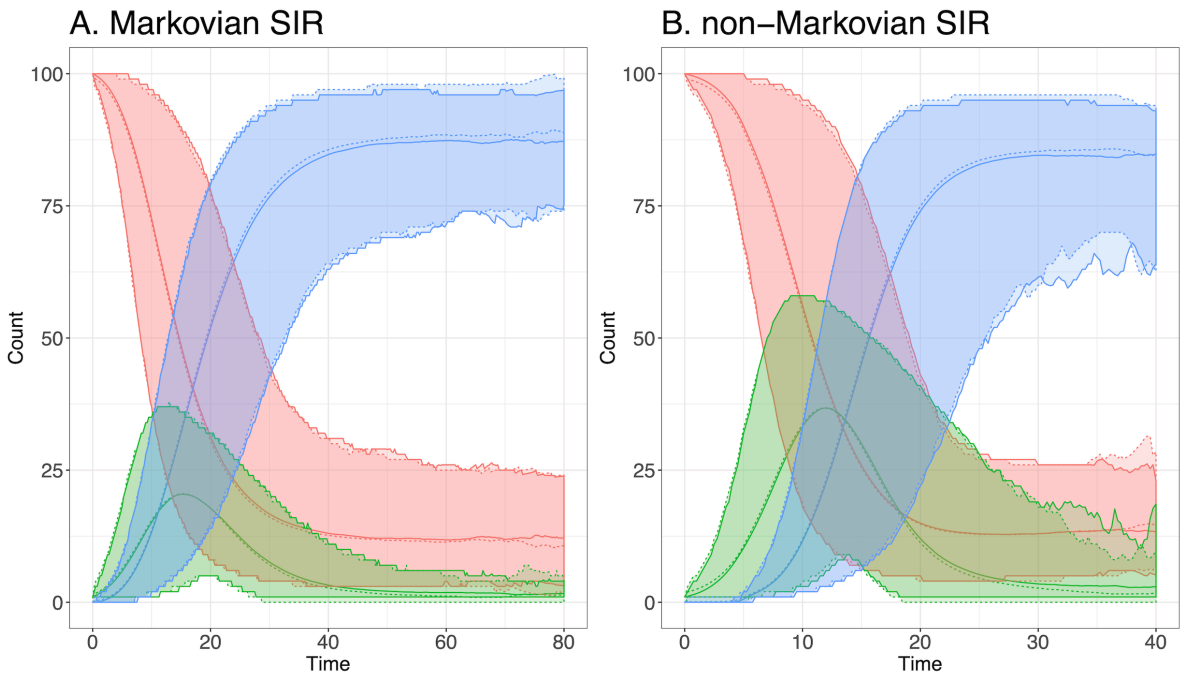

Figure E.3: **Comparison of simulation trajectories from exact stochastic simulation and ABM.** Panel A: Markovian SIR trajectories. Panel B: non-Markovian SIR trajectories. For each panel we drew 10^4 trajectories from the MNRM and ABM simulation algorithms and summarized the results by plotting the mean and 95% simulation interval. The MNRM trajectory is denoted by dashed lines and the ABM by solid lines.